

Doctoral theses at NTNU, 2021:13

Sanat Kumar Karmacharya

Simulating pressurized reservoir
flushing in scale models using
lightweight sediments

ISBN 978-82-471-9404-1 (printed ver.)
ISBN 978-82-471-9659-5 (electronic ver.)
ISSN 1503-8181 (printed ver.)
ISSN 2703-8084 (electronic ver.)

Doctoral theses at NTNU, 2021:13

NTNU
Norwegian University of
Science and Technology
Thesis for the degree of
Philosophiae Doctor
Faculty of Engineering
Department of Civil and Environmental
Engineering

 **NTNU**
Norwegian University of
Science and Technology

 NTNU

 **NTNU**
Norwegian University of
Science and Technology

Sanat Kumar Karmacharya

Simulating pressurized reservoir flushing in scale models using lightweight sediments

Thesis for the degree of Philosophiae Doctor

Trondheim, May 2021

Norwegian University of Science and Technology
Faculty of Engineering
Department of Civil and Environmental Engineering



Norwegian University of
Science and Technology

NTNU

Norwegian University of Science and Technology

Thesis for the degree of Philosophiae Doctor

Faculty of Engineering

Department of Civil and Environmental Engineering

© Sanat Kumar Karmacharya

ISBN 978-82-471-9404-1 (printed ver.)

ISBN 978-82-471-9659-5 (electronic ver.)

ISSN 1503-8181 (printed ver.)

ISSN 2703-8084 (electronic ver.)

Doctoral theses at NTNU, 2021:13



Printed by Skipnes Kommunikasjon AS

Abstract

The dissertation presents the findings from laboratory experiments conducted to study the pressurised flushing phenomena using lightweight materials as model sediment. The study resulted in four research papers, which are summarized in this thesis and the results are discussed in detail.

To speed up the recording of bed levels in the experiments and to produce better quality 3D models of the recorded bed levels, Structure from Motion (SfM) technique was applied. Before adopting to the experiments, different SfM tools available were compared and the suitable one was selected. Then, the applicability of SfM technique with the selected SfM tool was tested in three scale model studies of different scales.

Five sets of scaled model experiments on pressurised flushing of non-cohesive sediment deposit through bottom outlet were carried out. Natural sand and lightweight materials satisfying the scaling criteria were selected to be used as model sediments. The experiments were focused on predicting the dimensions and volume of flushing cones, so two empirical equations were proposed from regression analysis of the experimental data to predict the length and volume of flushing cones.

The prediction made by new proposed empirical equations were also compared with the empirical equations proposed by previous laboratory experiments conducted with sand as model sediment. Since the experiments in this study were conducted for variations in different parameters governing the flushing process, the proposed equations performed pretty well for both sand and lightweight materials as model sediment when compared to empirical equations from previous studies.

Preface

This thesis is submitted to the Norwegian University of Science and Technology (NTNU) in Trondheim for partial fulfilment of the requirements for the degree of 'Philosophiae Doctor (PhD)'.

This work is the result of a three-year PhD programme, which was conducted jointly at the Department of Civil and Environmental Engineering (NTNU) and Hydro Lab Pvt. Ltd., Nepal. The research has been supervised by Professor Nils R  ther as main supervisor and Professor Jochen Aberle & Dr. Meg Bahadur Bishwakarma as co-supervisors. This research was conducted as a joint collaboration between Norwegian Hydropower Center (NVKS), Norway, Department of Civil and Environmental Engineering (NTNU), Norway and Hydro Lab, Nepal under SediPASS programme with funding from The Research Council of Norway. The research was also supported by Energize Nepal (ENEP) which is a collaboration between NTNU (Norway), SINTEF (Norway), Kathmandu University (Nepal) and Hydro Lab (Nepal) and is funded by The Norwegian Ministry of Foreign Affairs (MFA).

In accordance with the guidelines of the Faculty of Engineering, this thesis comprises an introduction to the research that has resulted in four scientific journal papers.

Acknowledgements

This research work has been possible with direct/indirect contribution of various brilliant and helpful people in my academic, professional and personal life. I would like to thank all of them for their support and motivation throughout the research period.

To begin with, I would like to express my sincere gratitude to my supervisor Prof. Nils Ruther for being very supportive and guiding me with his valuable and constructive suggestions during the planning and development of this research work. I would also like to extend my sincere gratitude to my co-supervisor Prof. Jochen Aberle for sharing his knowledge on physical modelling and for his valuable support and suggestions in scientific writing of the research outcomes. And my deep gratitude extends to my co-supervisor Dr. Meg Bahadur Bishwakarma for continuous encouragement and for providing all the facilities available at the hydraulic laboratory of Hydro Lab as per requirement of this research.

A very special thanks to all colleagues from Department of Civil and Environmental Engineering (NTNU) and Hydro Lab, who facilitated my research with their skill, knowledge and constructive suggestions.

Last but not the least, my special thanks to my family and friends for their moral support over the years.

Thank you All!

Contents

Abstract.....	i
Preface.....	iii
Acknowledgements	v
Contents.....	vii
List of Papers.....	ix
List of Figures	xi
List of Tables	xiii
List of Abbreviations and Symbols.....	xv
Introduction.....	1
1.1 Scope and Aim	6
1.2 Thesis outline.....	6
Literature Review	9
2.1 Predicting geometry of a pressurized flushing cone	9
2.2 Similarity criteria for mobile bed models.....	14
2.3 Lightweight materials as model sediment	20
Research Methodology	23
3.1 Experimental setup.....	23
3.2 Design of mobile bed models.....	24
3.2.1 Model scales.....	24
3.2.2 Model sediments.....	25
3.3 Experimental procedure	26
3.4 Application of Structure from Motion (SfM) technique	27
Results and Discussions.....	31
4.1 Application of SfM in hydraulic model studies.....	31
4.2 Pressurized flushing experiments	33
4.2.1 Geometry of flushing cones.....	33
4.2.2 Performance of lightweight materials as model sediment.....	35
4.2.3 Comparison of empirical equations	36
4.2.4 Regression analysis and validation	39
Conclusions and Recommendations	43
References	47
Annex-A	53
Paper I	55
Paper II.....	67
Paper III.....	83
Paper IV.....	93
Annex-B.....	119
Annex-C.....	125

List of Papers

Paper I: Application of 'Structure from Motion' (SfM) technique in physical hydraulic modelling

Sanat Kumar Karmacharya, Meg Bishwakarma, Ujjwal Shrestha, Nils Rüther
CRHT IX, 2019, Journal of Physics: Conference Series 1266 012008

Paper II: Evaluating the Structure from Motion technique for measurement of bed morphology in physical model studies

Sanat Kumar Karmacharya, Nils Rüther, Ujjwal Shrestha, Meg Bahadur Bishwakarma
Water 2021, 13(7), 998; <https://doi.org/10.3390/w13070998>

Paper III: Physical modelling of pressurized flushing of non-cohesive sediment using lightweight material

Sanat Kumar Karmacharya, Pierre-Yves Henry, Meg Bishwakarma, Jochen Aberle, Nils Rüther
CRHT IX, 2019, Journal of Physics: Conference Series 1266 012012

Paper IV: Physical modelling of pressure flushing of sediment using lightweight materials

Sanat Kumar Karmacharya, Nils Rüther, Jochen Aberle, Sudhir Man Shrestha, Meg Bahadur Bishwakarma
Accepted: Journal of Applied Water Engineering and Research, 2021

List of Figures

Figure 1. Sketch of a flushing cone and its associated parameters.....	3
Figure 2: Schematic diagram of the experimental setup (not to scale)	24
Figure 3. General workflow for SfM technique.....	28
Figure 4. Overall statistical performance indices for prediction of (a) elevations, (b) lengths and (c) volumes by SfM technique using Photoscan	33
Figure 5. Non-dimensional cross-section profiles of flushing cones at 0.02 m upstream of the outlet.....	34
Figure 6. Non-dimensional centreline profiles of flushing cones.....	34
Figure 7. Comparison of $L_{max}H_{wnet}$ for Sand and Lightweight sediment pair	36
Figure 8. Comparison of $V_{s1/3}H_{wnet}$ for Sand and Lightweight sediment pair	36
Figure 9. Comparison of measured dimensionless volume $V_{s1/3}/H_{wnet}$ against that predicted using empirical equations proposed by (a) Emamgholizadeh et al. (2006), (b) Powell (2007), (c) Shahmirzadi et al. (2010), (d) Meshkati et al. (2010), (e) Fathi-Moghadam et al. (2010), (f) Dreyer & Basson (2018)	37
Figure 10. Comparison of measured dimensionless length L_{max}/H_{wnet} against that predicted using empirical equations proposed by (a) Powell (2007), (b) Shahmirzadi et al. (2010), (c) Meshkati et al. (2010), (d) Fathi-Moghadam et al. (2010), (e) Kamble et al. (2017) and (f) Dreyer and Basson (2018).....	38
Figure 11. Comparison of measured L_{max}/H_{wnet} against that predicted by (a) Eqn 18 and (b) Eqn 19.....	39
Figure 12. Plot of measured $V_{s1/3}/H_{wnet}$ against that estimated by Eqn 20 for (a) calibration dataset and (b) validation dataset.....	40
Figure 13. Plot of measured L_{max}/H_{wnet} against that estimated by Eqn 21 for (a) calibration dataset and (b) validation dataset.....	40
Figure 14. Prediction of $V_{s1/3}/H_{wnet}$ for experimental data from Fathi-Moghadam et al. (2010) using Eqn. 20.....	41

List of Tables

Table 2.1: Summary of sediment used by experimental studies on pressurised flushing of non-cohesive sediment	13
Table 2.2. Classification of movable bed models by Kamphuis (1985).....	20
Table 3.1. Scale ratio for mobile bed models used in the study	25
Table 3.2. Sediment used for the experiments and their properties.....	26
Table 3.3. Range of parameters.....	27
Table 3.4. Comparison of SfM software selected for the study.....	29
Table 4.1. Statistical performance indices for selected software in predicting elevations	32

List of Abbreviations and Symbols

A	Cross sectional area of the outlet opening	k_s	Roughness height
a	Opening height of bottom outlet	L_{max}	Length of the flushing cone at equilibrium
a_0	Height of bottom sill above flume bed	L_r	Model length scale ratio
B	Width of the flume	n	Manning-Strickler's coefficient of roughness
b	Opening width of bottom outlet	Q	Discharge
b_{oc}	Outlet width over the centreline	q_s	Volumetric bed load transport rate per unit width
b_{oe}	Outlet width at the edge	q_s	Volumetric bed load transport rate per unit width
C_s	Sorting coefficient of sediment particles	q_s^*	Taylor's dimensionless unit sediment discharge
C_u	Uniformity coefficient of sediment particles	R^*	Particle Reynolds number
D	Diameter of the circular bottom outlet	SfM	Structure from Motion
D^*	Dimensionless grain diameter	u	Average flow velocity at the orifice
d_{50}	Mean diameter of sediment particles	u^*	Average shear velocity
d_s	Characteristic sediment particle size	V_s	Equilibrium volume of the flushing cone
EFWL	Effective Flushing Water Level	W_{max}	Width of flushing cone at equilibrium
F	Froude Number	w_s	Settling velocity of sediment particles
F^*	Densimetric Froude number	Z_{max}	Depth of flushing cone at equilibrium
GCP	Ground Control Point	δ	Distortion ratio
G_s	Specific gravity of sediment particles	θ	Shields parameter
g	Acceleration due to gravity	θ_c	Critical Shields parameter
h_s	Sediment height above outlet's sill	μ	Dynamic viscosity of water
H_s	Sediment height above flume bed	ν	Kinematic viscosity of water
H_{snet}	Net sediment height above the centre of the outlet opening	ρ_s	Density of sediment particles
h_w	Flow depth above outlet's sill	ρ_w	Density of water
H_w	Flow depth above flume bed	σ_g	Geometric standard deviation of sediment sizes
H_{wnet}	Net flow depth above the centre of the outlet opening	τ	Bed shear stress

1

Introduction

Around the world, there are more than 50,000 large dams which are higher than 15 m and/or having storage capacity bigger than 3 million m³. The total reservoir storage capacity of dams around the world is estimated at about 7,000 km³ (UNESCO, 2009). Undoubtedly, damming a naturally flowing river was one of the biggest human achievement in harvesting natural water resources. Initially, dams were built to attenuate flood intensity, supply water for household uses and irrigating crops. In course of time, the purpose of dams distended to navigation, energy production, fish farming, recreation and many more.

Besides storing precious water, the dams also accumulate sediment fluxes into the reservoir. Sedimentation in reservoirs has many environmental, ecological and engineering effects including continuous loss of reservoir capacity itself. Globally, the annual loss rates relative to installed storage capacity are generally estimated to range between 0.5 and 1% (Atkinson, 1996; Mahmood, 1987; Schleiss et al., 2016; White, 2001). To cope with increasing population and decreasing reservoir capacity, new dams have to be built. But most of the feasible sites for dam construction have already been exploited and the environmental regulations regarding construction of dams have become very demanding. Hence, sustaining the storage capacity of a reservoir by reducing the sedimentation or restoring the reservoir storage lost due to sedimentation could be more feasible option than building a new reservoir. Regarding this, various reservoir sediment management strategies like reducing sediment yield in the river by watershed management or trapping sediment before entering the reservoir; routing the inflow sediment to downstream bypassing or through the reservoir; and evacuating deposited sediment mechanically or hydraulically have been practised to prolong the reservoir's life and to restore the lost storage capacity (Annandale et al.,

2016; Basson et al., 1997; Brandt, 2000; Morris & Fan, 2010; Schleiss et al., 2016; Wen Shen, 1999).

Hydraulic flushing is one of the strategies commonly used across the globe for evacuating deposited sediments from reservoirs (Lai & Shen, 1996), usually by releasing flow through low-level outlets at the dam (White, 1990). It is most often preferred in long and narrow valleys with ample water inflow as the river water itself is used to flush the deposited sediment from reservoirs and to pass incoming sediments through the reservoir to downstream. Paul & Dhillon (1988) analysed reservoir flushing data from the field and model studies in six countries and reported that the hydraulic flushing is effective in removing deposited sediments from small reservoirs (storage capacity less than 10^8 m³) as well as from large reservoirs (storage capacity up to 10^{10} m³). For hydraulic flushing to be significantly effective, the reservoir shall be drawn down to the extent of natural river flow condition existing before the dam was built (Atkinson, 1996; Scheuerlein et al., 2004; White, 1990). Such type of flushing with complete drawdown of reservoir is called 'free flow flushing'. Free flow flushing is not feasible for large reservoirs in water scarce regions since reservoirs shall be emptied for flushing sediment deposits. It requires curtailing of reservoir's function (e.g., power production, water supply etc.) during the flushing period, which makes it not suitable for reservoirs built to provide steady water supply e.g., for municipal or industrial users. In such cases, pressurized flushing, in which deposited sediments are evacuated through bottom outlets while maintaining the minimum reservoir operation level, can be a viable option.

Pressurized flushing is a type of hydraulic flushing in which sediment deposits are evacuated through bottom outlets while the reservoir water level is maintained not to be lower than the minimum operating level. Unlike free flow flushing in which reservoir is drawn down completely, pressurized flushing is less efficient and only scours sediment deposits locally in the vicinity of bottom outlet creating a funnel shaped crater commonly designated as flushing cone or flushing half-cone (Samad Emamgholizadeh et al., 2006; Mahmood, 1987; Meshkati et al., 2010; Sloff, 1991; Wen Shen, 1999). A simplified sketch of a flushing cone and its associated parameters are shown in Figure 1.

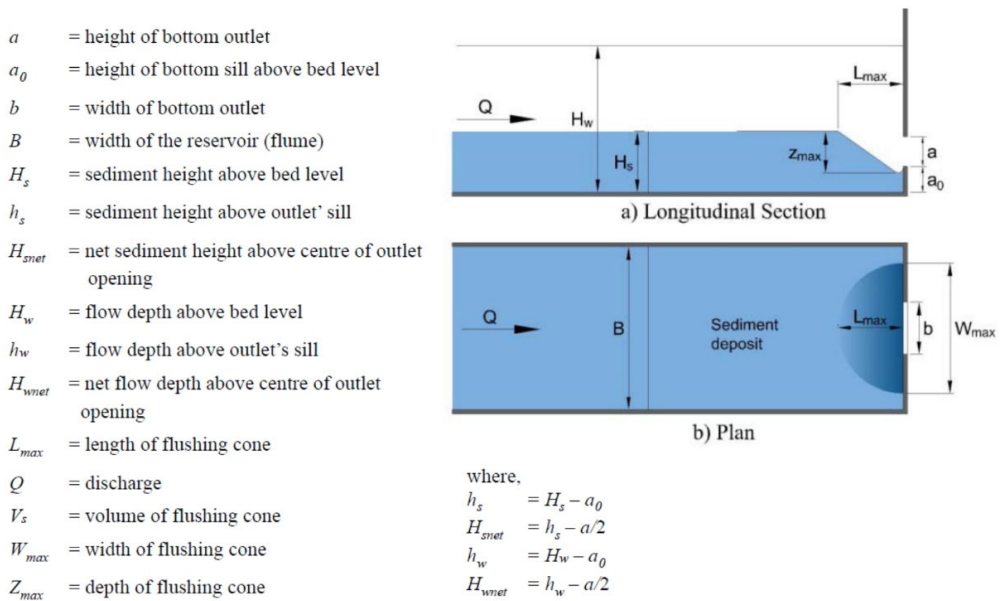


Figure 1. Sketch of a flushing cone and its associated parameters

As soon as the gate of the bottom outlet is opened for pressurized flushing, a scour is initiated due to excess shear stress (Powell & Khan, 2012) and large amounts of sediment are released in the beginning (Fang & Cao, 1996). After the formation of the scour cone, vortices with vertical axes occur randomly which further scour the sediment deposit by entraining sediment particles into the flow and hence discharging through the outlet (Powell & Khan, 2012). These random vortices ultimately govern the equilibrium size of the flushing cone (Powell, 2007; Powell & Khan, 2012). With progressing time, the scour cone becomes fairly stable in shape and size with no further sediment removal from the cone (Di Silvio, 1990).

Despite the pressurized flushing can clear deposited sediment up to a limited extent only, it is crucial especially for hydropower reservoirs, when sediment deposition levels near intakes have to be controlled to prevent passage of sand through the turbines while the hydropower plant is in operation (Basson & Rooseboom, 2008; Fang & Cao, 1996). Moreover, it can be the only feasible option for reservoirs in water scarce regions, which cannot afford emptying of the reservoir for free-flow flushing (Kondolf et al., 2014). Therefore, it is essential to predict the spatial extent and the volume of sediment that can be cleared for design of the outlets and to establish operational regime for efficient pressurized flushing. But the formation of a flushing cone during

pressurized flushing is a complex three-dimensional phenomenon involving numerous parameters, verification of which is problematic (Scheuerlein et al., 2004). Because of that, the theoretical treatment of pressurized flushing phenomenon is very difficult. Most of the flushing and sluicing practices are based more on experience than on understanding of the physical processes (Sloff, 1991). Hence, various empirical regression-based relationships have been proposed to predict the dimensions and the volume of a flushing cone within a dimensionless framework as described in Section 2.1. Almost all of the empirical relations available in literature to predict the dimensions and volume of a flushing cone were derived via flume experiments and scaled model studies except the one by Scheuerlein (1993) in which he proposed a simplified analytical approach. Most of such flume experiments and scaled model studies used sand as model sediment whereas some preferred lightweight materials, having density lower than natural sand but denser than water, as substitute for natural sand. But they did not clearly explain about scaling relation between different parameters associated to the model sediment and the prototype sediment.

In a reservoir project, the sediments depositing near the intake are mostly fine sediment since the coarse sediment carried by the inflowing river starts settling nearby the mouth of the reservoir due to very low flow velocity in the reservoir. Therefore, physical models replicating pressurized flushing in general have to properly represent fine prototype sediment. The common practice to model such scenario is to scale down the parameters of prototype into model scale based on Froude model law. Froude model law is applicable for open channel flows, in which gravitational force is the dominant hydrodynamic force. Hence, similarity in Froude number F between model and prototype is considered as the basic similarity criterion. Such models are also designated as Froude-scaled models or Froudeian-scale models. Undistorted Froude scaled models with fixed beds produce satisfactory results with reasonably understood scale effects (Heller, 2011). However, the degree of complexity increases by many folds for mobile bed physical models in which similarity in sediment transport needs to be considered.

Undistorted Froude scale models with natural sand as model sediment, the particle size of which is scaled down by model scale factor L_r (where the subscript ' r ' defines the ratio of prototype and model properties), provide satisfactory results with minimized scale effects. However, if such models are used to represent prototypes with fine sand which, when downscaled to model scale, may require sediment size in

cohesive range, they are prone to scale effects. Moreover, the scaling may also change the sediment transport phenomena from bed load in the prototype to suspended load in the model (Kamphuis, 1974). To avoid scale effects due to cohesion and changes in flow-grain interaction characteristics, the particle size of sand in models, d_{sm} , should be greater than 0.22 mm (Zarn, 1992) [$d_{sm}>0.5$ mm by Bretschneider (in Kobus, 1980), $d_{sm}>0.8$ mm by Oliveto & Hager (2005), $d_{sm}>1$ mm by Schmocker & Hager (2009)]. However, the prototype sediment size for a reservoir project is likely to dwell within that size range. To avoid downscaling fine prototype sand to model sediment size likely to be in cohesive range, lightweight materials can be used as model sediment to overcome the limitation in particle size of sand in model and to avoid cohesion in model sediment.

In the past, lightweight sediment models were designed based on trial and error using various materials available and selecting the one that calibrated well with the prototype data. Those models were most often intended to get qualitative results. Based on experiments on incipient motion of sediment by Shields (1936), various scaling laws were developed for quantitatively interpreting the model predictions. Since then, different laboratories around the world have been using lightweight materials as model sediment, and the scaling criteria and study methodologies were based on their experiences with such models and adjusted to the peculiarities of the problems at hand (Henry et al., 2018). But the details about the scaling laws and model techniques, especially about the failed attempts, were never published (Vollmers, 1990).

Therefore, a research project was initiated as a part of SediPASS program by Norwegian Hydropower Center (NVKS), Norway and Norwegian Institute of Science and Technology (NTNU), Norway in collaboration with Hydro Lab, Nepal in 2017 to fill the gap between physical hydraulic modelling of pressurized flushing of a reservoir and the methodological scaling of the sediment parameters by using lightweight sediments. Under the broad objective of SediPASS program to develop knowledge towards improved design and operation of sustainable hydropower exposed to high sediment yield, this study was focused on simulation of pressurized flushing in physical hydraulic models using lightweight sediment to predict the extent of resulting flushing cones. The study was funded by The Research Council of

Norway, Hydro Lab Nepal, Statkraft and the Norwegian Hydro Power Center (NVKS).

1.1 Scope and Aim

Narrowing down the broad objective of SediPASS program, the present PhD research specifically concentrates on conducting physical hydraulic modelling of pressurized flushing of non-cohesive sediment deposits from reservoir through bottom outlets by using properly scaled lightweight sediments to represent fine prototype sediment. The objectives of the research are to review the literature on pressurised flushing as well as on scaling laws for mobile bed models, to select suitable scaling laws for using lightweight sediments in scale models to represent non-cohesive sediment in prototype, to design physical models based on selected scaling laws and available lightweight sediment and to conduct physical modelling of pressurized flushing of sediment deposits through bottom outlets to validate the applicability of the model technique. The research is also intended to develop empirical relations for quantitative prediction of flushing scour cone geometry. Additionally, this study also aimed in adoption of Structure from Motion (SfM) technique to physical scale modelling for acquiring accurate data in high temporal and spatial resolution.

1.2 Thesis outline

This thesis is composed of five main chapters. The present chapter introduces the topic and describes the need and objective of the study. Chapter 2 presents theoretical background via literature review on pressurized flushing experiments and similarity criteria for mobile bed scale models using lightweight sediments. Chapter 3 describes the research methodology and acquaints an overview of the experimental setup, adopted modelling techniques and experimental procedure. In addition, one section in Chapter 3 is dedicated to describe application of Structure from Motion (SfM) technique in data acquisition during the model experiments. Chapter 4 summarises and discusses the results from the experiments including comparison of empirical relations available in the literature. Chapter 4 also covers multi-variate nonlinear regression analyses of experimental data to propose new empirical relations for prediction of dimensions and volume of a pressurized flushing cone. Chapter 5 summarizes the findings of this study and outlines potentials for further research. The thesis also contains manuscripts of the selected research articles in Annex-A. The dimensional analysis to derive dimensionless functional relationships for length and

volume of flushing cones; and the regression analysis of experimental data to derive empirical relations predicting length and volume of flushing cones are presented in Annex-B. The statement from co-authors are included in Annex-C at the end of the thesis.

2

Literature Review

2.1 Predicting geometry of a pressurized flushing cone

Various studies available in literature on pressurized flushing of non-cohesive sediment deposit through bottom outlet presented different empirical relations to predict dimensions and size of a pressurized flushing cone except Scheuerlein (1993), who presented a simplified analytical approach to identify the parameters governing flushing efficiency and to develop criteria for evaluation of the flushing efficiency. He suggested that the flushing efficiency will be maximum for a certain water level above the sediment deposit, which was designated as effective flushing water level (EFWL).

Emamgholizadeh et al. (2006) showed in their experiments with non-cohesive sediments that the maximum flushing efficiency can be achieved by lowering the reservoir water level during the flushing while the outlets are fully opened. They proposed an empirical relation for estimating the flushing cone volume:

$$\frac{V_s^{1/3}}{H_{snet}} = 0.6139 \left(\frac{u}{\sqrt{g H_{wnet}}} \right)^{0.0062} \left(\frac{H_{snet}}{d_s} \right)^{0.05} \left(\frac{H_{snet}}{H_{wnet}} \right)^{0.0036} \quad (1)$$

where, V_s = equilibrium volume of the flushing cone, H_{snet} = net sediment height above the centre of the outlet opening, u = flow velocity at the entrance of the outlet and H_{wnet} = net flow depth above the centre of the outlet opening.

The experimental investigations of Powell (2007) and Powell & Khan (2012) showed that the flushing cone geometry is similar for different net heads and sediment sizes if it is described in a dimensionless framework. They concluded that the maximum scour depth Z_{max} increases with increasing net head H_{wnet} and it decreases with increasing sediment size d_s . Powell (2007) also provided explicit relationships for maximum depth

of flushing cone Z_{max} , maximum width of flushing cone W_{max} , maximum length of flushing cone L_{max} and volume of flushing cone V_s at equilibrium as follows:

$$Z_{max} = \frac{18576 \frac{H_{wnet}}{D} + 33273}{\frac{\rho u \left(\frac{d_s}{H_{wnet}} \right)^{0.1}}{\mu}} \quad (2.1)$$

$$\frac{W_{max}}{2} = \frac{55789 \frac{H_{wnet}}{D} + 144557}{\frac{\rho u \left(\frac{d_s}{H_{wnet}} \right)^{0.1}}{\mu}} \quad (2.2)$$

$$L_{max} = \frac{72017 \frac{H_{wnet}}{D} + 45656}{\frac{\rho u \left(\frac{d_s}{H_{wnet}} \right)^{0.1}}{\mu}} \quad (2.3)$$

$$V_s = 0.673 L_{max} \frac{W_{max}}{2} Z_{max} \quad (2.4)$$

Shahmirzadi et al. (2010) showed that the length and volume of the flushing cone increases with increase in area of outlet opening under constant reservoir level. They proposed the following empirical relations for predicting the length and volume of flushing cones:

$$\frac{V_s}{H_{wnet}^3} = 0.042 \left(\frac{u}{\sqrt{g H_{wnet}}} \right)^{0.149} \left(\frac{H_{snet}}{H_{wnet}} \right)^{3.082} \left(\frac{A}{H_{wnet}^2} \right)^{0.174} \quad (3.1)$$

$$\frac{L_{max}}{H_{wnet}} = 0.031 \left(\frac{u}{\sqrt{g H_{wnet}}} \right)^{0.104} \left(\frac{H_{snet}}{H_{wnet}} \right)^{0.733} \left(\frac{A}{H_{wnet}^2} \right)^{0.146} \quad (3.2)$$

where, A = cross sectional area of the outlet opening.

Conducting similar experiments, Meshkati et al. (2010) concluded that the flushing cone dimensions for a constant outlet discharge can be increased by regulating the discharge under lower reservoir level. They also showed that the flushing cone volume can be increased by increasing the outlet discharge for a constant reservoir water level. They finally proposed empirical relations for the estimation of the flushing cone volume and length:

$$\frac{V_s}{H_{wnet}^3} = 4.6 \left(\frac{u}{\sqrt{g(G_s-1)d_s}} \right)^{0.21} \left(\frac{H_{snet}}{H_{wnet}} \right)^{2.2} \left(\frac{D}{H_{wnet}} \right)^{0.89} \quad (4.1)$$

$$\frac{L_{max}}{H_{wnet}} = 0.02 \left(\frac{u}{\sqrt{g(G_s-1)d_s}} \right)^{0.1} \left(\frac{H_{snet}}{H_{wnet}} \right)^{0.75} \left(\frac{D}{H_{wnet}} \right)^{0.34} \quad (4.2)$$

where D is diameter of the circular bottom outlet. Only a single sand sample of a constant thickness was used in their experiments i.e. the experiments were carried out for constant values for G_s , d_s and H_{snet} .

Fathi-Moghadam et al. (2010) carried out experiments with three different sand sizes and showed that the size of the flushing cone increases with decreasing sediment size d_s . They proposed the following empirical relations to predict the flushing cone's volume and length:

$$\frac{V_s^{1/3}}{D} = 5.28 \left(\frac{u}{\sqrt{g(G_s-1)d_s}} \right)^{0.1} \left(\frac{H_{wnet}}{H_{snet}} \right)^{-0.046} \quad (5.1)$$

$$\frac{L_{max}}{D} = 8.19 \left(\frac{u}{\sqrt{g(G_s-1)d_s}} \right)^{0.1} \left(\frac{H_{wnet}}{H_{snet}} \right)^{-0.033} \quad (5.2)$$

Atmodjo & Suripin (2012) performed physical model tests of pressurized flushing of Wonogiri Reservoir in Indonesia and concluded that the effective flushing water level (*EFWL*), under which the flushing is most effective as defined by Scheuerlein (1993), depends on the thickness of sediment deposit H_s as derived in the equation $EFWL=10.58H_s^{-0.12}$. Emamgholizadeh et al. (2013) used data from Emamgholizadeh et al. (2006), Meshkati et al. (2010) and Fathi-Moghadam et al. (2010) to train and test an Artificial Neural Network (ANN) and an Adaptive Neuro-Fuzzy Inference System (ANFIS), and concluded that both artificial intelligence (AI) based models predicted the flushing cone volume and length more accurately than the empirical regression-based relations according to Eqn. 1 and Eqn.s 3-5. They performed sensitivity analyses and listed the most significant parameters regarding the flushing cone dimension and volume in descending order of their significance as: net sediment height above the centreline of outlet opening H_{snet} , characteristic sediment size d_s , diameter of outlet opening D , average velocity at the outlet u and net flow depth above the centerline of outlet opening H_{wnet} . It means that the geometry of flushing cones are more sensitive to sediment properties H_{snet} and d_s than the hydraulic parameters u and H_{wnet} .

Kamble et al. (2017) studied pressurized flushing cones in a physical model of Chamera II Hydroelectric Project – Stage II (CHEP-II), India. The experimental results consolidated the findings from previous studies. Additionally, they derived empirical equations for dimensionless length and depth of flushing cones by non-linear multiple regression analysis of experimental data.

$$\frac{L_{max}}{H_{wnet}} = e^{1.0675} \left(\frac{u}{\sqrt{g H_{wnet}}} \right)^{-0.4411} \left(\frac{H_{snet}}{H_{wnet}} \right)^{0.5089} \left(\frac{A}{H_{wnet}^2} \right)^{0.31162} \quad (6.1)$$

$$\frac{Z_{max}}{H_{wnet}} = e^{-0.0706} \left(\frac{u}{\sqrt{g H_{wnet}}} \right)^{0.5719} \left(\frac{H_{snet}}{H_{wnet}} \right)^{0.9859} \left(\frac{A}{H_{wnet}^2} \right)^{0.2309} \quad (6.2)$$

Hajikandi et al. (2018) performed pressurized flushing experiments for square and circular orifices having equivalent opening area to confirm that the flushing cone dimensions for square orifices are bigger than those for circular orifices under the same reservoir level condition. Their experimental results showed that width of a flushing cone is most sensitive to shape of outlet opening and least sensitive to sedimentation parameter $[G = \rho v^2 / (\rho_s - \rho) g d_s^3]$. Similarly, Dreyer & Basson (2018) performed experiments with outlets of four different shapes and concluded that square outlets produce bigger flushing cones than circular outlets but smaller flushing cones than flat rectangular outlets having equivalent opening area. They also presented non-dimensional equations to predict scour cone dimensions and volume:

$$\frac{L_{max}}{h_w} = 1.206 \ln \left(\frac{h_w}{h_w - h_s} \right) - 1.4594 \ln \left(\frac{u}{\sqrt{g h_w}} \right) + 0.0536 \ln \left(\frac{b_{oc} + b_{oe}}{h_w} \right) \quad (7.1)$$

$$\frac{W_{max}}{h_w} = 2.3065 \ln \left(\frac{h_w}{h_w - h_s} \right) - 3.4197 \ln \left(\frac{u}{\sqrt{g h_w}} \right) + 0.136 \ln \left(\frac{b_{oc} + b_{oe}}{h_w} \right) \quad (7.2)$$

$$\frac{Z_{max}}{h_w} = 0.7615 \ln \left(\frac{h_w}{h_w - h_s} \right) - 0.7519 \ln \left(\frac{u}{\sqrt{g h_w}} \right) + 0.0278 \ln \left(\frac{b_{oc} + b_{oe}}{h_w} \right) \quad (7.3)$$

$$\frac{V_s}{h_w^3} = \left(\frac{L_{max}}{h_w} \right)^{1.9529} \left(\frac{W_{max}}{h_w} \right)^{-0.3787} \left(\frac{Z_{max}}{h_w} \right)^{1.3663} \quad (7.4)$$

where h_w is flow depth above outlet's sill, h_s is sediment height above outlet's sill, b_{oc} is outlet width over the centreline and b_{oe} is outlet width at the edge.

Mohammad et al. (2018) carried out laboratory experiments on pressurized flushing in straight wall reservoirs to conclude that maximum volume of sediment was flushed for optimal value of H_{wnet}/H_{snet} which was found to be 2.26. They presented that volume of sediment flushed can be optimized by providing the outlet with an optimal length of internal offset. They provided four different dimensionless equations to predict the scour cone volume and proposed that uniformity coefficient of the sediment $C_u = d_{60}/d_{10}$ can be used instead of d_{50} (median diameter of sediment particles) to estimate the scour cone volume. The equations put forward by Mohammad et al. (2018) consisted of

outlet's length of internal offset L_v as an important parameter. But the proposed equations are not applicable to the condition $L_v = 0$ resulting $V_s = 0$, which is not true.

The summary of the sediment used by above mentioned studies as shown in Table 2.1 demonstrates that the sand size used in the pressurized flushing experiments ranged from 2 mm to finer than 0.25 mm. Only experiments by Atmodjo & Suripin (2012) and Kamble et al. (2017) were performed as model studies of respective prototypes scaled down with proper scale factors whereas others were performed as generalized experiments to study the relationship among different parameters associated with pressurized flushing phenomenon. However, both Atmodjo & Suripin (2012) and Kamble et al. (2017) did not describe about the downscaling of prototype sediment into model scale. Moreover, Atmodjo & Suripin (2012) used coal dust as model sediment but they did not even mention the size of model sediment particles. They concluded that more research is needed with the sediment material i.e., coal dust of various sizes. This study was focused on addressing such deficiency by implementing proper scaling for model sediment based on available theoretical scaling criteria as described in following sections.

Table 2.1: Summary of sediment used by experimental studies on pressurised flushing of non-cohesive sediment

Reference	Sediment material	Sediment size (d_{50})	Model scale
Emamgholizadeh et al. (2006)	Sand	2 mm – 0.595 mm 0.595 mm – 0.25 mm finer than 0.25 mm	N/A
Shahmirzadi et al. (2010)	Sand	1 mm (uniform)	N/A
Meshkati et al. (2010)	Sand	1 mm (uniform)	N/A
Fathi-Moghadam et al. (2010)	Sand	1.2 mm 0.42 mm 0.27 mm	N/A
Powell and Khan (2012)	Sand	0.89 mm 0.73 mm 0.29 mm	N/A
Atmodjo and Suripin (2012)	Coal dust ($G_s = 1.558$)	N/A	1:66.67
Kamble et al. (2017)	Sand	0.25 mm	1:55
Hajikandi et al. (2018)	Sand	0.87 mm 0.28 mm	N/A
Dreyer and Basson (2018)	Silica sand	0.095 mm	N/A
Mohammad et al. (2018)	Sand	1.44 mm 0.84 mm	N/A

2.2 Similarity criteria for mobile bed models

Physical hydraulic modelling is a well-established approach to study real world hydraulics by replicating the prototype and its hydraulic phenomena via a properly scaled physical hydraulic model. Physical hydraulic models in general are scaled down representations of their prototypes which makes them both economically and practically feasible. Theoretically an ideal physical model shall have similitude with its prototype in every aspect, which requires scaling down the whole prototype system including geometry, fluid properties, gravitational acceleration and atmospheric pressure. Though it is possible to scale down gravitational acceleration, g as implemented in geotechnical experiments using centrifuges (Taylor, 1994), it is not practical in case of physical hydraulic models. Similarly, scaling of fluid properties can be achieved by different methods e.g. using glycerine instead of water (Kobus, 1980), adding surfactant to water to reduce surface tension effects [Miller (2015); Ghetti & D'Alpaos (1977)] and modelling in wind tunnels using air as model fluid [Rouse et al. (1958), Westrich in Kobus (1980)]. However, using chemical additives to water or using completely different fluid in physical hydraulic models is highly expensive and difficult to handle. Considering overall economic and practical feasibility, water is the most suitable and the only option to be used as model fluid (Kamphuis, 1985). Since fluid properties, gravitational acceleration and atmospheric pressure are almost same in prototype and models, a complete similitude between model and prototype is practically not possible except for 1:1 scale. The imperfect similitude between model and prototype for model scale other than 1:1 will bestow some discrepancies in model predictions known as 'scale effects'. Scale effects are inevitable and become more significant with increasing model scale factor and their size depends on the investigated phenomenon (Heller, 2011). Nevertheless, scale effects can be confined to acceptable limits by maintaining similarity in dominant hydrodynamic forces while neglecting insignificant ones.

Mobile bed models represent two-phase flow with sediments and water. They are utilized to study sediment transport processes in fluvial and coastal environments. Evidently the basic requirement for a mobile bed model shall be its ability to achieve similarity in both hydrodynamics and sediment motion. One of the first successful mobile bed physical model was used by Osborne Reynolds in 1885 to study the patterns of tidal currents in the estuary of the River Mersey in England (Reynolds,

1901). At that time, there was not any systematic basis for scaling model sediment until Einstein & Chien (1956) proposed similarity criteria for distorted river models with movable bed. They carried out semi-theoretical derivation of each criterion using theoretical and empirical equations for hydraulics and sediment transport. They recommended satisfying similarity in both Shields parameter $\theta = \tau/[\rho g(G_s - 1)d_s]$ and sediment transport intensity $\Phi = q_s/\sqrt{[g(G_s - 1)d_s^3]}$ (τ is bed shear stress, G_s is specific gravity of the sediment particles, d_s is characteristic size of sediment particles, g is gravitational acceleration and q_s is volumetric bed load transport rate per unit width). Komura (1962) excluded similarity in Shields parameter and derived similarity conditions from the equations of motion and continuity for flowing water and sediment transport and equation of resistance law for sediment laden water flow. He used empirical relations from other Japanese researchers relating the ratio k_s/d_s (where, k_s is roughness height) to the entrainment function θ . Kishi et al. (1975) proposed similarity in $B \times S/h$ and θ/θ_c (where, B is the channel width, S is average bed slope, h is flow depth and θ_c is critical Shields parameter for incipient motion).

Yalin (1971) carried out dimensional analysis of seven characteristic parameters [ν , ρ_w , ρ_s , d_s , S , h and g] that can describe the two phase phenomenon of sediment transport in water (where, ν is kinematic viscosity of water, ρ_w is density of water, ρ_s is density of sediment particles). He arrived at four dimensionless parameters [R^* , F^* or θ , h/d_s and ρ_s/ρ_w] and proposed that similarity in all these four dimensionless parameters shall achieve dynamic similarity in sediment transport phenomenon. Here, R^* represents particle Reynolds number and F^* represents densimetric Froude number. Similarly, Zwamborn (1966) concluded that similarity in Froude number F , relative fall speed w_s/u^* of sediment particles and relative roughness (h/d_s) shall be satisfied to achieve a good similarity in river morphology between model and prototype (where, w_s is settling velocity of sediment particles and u^* is average shear velocity). He also concluded that similarity in particle Reynolds number R^* shall necessarily be compromised, which is applicable for rough turbulent flows, to arrive at comparable sediment behaviour in model and prototype.

Pugh & Dodge (1991) proposed that sediment discharge can be properly simulated in Froude scaled models by maintaining similarity in Taylor's dimensionless unit sediment discharge $q_{s*} = q_s/u_*d_s$. Assuming natural sand as the model sediment, this condition can be achieved when magnitude of R^* in model is above 100 or model

sediment particle size is greater than 1 mm. For models with $5 < R_* < 100$, either the model sediment size or the specific gravity of sediment particles shall be adjusted according to required settling velocity of model sediment particles as per Froude scaling. United States Army Corps of Engineers (USACE) proposed the use of micro scale physical models which ignore similarity in both Froude number and Shields parameter (Gaines & Smith, 2002). Though these model types could be useful for qualitative studies, their results have huge discrepancies when compared to prototype measurements. According to Julien (2018), similitude in mobile bed models can be achieved by simultaneously satisfying similarity in Froude number F , resistance e.g. Manning-Strickler's coefficient of roughness n , dimensionless grain diameter D^* and Shields parameter θ .

Besides the above mentioned scaling conditions, many different scaling criteria have been proposed by various researchers that selecting an appropriate set for a given model is sometimes very problematic (Hudson et al., 1979). Hence, the selection of scaling criteria for a mobile bed scale model shall be based on objectives of the study, assumptions made and constraints. All the proposed scaling criteria have their own constraints.

For the similarity criteria proposed by Einstein & Chien (1956), similarity in Shields parameter θ and sediment transport intensity Φ can be simultaneously achieved for only a very narrow range of sediment transport rates. The similarity in Shields parameter, also known as the zero-sediment load criterion, can only satisfy the similarity in flow conditions at the beginning of sediment motion i.e. similarity condition of critical tractive force but is unable to satisfy similarity in flow having large sediment transport rates (Komura, 1962). The similarity criteria suggested by Kishi et al. (1975) is suitable for investigating bar formation as dominant process in scale models.

The limitation in scaling criteria proposed by Yalin (1971) is that it demands lightweight material as model sediment for distorted model experiments (Wei et al., 2011). Similarity in relative fall speed w_s / u^* proposed by Zwamborn (1966) can be achieved only in undistorted models if settling velocity is scaled according to Froude scaling as suggested by Pugh and Dodge (1991). Taylor (1972) performed dimensional analysis and showed $q_{s*} = f\left(R_*, \theta, \frac{\rho_s}{\rho_w}, \sigma_g, SF\right)$, which means similarity in θ , R^* and

ρ_s/ρ_w will ultimately represent similarity in q_{s^*} for properly scaled model sediment (for the given value of σ_g and $S.F.$). Here, σ_g is geometric standard deviation of sediment sizes and $S.F.$ is sediment particle's shape factor. The criteria of similarity in θ and D^* as proposed by Julien (2018) also imply the similarity in R^* since $R_*^2 = \theta D_*^3$.

Based on the available literature, the similarity criteria required for designing mobile bed scale models can be summarized as:

A. Similarity in hydrodynamics:

- i. Froude number F : For modelling turbulent open channel flow systems in which gravitational force is dominant, Froude scale modelling (FSM) approach is generally adopted for similarity in hydrodynamics. While designing such models, similarity in Froude number in prototype and model is maintained in all cases. This similarity criteria can be written mathematically as:

$$F_r = \frac{u_r}{\sqrt{g_r h_r}} = \frac{u_r}{\sqrt{h_r}} = 1 \quad (8)$$

where, $X_r = X_p/X_m$

X_p = magnitude of parameter X in prototype

X_m = magnitude of parameter X in model

- ii. Reynolds number R : The tractive forces on sediment particles is due to drag force and turbulence, both of which depends on Reynolds number. Therefore, achieving similarity in Froude number only does not necessarily ensure similarity in the tractive forces and hence the sediment transport accurately (Pugh & Dodge, 1991).

$$R_r = \frac{u_r h_r}{\nu_r} = u_r h_r = 1 \quad (9)$$

Satisfying both criteria $F_r = 1$ and $R_r = 1$ simultaneously is practically not possible except for 1:1 scale. However, this criterion can be relaxed when both prototype and model have turbulent flows i.e. $R > 2000$ (Gill & Pugh, 2009) for which viscous forces are not significant.

B. Similarity in sediment transport

- i. Shield's parameter or Densimetric Froude number θ

$$\theta_r = \frac{\rho_r u_{*r}^2}{(\rho_s - \rho)_r g_r d_{sr}} = \frac{u_{*r}^2}{(G_s - 1)_r d_{sr}} = 1 \quad (10)$$

- ii. Particle Reynold's number R_*

$$R_{*r} = \frac{u_{*r} d_{sr}}{\nu_r} = u_{*r} d_{sr} = 1 \quad (11)$$

- iii. Relative particle density,

$$\frac{\rho_{sr}}{\rho_r} = 1 \quad (12)$$

- iv. Relative roughness

$$\frac{d_{sr}}{h_r} = 1 \quad (13)$$

- v. Relative fall speed

$$\frac{w_{sr}}{u_{*r}} = 1 \quad (14)$$

For complete similitude in sediment transport, all these five criteria (Eqns. 10-14) must be satisfied simultaneously, which is again practically not possible for model scale other than 1:1. Hence based on the objectives of the model study, incomplete similitude models shall be designed by satisfying similarity in significant parameters while relaxing the remaining. Since the relative fall speed accounts for sediment transport in suspension occurring simultaneously with bed-load transport, the criterion of similarity in relative fall speed (Eqn. 14) can be compromised for bed load dominant models. Likewise, the similarity in particle Reynolds number (Eqn. 11) can be compromised if its value is greater than a certain critical value, for which the fluid viscosity and the particle Reynolds number become insignificant regarding the detachment and motion of sediment particles. This critical value of R_* depends on the flow depth, grain size distribution and shape of sediment particles. Hence, a definite value of R_* may not be valid to generalize for all type of scenarios to be modelled. However, literature shows that the critical value should be somewhere in the range $70 < R_* < 150$ (Yalin, 1971) [also $R_* > 100$ (Bogardi, 1959), $R_* > 70$ (Vollmers, 1990) and $R_* > 60$ (Chauvin, 1962; Gehrig, 1980)].

Kamphuis (1985) proposed different types of models with incomplete similitude based on the similarity criteria that are satisfied (see Table 2.2). He designated models which satisfy the most number of criteria (three out of five) as '*Best Models*'. Best models are basically undistorted models with model sediments having same density as that of prototype sediments. Since the Best models require the size of the sediment particles to be scaled down as per the model length scale factor, it poses a limitation to the applicability of such models when the sediment particles are very fine in prototype and scaling it down to model scale may demand model sediment sizes in the cohesive range. Using cohesive sediments in model to represent non-cohesive sediments in prototype will inevitably produce erroneous results due to the difference in sediment properties. To overcome this limitation in scaling down fine prototype sediments, the similarity criteria for relative sediment density, relative roughness and relative fall velocity can be relaxed while satisfying similarity criteria for Shields parameter and particle Reynolds number. Kamphuis (1985) named such models as '*Lightweight models*' and suggested that the specific gravity of model sediments shall be within a range of 1.05 to 2.65. The use of lightweight sediments can introduce additional scale effects through the incorrect scaling of the relative density (Gorrick & Rodríguez, 2014; Kamphuis, 1985; Keen, 2011; Sutherland & Soulsby, 2011). However, it can be taken as better option against using fine cohesive model sediment or incorrectly scaled coarser model sediment.

For the model studies that require large volume of lightweight sediments, it will be economically feasible to use easily available or locally producible materials. However, such materials are available in very limited range in size and density and seldom satisfies the size-density relation (derived from Eqns 10 and 11) mandatory for the lightweight models i.e.

$$d_{sr}^3 = (G_s - 1)_r^{-1} \quad (15)$$

While designing lightweight models, the designer can independently choose only one scale ratio for parameters among horizontal length L_r , sediment size d_{sr} and specific gravity of sediment particles G_{sr} . It will be practically convenient to select locally available lightweight materials to conduct model studies if the size and density of such materials can be chosen independently. This freedom can be achieved by further relaxing the similarity in particle Reynolds number and maintaining similarity in Shields parameter only. Kamphuis (1985) designated such models as '*Densimetric*

Froude models' based on the only scaling criteria that is satisfied. The generalized scaling relation for a densimetric Froude model can be derived from Eqns 8 and 10 as;

$$L_r = \delta^2 (G_s - 1)_r d_{sr} \quad (16)$$

where, $\delta = L_r/h_r$ is distortion ratio

It should be noted that the extra flexibility in choosing model parameters for densimetric Froude models comes with additional exposure to scale effects. Such models have to deal with combined scale effects inherent to Best models and Lightweight models.

Table 2.2. Classification of movable bed models by Kamphuis (1985)

Model	Similarity Criteria				
	$\theta_r=1$	$R_{*r}=1$	$(\rho_s/\rho_w)_r$	$(d/h)_r = 1$	$(w_s/u_{*r}) = 1$
Best Model	✓	✗	✓	✓	✗
Lightweight model	✓	✓	$\rho_{sm}/\rho_{wm} = 1.05$ to 2.65	✗	✗
Densimetric Froude model	✓	✗	$\rho_{sm}/\rho_{wm} = 1.05$ to 2.65	✗	✗
Sand model	✗	✗	✓	✗	✗

Note: ✓ satisfied ✗ not satisfied

2.3 Lightweight materials as model sediment

In the past, there were no systematic basis for scaling model sediment to be used in mobile bed models, so natural sand itself was used as model sediment. When fine sediment in prototype had to be modelled, the model sediment was likely to be coarser than required due to the limitation on using model sediment size within non-cohesive range. In such cases, the slopes in the models were exaggerated by the modeller to facilitate sediment motion. The modelling process most often involved tedious trial and error to select suitable model sediment size and model boundary conditions which successfully reproduce prototype conditions.

During 1935-36, Lieutenant Francis H. Falkner who was the Director of Waterways Experiment Station (WES) located in Vicksburg, Mississippi supervised a comprehensive investigation of model methods and theories including a search for

better bed materials for movable bed models. Based on physical and chemical properties, cost and availability, four out of 60 materials under consideration were proposed as potential candidates for practical use in models. The shortlisted materials were; gilsonite, limed resin, Kansas coal and haydite. All those four materials were lightweight, having density lower than natural sand, and produced better model predictions (Fatherree, 2004).

Shields (1936) performed flume studies on bed load movement using various bed materials with specific gravities ranging from 1.06 to 4.3. He concluded that lightweight materials are very advantageous to be used in river model experiments as bed-load materials since they have lower critical tractive forces which can easily be attained in laboratory models. He also added that the possibility to use bigger grains of lightweight materials make it suitable for distorted models as well. Bagnold (1955) used lightweight grains, having specific gravity 1.004, made of 50% mixture of micro-crystalline paraffin wax and lead stearate. He concluded that use of lightweight materials makes it possible to achieve dynamically similar shear stresses in small and inexpensive laboratory apparatus, which otherwise could not be achieved with natural sand due to practical limitations. Before Bagnold (1955), the lightest materials used in hydraulic experiments were amber and polystyrene (specific gravity of 1.06). Le Mehaute (1970) concluded that even though using similar sediment material in model as in prototype will ensure similarity in densimetric Froude number F^* and particle Reynolds number R^* , the scale effects will be too large. In such cases, use of distorted models with lightweight materials as model sediment will ensure better predictions.

Kamphuis (1985) suggested that the specific gravity of lightweight materials shall be between 1.05 and 2.65. There is a wide range of materials having specific gravity between 1.05 and 2.65, but only a few have potential to be used in mobile bed model studies. Bettess (1990) conducted a survey on the use of lightweight sediments in mobile bed models by different laboratories around the world. Based on responses from 16 institutions in 11 different countries, he documented the list of lightweight materials used by those institutions along with properties, advantages and disadvantages of each material. A list of lightweight materials commonly used in mobile bed experiments were also published in Julien (2018). A comprehensive review of morphodynamic investigations using lightweight sediments in riverine and estuarine models as well as in coastal models was presented by Henry et al. (2018).

3

Research Methodology

3.1 Experimental setup

The experiments were carried out at the hydraulic laboratory of Norwegian Institute of Science and Technology (NTNU) in Trondheim, Norway and the hydraulic laboratory of Hydro Lab in Lalitpur, Nepal. In the hydraulic laboratory at NTNU, an existing hydraulic flume was used. The flume was 12 m long, 0.6 m wide and 0.75 m high and had a horizontal bed. The flume had an inlet tank at upstream and an outlet tank at downstream. The outlet tank was connected to the inlet tank through a pipe via an electric pump with a variable frequency drive (VFD) so that controlled discharge could be circulated within the system. Before running the system, the outlet tank had to be primarily filled with water supply from laboratory's reservoir. The pipe supplying discharge into the inlet tank was equipped with an electro-magnetic flow meter to measure the inflow discharge. To simulate pressure flushing, the flume was blocked at 6 m downstream from the inlet tank and a 50 mm x 50 mm orifice was provided at the centerline representing a sluice gate i.e. bottom outlet. The sill level of the orifice was kept 60 mm above the flume bed (i.e. $a_0 = 60$ mm) to allow free formation of the flushing cone and to avoid influence of the downstream flow. The opening height of the outlet a could be varied from 0 to 50 mm by a vertical slide gate. A netted basket was provided at the downstream end of the flume to collect flushed sediments.

For the experiments at the hydraulic laboratory of Hydro Lab, similar setup was constructed so that the results could be directly compared. Since the study was focused on flushing scour upstream of the bottom outlet, only 6 m long flume was constructed up to the bottom outlet and an outlet tank was provided at immediate downstream. The inlet tank at upstream of the flume was connected to the laboratory's water storage reservoir via a pump and supply pipe. A box with calibrated V-notch was installed at the end of the supply pipe to measure the discharge fed into the inlet tank. The outlet

tank was also connected to the laboratory's reservoir to release back the outlet discharge. A schematic diagram of the experimental setup is shown in Figure 2.

Unlike the experimental setups used by Emamgholizadeh et al. (2006), Shahmirzadi et al. (2010), Meshkati et al. (2010) and Fathi-Moghadam et al. (2010) in which the discharge through the bottom outlet could be regulated to vary for a given area of outlet opening under constant water level, the experimental setup in this study was purely gravitational i.e. water level, outlet discharge and outlet opening area were interdependent. In this experimental setup, the outlet discharge increases with increasing water level and vice versa for a given outlet opening area. Similarly, the outlet discharge is proportional to outlet opening area under a constant water level.

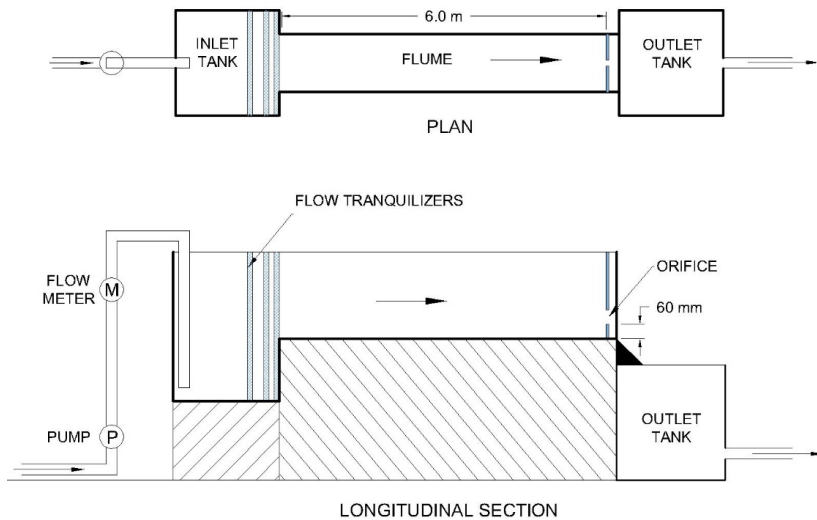


Figure 2: Schematic diagram of the experimental setup (not to scale)

3.2 Design of mobile bed models

3.2.1 Model scales

Three pairs of mobile bed models were designed for the pressurized flushing experiments, each pair consisting of a sand model and a lightweight sediment model. Due to limitations in resources and laboratory facilities, sand models could not be built in bigger scale to represent as prototype of lightweight sediment models. Hence, the models were designed in such a way that both sand model and lightweight sediment model in each pair can be scaled up to represent a common fictitious prototype. Based

on literature review, scaling criteria for ‘Best models’ (see section 2.2) were elected to be suitable for sand models while scaling criteria for ‘densimetric Froude models’ (see section 2.2) were selected for lightweight sediment models. Accordingly, the sand models were designed as ‘Best models’ and the lightweight sediment models were designed as undistorted ‘Densimetric Froude models’, such that both the sand model and the lightweight sediment model in each pair were scaled down by the same length ratio L_r . It is assumed that a ‘Best model’ can be treated as scaled down version of its prototype since a ‘Best model’ is known to produce satisfactory results with minimized scale effects. This assumption accorded the use of same experimental setup for both sand models and lightweight sediment models and also allowed direct comparison of experimental results from models within each pair. The scale factors for the models were estimated as shown in Table 3.1.

Table 3.1. Scale ratio for mobile bed models used in the study

Model Parameter	Symbology	Best model	densimetric Froude model	
			distorted	undistorted
Length	L_r	L_r	L_r	L_r
Depth	h_r	L_r	h_r	L_r
Distortion ratio	δ	1	$L_r h_r^{-1}$	1
Velocity	v_r	$\sqrt{L_r}$	$\sqrt{h_r}$	$\sqrt{L_r}$
Discharge	Q_r	$L_r^{2.5}$	$L_r h_r^{1.5}$	$L_r^{2.5}$
Time (flow)	t_{fr}	$\sqrt{L_r}$	$L_r h_r^{-1/2}$	$\sqrt{L_r}$
Submerged specific gravity of sediment	$(G_s - 1)_r$	1	$(G_s - 1)_r$	$(G_s - 1)_r$
Sediment size	d_{sr}	L_r	$h_r^2 L_r^{-1} (G - 1)_r^{-1}$	$L_r (G - 1)_r^{-1}$
Dimensionless unit sediment discharge	q_{sr}	$L_r^{1.5}$	$h_r^3 L_r^{-1.5} (G - 1)_r^{-1}$	$L_r^{1.5} (G - 1)_r^{-1}$

3.2.2 Model sediments

Three lightweight materials, designated in this study as LW-1, LW-2 and LW-3, were selected as lightweight sediment. Acrylic and polystyrene materials were selected because they are easily available in local market and they do not

decompose/breakdown or changes in the material occur over time like organic materials e.g., crushed coal, crushed walnut shells etc. Moreover, these materials can be re-used in experiments repeatedly.

Three model sediments composed of natural sand, designated in this study as Sand-1, Sand-2 and Sand-3, were selected to pair with the three lightweight materials LW-1, LW-2 and LW-3 respectively. The characteristic particle sizes d_s and specific gravity G_s of the selected model sediments were chosen as per the scaling criteria discussed in Section 3.2.1. Sand-1 and Sand-2 were composed of poorly graded sand keeping the particle size distribution as close as possible to be uniform near the calculated d_s . The experiments with model sediment Sand-3 were not conducted since the characteristic particle size of Sand-3, as per the adopted scaling criteria, was required to be 0.07 mm which is close to the sand-silt boundary and possibly be subjected to cohesion. The properties of model sediments used in this study are listed in Table 3.2. Two sets of experiments with model sediment LW-1 and LW-3 were conducted at hydraulic laboratory of NTNU in Norway whereas the remaining three sets of experiments with model sediments Sand-1, LW-2 and Sand-2 were carried out at hydraulic laboratory of Hydro Lab in Nepal.

Table 3.2. Sediment used for the experiments and their properties

Exp set no.	Sediment material ID	Name of Material	Calculated size (d_s) mm	Adopted size (d_s) mm	Sp. Gr. (G_s)	Geometric mean size (d_g)	Geometric standard deviation (σ_g)	Uniformity coefficient, $C_u = d_{60}/d_{10}$
1	LW-1	Poly-methyl methacrylate (PMMA)	2.40	2.40	1.180	2.40	1.00	1.00
2	Sand-1	Natural sand	0.26	0.30	2.650	0.30	1.67	2.50
3	LW-2	Masterbatch	4.00	4.00	1.400	4.00	1.00	1.00
4	Sand-2	Natural sand	0.97	1.05	2.650	0.93	1.25	1.76
5	LW-3	Polystyrene	2.00	2.00	1.058	2.00	1.00	1.00

3.3 Experimental procedure

Five sets of experiments were carried out with five model sediments (see Table 3.2). Each set consisted of 32 tests; 16 tests for $H_s = 120$ mm and 140 mm each. Additional 16 tests were carried out for $H_s = 100$ mm with each of LW-1 and Sand-1 to provide extra data for validation purposes. Hence, in total 192 tests were performed in this study.

The tests were carried out under steady flow conditions for a range of parameters shown in Table 3.3. The detailed experimental procedure is presented in [Paper IV].

Table 3.3. Range of parameters

Parameters	Range
Discharge (Q)	0.9 – 5.0 Lps
Net flow depth (H_{wnet})	107 – 408 mm
Thickness of sediment deposit above flume bed (H_s)	120 and 140 mm
Opening height of outlet orifice (a)	20, 30, 40 and 50 mm
Specific gravity of sediment particles (G_s)	1.058, 1.18, 1.4 and 2.65

3.4 Application of Structure from Motion (SfM) technique

During experiments in the hydraulic laboratory at NTNU, the surface profiles of flushing cones were measured using SeaTek 5 MHz ranging system consisting of 32 acoustic transducers [Paper III]. The instrumentation helped in quick scanning of the bed profile upstream of the bottom outlet. Whereas a manual point gauge was used for the bed measurements when conducting experiments in the hydraulic laboratory of Hydro Lab. Though being low-cost, simple to operate and satisfactorily precise, manual gauge measurements are time consuming and also require additional manpower for assistance. The manual gauge measurements most often involve taking measurements at a number of cross-sections at certain intervals and the data are interpolated in between. While doing so, sometimes significant details in between the measured cross-sections are probably lost. Hence, Hydro Lab was keen on adopting an economical, portable, quick and flexible method to record bed surface profiles in laboratory models. Regarding this, a methodology was developed for application of Structure from Motion (SfM) technique as a complete method to record model's bed topography and to produce high resolution 3D models with high quality of color information. SfM is a widely used photogrammetric technique to produce high resolution 3D models of a target object from a series of overlapping 2D images (Westoby et al., 2012). The SfM technique has already been applied in various fields like archaeology, geosciences, robotics, terrestrial surveying, real state, film and entertainment, sports etc. including hydraulic engineering. A few researchers have also used it to study fluvial geomorphology in laboratory flume experiments (Morgan et al., 2017).

A hydraulic laboratory has to deal with physical models of various size and geometry ranging from simple flume models to complicated coastal or river models. Therefore, the instrumentation shall be portable and flexible in addition to being quick and economical. All these conditions can be satisfied by the SfM technique. A complete methodology was developed for Hydro Lab to implement the SfM technique in recording three-dimensional information from laboratory models. The general workflow of the methodology is shown in Figure 3. To make the method more flexible and quicker, free handheld photography was adopted for capturing images rather than installing cameras in moving trollies. Use of handheld photography also reduced the overall cost for instrumentation. Another advantage of this technique is that a low-cost consumer grade camera and even the inbuilt camera in smartphones, can be used for image acquisition.

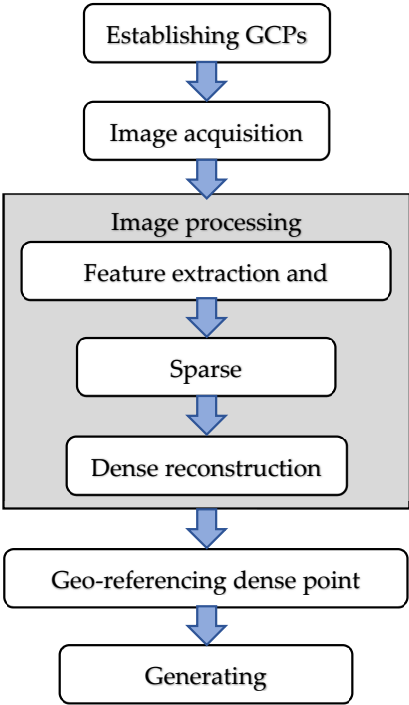


Figure 3. General workflow for SfM technique

The study was initiated with trials for capturing effective images by free handheld photography in contrasting lighting conditions of the laboratory. Another method for image acquisition was also tried by capturing the target object in a video shot by moving the camera steadily around the object and then extracting frames from the




video by using software like VirtualDub. But the quality of the images extracted from the video was found to be drastically lower than the photographs taken. Hence, free handheld photography was finally adopted for image acquisition. Then six potential SfM tools consisting of four freely available software (ColMap, Meshroom, Regard3D and VisualSfM) and two commercial software (ReCap and Photoscan) were reviewed (see Table 3.4).

Table 3.4. Comparison of SfM software selected for the study

Tools	Feature Extraction and Matching	Sparse Reconstruct	Dense Reconstruct	Mesh Generation	Post Processing	Developer	License
Colmap	✓	✓	MVS	Delaunay or Poisson surface reconstruction	Meshlab	Johannes L. Schönberger, Switzerland	Free
Meshroom	✓	✓	✓	✓	✓	AliceVision	Free and Open source
Photoscan	✓	✓	✓	✓	✓	Agisoft LLC, Russia	Commercial
ReCap	✓	✓	✓	✓	✓	Autodesk Inc, USA	Commercial and Academic
Regard3d	✓	✓	✓	✓	✓	Roman Hiestand, Switzerland	Free and Open source
VisualSfM	✓	✓	PMVS/CMVS	Meshlab	Meshlab	Changchang Wu	Free but not for commercial use

Notes:

MVS Multi View Stereo
 PMVS Patch-based Multi-View Stereo
 CMVS Clustering views for Multi-View Stereo

 enabled in same software
 run from same software environment
 different software with exported result

All the selected software were tested by processing a set of images from a 3 m long physical hydraulic model of a river stretch. Different aspects of the software were compared including quality of outputs and time taken for processing. The detailed description of the comparison is presented in [Paper I]. Based on the results, Photoscan was selected for application of SfM technique in the laboratory and it was further tested for three different case studies of varying scales and scopes, including the generation of 3D surface models of flushing scour cones for the laboratory experiments

conducted under this research. The details about the study and the results are presented in [Paper II].

4

Results and Discussions

In this chapter, the results of this PhD research are summarized and discussed. This chapter is divided into sections based on the main outcomes. The respective papers, from which the results are summarized, are mentioned as parenthesis in each section's heading. This chapter also contains some additional results and discussion which are not included in any of the mentioned papers.

4.1 Application of SfM in hydraulic model studies

[Paper I and II]

The selected six SfM software (Table 3.4) were compared by processing a set of images from a 3 m long physical hydraulic model of a river stretch. Comparison of the selected software were made regarding user friendliness, processing time, quality of outputs, and precision in reproducing model geometry especially in vertical direction. It was observed that the commercial software Photoscan and ReCap have comparatively better graphical user interface (GUI) and are more user friendly. Likewise, free software Meshroom also has those qualities matchable to commercial software. Colmap and Visual SfM slightly lack behind as they need little extra effort for installation and require additional third-party tools for dense reconstruction and post processing. Regarding the quality of 3D model output, all the selected software produced competitive results (see Table 4.1). [Paper I]

Free and open-source software are more flexible and offer more control to users compared to black-box type commercial software. However free software are under continuous development and are prone to bugs, vulnerable to crashes and most of them are restricted by their developers to be used in commercial projects. Even though some free software allow their usage in commercial projects, it lacks credibility to the Clients. Commercial software ReCap has top notch features and processing

capabilities under the reliable branding of Autodesk. Additionally, ReCap being a cloud-based service does not require high end computing facilities. But it requires a stable and high-speed internet connection which is still a privilege in countries like Nepal. After considering all aspects, Photoscan was chosen for further application of SfM technique in physical hydraulic model studies.

Table 4.1. Statistical performance indices for selected software in predicting elevations

Software	Mean Absolute Error (MAE), mm	Root Mean Square Error (RMSE), mm	Coefficient of determination (R^2)
PhotoScan	3.9	4.9	0.9965
Colmap	4.0	5.4	0.9958
Recap	4.1	5.5	0.9962
Visual SfM	4.4	5.7	0.9956
Meshroom	4.4	5.8	0.9956
Regard3d	5.8	7.3	0.9946

The SfM technique was then applied on three different case studies regarding river bed morphology (case study I), free flushing of sediment deposit near hydropower intakes (case study II) and small-scale flume study on pressurized flushing of sediment deposit (case study III) [Paper II]. Analyses of results from the three case studies show that the accuracy of the SfM technique was estimated to be below 5 mm for reproducing point coordinates and below 3 mm for estimating linear distances in the model scale (see Figure 4). The accuracy in estimating volume changes was found to be below 5% of measured volumes. The fine accuracy in estimating volume changes could be due to compensation of errors while subtracting two 3D models to calculate change in volume. During the study, it was observed that the final accuracy of outputs from SfM technique highly depended on the quality of images and the accuracy of established GCPs. Number of images more than an optimum number does not necessarily improve the quality of output. But the optimum number of images required increases with increase in size of the model. The increase in number of images to be processed ultimately results in longer processing time. Despite of the longer processing time, SfM technique used lesser total manhour than manual measurements as most of the image processing steps were automatized. The results from case study

It showed that plain (non-textured) surfaces of headworks structures in the model were not well reproduced so they were excluded while performing volume calculations.

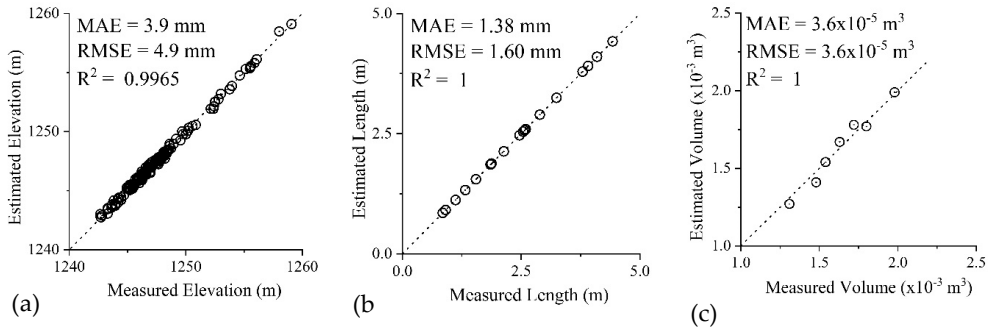


Figure 4. Overall statistical performance indices for prediction of (a) elevations, (b) lengths and (c) volumes by SfM technique using Photoscan

The successful application of SfM technique in river model studies of varying scales and scopes justified the potential application of SfM technique in different kinds of physical hydraulic model studies. Hence by following proper methodology, the SfM technique can be used as a quick, cost effective and accurate method to record three-dimensional information from physical hydraulic models.

4.2 Pressurized flushing experiments

4.2.1 Geometry of flushing cones

[Paper IV]

The geometry of flushing cones achieved after each test consolidated the results from previous studies by Hajikandi et al. (2018), Meshkati et al. (2010), Powell & Khan (2012) and Shahmirzadi et al. (2010). The plan area of flushing cones were close to semi-circular with their center at the middle of outlet's width i.e. $W_{max} \approx 2 L_{max}$. The experimental results show that for $W_{max} = k L_{max}$, the value of k ranged from 1.80 to 2.88 with an average value of 2.08. The flushing cones had the maximum length along the centerline of the outlet, and had the maximum width and maximum depth near the dam wall. The maximum depths were observed to be close to edges of the outlet opening forming a small ridge along the centerline of the outlet.

Figure 5 shows cross-section profiles of flushing cones at 0.02 m upstream of the outlet. The profiles were plotted with non-dimensional width Y and non-dimensional depth

D defined as $Y = y/(W_{max}/2)$ and $D = d/d_{cl}$ (y is distance in transverse direction, d is depth of cone at y , d_{cl} is scour depth along centerline). Similarly, Figure 6 shows centerline profile of flushing cones in which the length along the centerline and the depth were non-dimensionalised by length of flushing cone L_{max} and maximum depth along the centerline d_m respectively as $X = x/L_{max}$ and $D_c = d_{cl}/d_m$ (x is distance upstream of orifice, d_{cl} is scour depth along the centerline at x distance from the orifice). The comparisons show that the transverse and centerline profiles of the flushing cones formed with different model sediments under different boundary conditions had almost similar trend when described in dimensionless framework. The data fitted pretty well with the approximate relations for transverse and centerline profiles proposed by Powell (2007).

For a constant outlet opening area, the size (volume and dimensions) of flushing cones increased with increasing water level i.e. net head H_{wnet} due to increase in outlet discharge Q . Likewise the size of flushing cones were observed to be increased with increase in outlet's opening area A under constant net head H_{wnet} . The experiments with Sand-1 and Sand-2 also showed that size of flushing cones increased with decrease in sediment size. Finer non-cohesive sand produces bigger flushing cone because finer sand has lower angle of repose and is subjected to higher buoyant forces. Among the dimensions of the flushing cone, W_{max} was observed to be more sensitive to changes in hydraulic and sediment parameters.

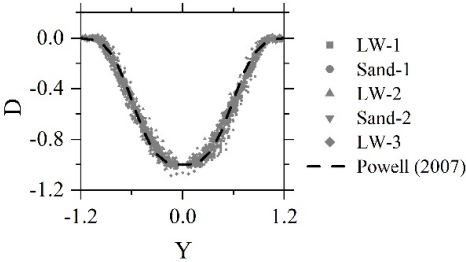


Figure 5. Non-dimensional cross-section profiles of flushing cones at 0.02 m upstream of the outlet

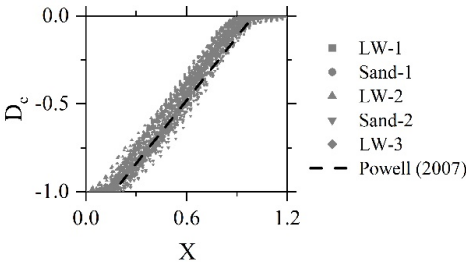


Figure 6. Non-dimensional centreline profiles of flushing cones

4.2.2 Performance of lightweight materials as model sediment

[Paper III and IV]

Initially, a dimensionless functional relationship for flushing cone volume (see Eq 17) was derived by dimensional analysis of parameters influencing the volume of a flushing cone. The parameters were selected as suggested by Fathi-Moghadam et al. (2010) and Meshkati et al. (2010).

$$\frac{V_s^{1/3}}{H_{wnet}} = f\left(\frac{u}{\sqrt{g(G_s-1)d_s}}, \frac{h_s}{H_{wnet}}, \frac{A}{H_{wnet}^2}\right) \quad (17)$$

where, $u = Q/A$ and $h_s = H_s - a_0$. The evaluation of dimensionless parameters in Eq 17 from experimental results shows that all the model sediments including the lightweight sediments satisfy the derived functional relationship. Moreover, plots of $\frac{V_s^{1/3}}{H_{wnet}}$ against each of the three dimensionless parameters at right hand side of Eq. 17 show that the data points for lightweight material and sand in each pair are almost overlapping and exhibit similar trend under identical test conditions [Paper IV]. That means lightweight materials LW-1 and LW-2 produced results comparable to their respective sediment pair Sand-1 and Sand-2. Figure 5 and Figure 6 respectively show that transverse and centerline profiles of flushing cones produced by lightweight materials were similar to that obtained with sand. This can be taken as the basic evidence of the similarity between lightweight sediments and their respective paired sand while simulating the flushing scour cone. Comparison of the dimensionless length $\left(\frac{L_{max}}{H_{wnet}}\right)$ and volume $\left(\frac{V_s^{1/3}}{H_{wnet}}\right)$ of flushing cones for lightweight sediment and sand in each pair showed good agreement in the prediction of those parameters (see Figure 7 and Figure 8). Hence, it can be confirmed that properly scaled lightweight sediment in physical hydraulic models can replicate the pressurized flushing of non-cohesive sediment in prototype.

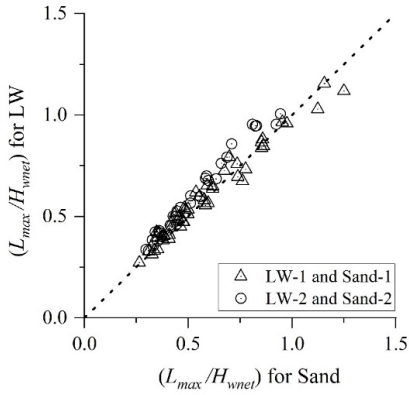


Figure 7. Comparison of $\frac{L_{max}}{H_{wnet}}$ for Sand and Lightweight sediment pair

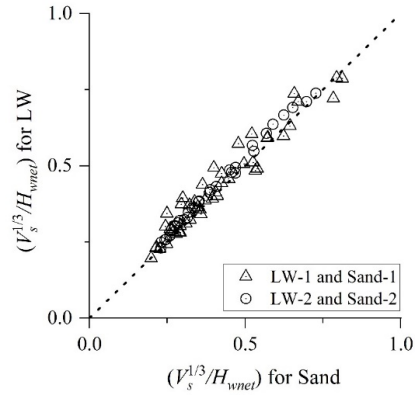


Figure 8. Comparison of $\frac{V_s^{1/3}}{H_{wnet}}$ for Sand and Lightweight sediment pair

4.2.3 Comparison of empirical equations

[Paper III and IV]

The empirical equations proposed by different researchers to predict dimensions and volume of flushing cones (Eqns. 1 – 7) were reviewed and the equations to predict volume of flushing cones were applied on the experimental data from this study for comparison. Figure 9 shows the comparison of measured dimensionless volume $V_s^{1/3}/H_{wnet}$ against that predicted by Eqns 1-7 except Eqn 6 since Kamble et al. (2017) did not propose any relation to predict flushing cone volume. It can be observed that the equations proposed by Emamgholizadeh et al. (2006), Shahmirzadi et al. (2010), Meshkati et al. (2010) and Dreyer & Basson (2018) underestimated the dimensionless volume of flushing cone. All these equations except the one by Dreyer & Basson (2018) were derived for circular outlets whereas the experiments in this study were carried out for square and flat rectangular outlets. Since circular outlets produce smaller flushing cones compared to square or flat rectangular outlets having equivalent opening area (Dreyer & Basson, 2018; Hajikandi et al., 2018), the equations derived for circular outlets are most likely to underestimate the flushing cone volume for square and flat rectangular outlets.

However, the empirical equations proposed by Powell (2007) over-estimated the dimensionless flushing volume. The reason behind this could be that the equations were derived for constant thickness of sediment deposit with its surface at the level of

outlet's sill i.e., $h_s = 0$. It may overestimate the volume while extrapolating for $h_s > 0$. Fathi-Moghadam et al. (2010) also over-estimated the dimensionless flushing volume which consolidated the conclusion made by Emamgholizadeh et al. (2013).

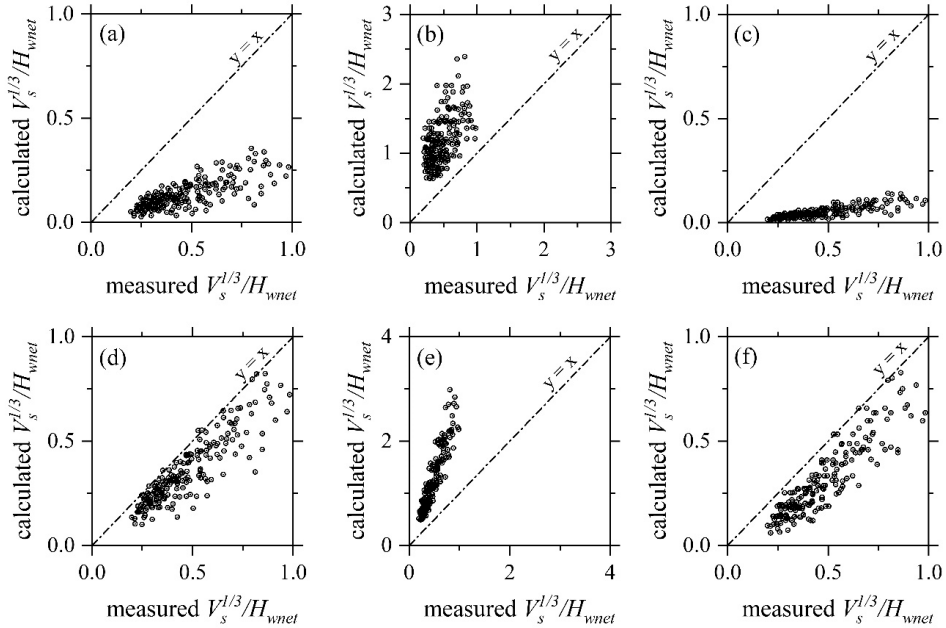


Figure 9. Comparison of measured dimensionless volume $V_s^{1/3}/H_{wnet}$ against that predicted using empirical equations proposed by (a) Emamgholizadeh et al. (2006), (b) Powell (2007), (c) Shahmirzadi et al. (2010), (d) Meshkati et al. (2010), (e) Fathi-Moghadam et al. (2010), (f) Dreyer & Basson (2018)

Sensitivity analysis by Emamgholizadeh et al. (2013) concluded that H_{snet} is the most significant parameter that influences flushing cone geometry. But each of the Eqns. 1-5 was derived by using experimental data for a constant H_{snet} , which could be one of the reasons for discrepancies in prediction made by these equations. Here, predictions made by Meshkati et al. (2010) and Dreyer & Basson (2018) seem to have lower discrepancies possibly because H_{snet} used in experiments by them are closer to H_{snet} in this study. In addition, Dreyer & Basson (2018) had also considered the effect of outlet's shape which could be another reason for its better prediction.

The available empirical equations were further tested for predicting dimensionless length of flushing cones L_{max}/H_{wnet} . Eqns 2-7 were used to predict L_{max}/H_{wnet} for experimental data from this study (see Figure 10). Powell (2007) and Fathi-Moghadam

et al. (2010) also over-estimated the dimensionless length in similar manner as the dimensionless volume of flushing cones.

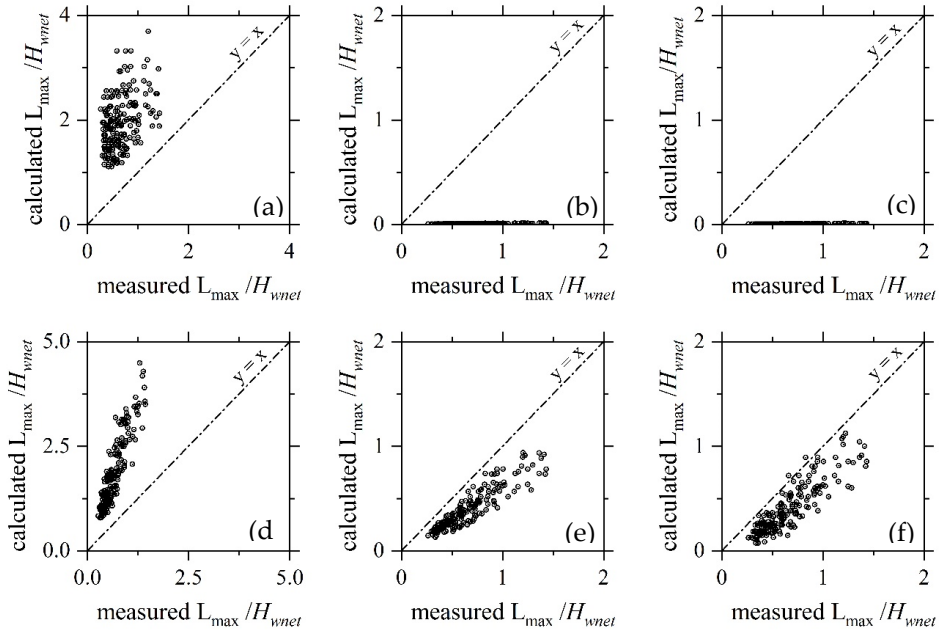


Figure 10. Comparison of measured dimensionless length L_{max}/H_{wnet} against that predicted using empirical equations proposed by (a) Powell (2007), (b) Shahmirzadi et al. (2010), (c) Meshkati et al. (2010), (d) Fathi-Moghadam et al. (2010), (e) Kamble et al. (2017) and (f) Dreyer and Basson (2018)

whereas, Eqn 6.1 (Kamble et al., 2017) and Eqn 7.1 (Dreyer & Basson, 2018) made better predictions close to the measured values since both equations were derived for varying H_{snet} and both equations also consider rectangular outlets. Eqn 3.2 (Shahmirzadi et al., 2010) and Eqn 4.2 (Meshkati et al., 2010) showed very poor prediction with very large discrepancies. However, another equation (Eqn 18) proposed by Meshkati et al. (2010) to predict dimensionless length of flushing cones was found as cited in Emamgholizadeh et al. (2013).

$$\frac{L_{max}}{H_{wnet}} = 1.98 \left(\frac{u}{\sqrt{g H_{wnet}}} \right)^{0.143} \left(\frac{H_{snet}}{H_{wnet}} \right)^{0.895} \quad (18)$$

When Eqn. 18 was used to predict the dimensionless length for the experimental data from this study, it made significantly better predictions than Eqns. 3.2 and 4.2 [Figure 11(a)]. Since Meshkati et al. (2010) considered $\frac{u}{\sqrt{g(G_s-1)d_s}}$ instead of $\frac{u}{\sqrt{g H_{wnet}}}$, we

hypothetically modified Eqn 18 to Eqn 19 and applied on the experimental data. Eqn 19 produced the best predictions over all the selected empirical relations [Figure 11(b)]. However, no literatures are available to justify the derivation of Eqn. 19.

$$\frac{L_{max}}{H_{wnet}} = 1.98 \left(\frac{u}{\sqrt{g(G_s-1)d_s}} \right)^{0.143} \left(\frac{H_{snet}}{H_{wnet}} \right)^{0.895} \quad (19)$$

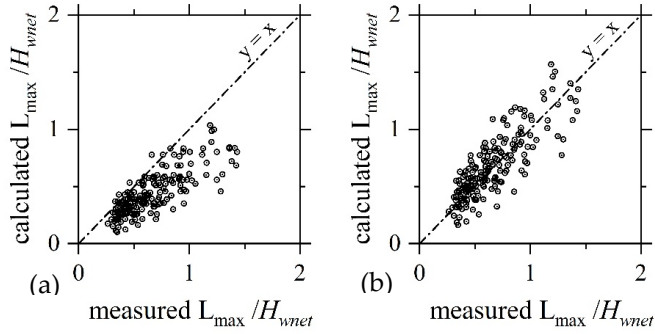


Figure 11. Comparison of measured L_{max}/H_{wnet} against that predicted by (a) Eqn 18 and (b) Eqn 19

Considering the discrepancies in predictions by selected empirical equations to predict volume and length of flushing cones, new empirical relations are proposed based on the experimental data.

4.2.4 Regression analysis and validation

[Paper IV]

Based on the functional relationship derived by dimensional analysis (Eqn. 17), multivariate non-linear regression analyses of the experimental data were carried out to derive empirical relations to predict dimensionless volume $V_s^{1/3}/H_{wnet}$ and dimensionless length L_{max}/H_{wnet} of flushing cones (Eqns. 20 and 21 respectively). 120 experimental data points were randomly selected out of total 160 data (16 tests for each of 5 model sediments with $H_s = 120$ mm and 140 mm) to calibrate the regression equations. The remaining 40 data points were combined with the additional 32 data points (16 tests for each of LW-1 and Sand-1 model for $H_s = 100$ mm) and used for validation of the regression equations.

$$\frac{V_s^{1/3}}{H_{wnet}} = 1.173 \left(\frac{u}{\sqrt{g(G_s-1)d_s}} \right)^{0.203} \left(\frac{h_s}{H_{wnet}} \right)^{0.522} \left(\frac{A}{H_{wnet}^2} \right)^{0.221} \quad (20)$$

$$\frac{L_{max}}{H_{wnet}} = 1.311 \left(\frac{u}{\sqrt{g(G_s-1)d_s}} \right)^{0.286} \left(\frac{h_s}{H_{wnet}} \right)^{0.588} \left(\frac{A}{H_{wnet}^2} \right)^{0.203} \quad (21)$$

The statistical performance indices for calibration and validation of Eqns. 20 and 21 (Figure 12 and Figure 13 respectively) confirmed that the proposed equations can make good predictions of volume and length of flushing cones respectively.

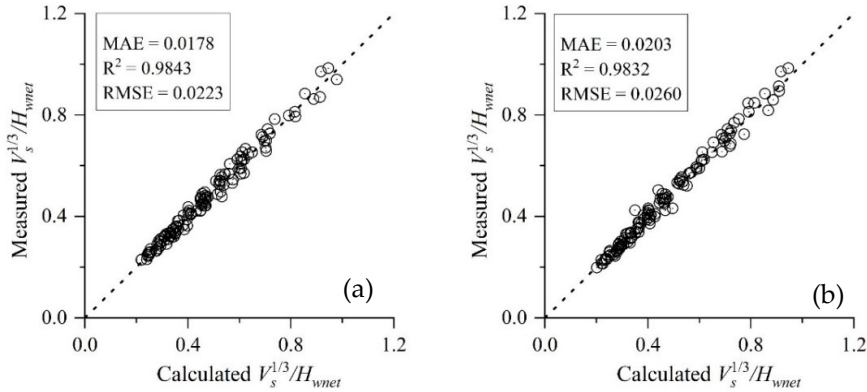


Figure 12. Plot of measured $V_s^{1/3}/H_{wnet}$ against that estimated by Eqn 20 for (a) calibration dataset and (b) validation dataset

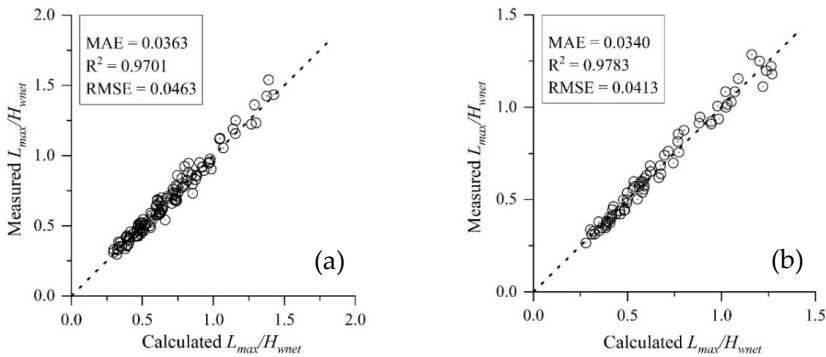


Figure 13. Plot of measured L_{max}/H_{wnet} against that estimated by Eqn 21 for (a) calibration dataset and (b) validation dataset

Although the calibration dataset contained test data for $H_s = 120$ mm and 140 mm only, the proposed equations provided good predictions for validation dataset including test data for $H_s = 100$ mm. Thus, the proposed equations are assumed to be capable of making predictions for different range of parameters. To test this assumption, Eqn. 20 was further validated against 45 experimental data from Fathi-Moghadam et al. (2010),

which were extracted by digitizing the published plots. The comparison of measured $V_s^{1/3}/H_{wnet}$ against that predicted by Eqn. 20 for the experimental data from Fathi-Moghadam et al. (2010) showed good agreement with satisfactory performance indices (see Figure 14).

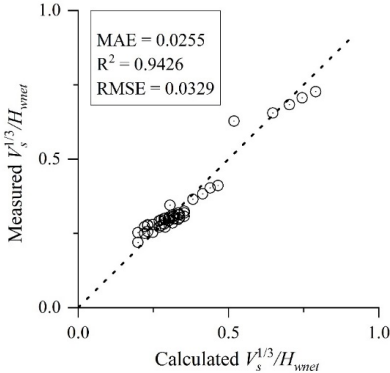


Figure 14. Prediction of $V_s^{1/3}/H_{wnet}$ for experimental data from Fathi-Moghadam et al. (2010) using Eqn. 20

5

Conclusions and Recommendations

The present PhD research was designed to study the pressurized flushing of non-cohesive sediment deposit through a bottom outlet via physical scale models using lightweight material as model sediment. The effective criteria for scaling down sediment parameters into model scale were reviewed. The most suitable criteria for designing sand models and lightweight models were selected. Three pairs of sand and lightweight material, each pair fulfilling the selected scaling criteria, were chosen to be used as model sediment. Physical model studies of pressurized flushing of sediment deposit through a bottom outlet were carried out using the selected model sediments except the sand for third pair which was excluded due to practical limitation in particle size of the model sediments. The results from the 192 tests from the five sets of experiments practically verified the applicability of selected lightweight materials as model sediments since the final flushing cones achieved with sand and lightweight material from each pair were comparable in terms of dimensions and volume. This study also increased the knowledge on designing mobile bed models utilizing locally available lightweight materials and yet not compromising accuracy of model predictions.

Simultaneously, application of SfM technique in physical model studies was also tested. Starting from image acquisition methods to selection of software from six available options were trialed to develop an effective methodology. Free handheld photography was selected for quick and flexible image acquisition. The set of images were processed in Photoscan software to implement SfM technique producing 3D models as dense point clouds or textured meshes. The SfM technique was further applied in three physical hydraulic model studies of different scopes and scales. The results showed satisfactory accuracy of the technique in estimating the point location,

linear distances and volume changes. The SfM technique was also applied in the experiments of this study to generate 3D models of the flushing cones.

After verifying the applicability of lightweight sediment in scaled model studies, the empirical equations proposed by past researchers to predict the geometry of flushing cones were reviewed. When all the available empirical equations were applied on the experimental data from this study, it was found that all the available empirical relations produce significantly contrasting predictions. Therefore, new empirical equations to predict volume and length of flushing cones were derived via regression analyses of the experimental data. Finally, the derived empirical equations were validated against experimental data extracted from Fathi-Moghadam et al. (2010). The new empirical equations proposed by this study performed well in predicting the length and volume of flushing cone for the validating data set from this study as well as for the experimental data extracted from Fathi-Moghadam et al. (2010).

In overall, the study provided some insights into using lightweight model sediments in physical scale modeling to study pressurized flushing phenomena. Moreover, the study also provided a methodology to implement SfM technique in physical hydraulic model studies. The SfM technique has huge potential against conventional manual measurements and it has already been applied successfully in selected model studies in Hydro Lab.

Recommendation for further research

Based on the experiences and results obtained from the present study, some scopes for further research are recommended.

- The present study assumed that a sand model (“Best model”) correctly represents its prototype with minimized scale effects. Further research could be carried out to validate the lightweight sediment models against real world prototype or at least prototype of bigger scale. Studies regarding geometrical distortion in lightweight models can also be included.
- During the experiments, it was noted that duration of tests (time to achieve equilibrium of flushing cones) were significantly shorter for lightweight sediment models compared to sand models. Yalin 1971 had already suggested

that time scales related to different morphological processes do not necessarily coincide in physical models. In this study, the pressurized flushing reached the equilibrium state in very short time, so no analyses regarding scaling of time frame were carried out. The distortion in time scale among hydrodynamic processes and different morphological and sedimentological processes specially for unsteady flow conditions can be interesting area for further research. Henry et al. (2018) had reviewed available literature on time scale distortion in lightweight models and it would be interesting to study how all the time scale ratio of the dominating sedimentological and morphological processes can be synchronized to the time scale ratio of driving hydrodynamic events. Physical model study of morphological processes over a distinct time period e.g., change in morphology of a river bed or migration of river bedform can be carried out focusing on scaling of time frame for different processes.

References

- Annandale, G. W., Morris, G. L., & Karki, P. (2016). *Extending the Life of Reservoirs: Sustainable Sediment Management for Dams and Run-of-River Hydropower*. The World Bank.
<https://doi.org/10.1596/978-1-4648-0838-8>
- Atkinson, K. (1996). *Close range photogrammetry and machine vision*. Whittles Publ.
<http://cds.cern.ch/record/2230204>
- Atmodjo, P. S., & Suripin. (2012). The Effect of Water Level on The Effectiveness of Sediment Flushing. *International Journal of Waste Resources*, 2(2), 0–0.
<https://doi.org/10.4172/2252-5211.1000114>
- Bagnold, R. A. (1955). Some flume experiments on large grains but little denser than the transporting fluid, and their implications. *Proceedings of the Institution of Civil Engineers*, 4(2), 174–205. <https://doi.org/10.1680/ipeds.1955.11843>
- Basson, G. R., & Rooseboom, A. (2008). Mathematical modeling of sediment transport and deposition in reservoirs (Bulletin). *International Commission on Large Dams*.
- Basson, G. R., Rooseboom, A., South Africa, & Water Research Commission. (1997). *Dealing with reservoir sedimentation* (Technical Report TT 91/97). Water Research Commission.
- Bettess, R. (1990). Survey of Lightweight Sediments for Use in Mobile-Bed Physical Models. In H. W. Shen (Ed.), *Movable Bed Physical Models* (pp. 115–123). Springer Netherlands.
https://doi.org/10.1007/978-94-009-2081-1_12
- Bogardi, J. (1959). *Hydraulic similarity of river models with movable bed*. 24, 417–445.
- Brandt, A. (2000). A review of reservoir desiltation. *International Journal of Sediment Research*, 15–3, 321–342.
- Chauvin, J. L. (1962). Similitude in movable bed river models. *Bull. Centre Rech. Essais Chatou*, 1, p 64.
- Di Silvio, G. (1990). Modeling Desiltation of Reservoirs by Bottom-Outlet Flushing. In H. W. Shen (Ed.), *Movable Bed Physical Models* (pp. 159–171). Springer Netherlands.
https://doi.org/10.1007/978-94-009-2081-1_16
- Dreyer, S., & Basson, G. (2018, November 9). *Investigation of the shape of low-level outlets at hydropower dams for local pressure flushing of sediments*. SANCOLD 2018, Cape Town.
- Einstein, H. A., & Chien, N. (1956). Similarity of Distorted River Models with Movable Beds. *Transactions of the American Society of Civil Engineers*, 121(1), 440–457.
- Emamgholizadeh, S., Bateni, S. M., & Jeng, D.-S. (2013). Artificial intelligence-based estimation of flushing half-cone geometry. *Engineering Applications of Artificial Intelligence*, 26(10), 2551–2558. <https://doi.org/10.1016/j.engappai.2013.05.014>
- Emamgholizadeh, Samad, Bina, M., Fathi-moghadam, M., & Ghomeysi, M. (2006). Investigation and Evaluation of the Pressure Flushing Through Storage Reservoir. *ARPJ Journal of Engineering and Applied Sciences*.
- Fang, D., & Cao, S. (1996). *An experimental study on scour funnel in front of a sediment flushing outlet of a reservoir*. I.78-I.84.

- Fatherree, B. H. (2004). *The First 75 Years: History of Hydraulics Engineering at the Waterways Experiment Station*. US Army Corps of Engineers, Engineer Research and Development Center.
<https://usace.contentdm.oclc.org/digital/collection/p16021coll4/id/157/>
- Fathi-Moghadam, M., Emamgholizadeh, S., Bina, M., & Ghomeshi, M. (2010). Physical modelling of pressure flushing for desilting of non-cohesive sediment. *Journal of Hydraulic Research*, 48(4), 509–514. <https://doi.org/10.1080/00221686.2010.491691>
- Gaines, R. A., & Smith, R. H. (2002). Micro-Scale Loose-Bed Physical Models. *Hydraulic Measurements and Experimental Methods 2002*, 1–12.
[https://doi.org/10.1061/40655\(2002\)78](https://doi.org/10.1061/40655(2002)78)
- Gehrig, W. (1980). River models with movable bed. In *in H. Kobus (ed). Hydraulic Modelling* (pp. 49–70).
- Ghetti, A., & D'Alpaos, L. (1977). Effets des forces de capillarité et de viscosité dans les écoulements permanents examinées en modèle physique. *17th IAHR Congress*, 389–396.
- Gill, T. W., & Pugh, C. A. (2009). Sediment transport similitude for scaled physical hydraulic modeling. *Proceedings of the 33rd IAHR Congress*, 9–14.
- Gorrick, S., & Rodríguez, J. F. (2014). Scaling of sediment dynamics in a laboratory model of a sand-bed stream. *Journal of Hydro-Environment Research*, 8(2), 77–87.
<https://doi.org/10.1016/j.jher.2013.12.001>
- Hajikandi, H., Vosoughi, H., & Jamali, S. (2018). Comparing the Scour Upstream of Circular and Square Orifices. *International Journal of Civil Engineering*, 16(9), 1145–1156.
<https://doi.org/10.1007/s40999-017-0269-5>
- Heller, V. (2011). Scale effects in physical hydraulic engineering models. *Journal of Hydraulic Research*, 49(3), 293–306. <https://doi.org/10.1080/00221686.2011.578914>
- Henry, P.-Y., Aberle, J., Anquetin, P.-G., Grasso, F., Bodewes, B., Fernandez, R. L., McLelland, S., Vettori, D., Caceres, I., Marzeddu, A., & Pinto, F. T. (2018). *Hydralab+ Deliverable D8.3 Protocols for scaling morphodynamics in time (Hydralab+ Deliverable D8.III)*. Zenodo. <https://doi.org/10.5281/zenodo.2420824>
- Hudson, R. Y., Herrmann, F. A., & Sager, R. A. (1979). *Coastal hydraulic models*.
<https://trid.trb.org/view/388546>
- Julien, P. Y. (2018). *River Mechanics* (2nd ed.). Cambridge University Press.
<https://doi.org/10.1017/9781316107072>
- Kamble, S. A., Kunjeer, P. S., B, S., & Isaac, N. (2017). Hydraulic model studies for estimating scour cone development during pressure flushing of reservoirs. *ISH Journal of Hydraulic Engineering*, 24(3), 337–344. <https://doi.org/10.1080/09715010.2017.1381577>
- Kamphuis, J. W. (1974). Practical Scaling of Coastal Models. *Coastal Engineering Proceedings*, 14, 121–121. <https://doi.org/10.9753/icce.v14.121>
- Kamphuis, J. W. (1985). On understanding scale effect in coastal mobile bed models. In R. A. Dalrymple (Ed.), *Physical modelling in Coastal Engineering* (pp. 141–162). A. A. Balkema.

- Keen, A. S. (2011). *Erosive bar migration using density and diameter scaled sediment* [Masters Thesis, TU Delft]. <https://repository.tudelft.nl/islandora/object/uuid%3A42438f18-4a91-45e3-ae52-f716ab7cdadd>
- Kishi, T., Kuroki, M., & Imaizumi, S. (1975). An experimental study on the meandering flow in straight channel with fixed side bank. *30th Annual Conference of the Japan Society of Civil Engineers*.
- Kobus, H. (1980). *Hydraulic Modelling* (Bulletin 7). German Association for Water Research and Land Development.
- Komura, S. (1962). Similarity and design methods of river models with movable bed. *Transactions of the Japan Society of Civil Engineers*, 1962(80), 31–41. https://doi.org/10.2208/jscej1949.1962.80_31
- Kondolf, G. M., Gao, Y., Annandale, G. W., Morris, G. L., Jiang, E., Zhang, J., Cao, Y., Carling, P., Fu, K., Guo, Q., Hotchkiss, R., Peteuil, C., Sumi, T., Wang, H.-W., Wang, Z., Wei, Z., Wu, B., Wu, C., & Yang, C. T. (2014). Sustainable sediment management in reservoirs and regulated rivers: Experiences from five continents. *Earth's Future*, 2(5), 256–280. <https://doi.org/10.1002/2013EF000184>
- Lai, J.-S., & Shen, H. W. (1996). Flushing sediment through reservoirs. *Journal of Hydraulic Research*, 34(2), 237–255. <https://doi.org/10.1080/00221689609498499>
- Le Mehaute, B. (1970). A comparison of fluvial and coastal similitude. *Coastal Engineering Proceedings*, 1(12). <https://doi.org/10.9753/icce.v12.%p>
- Mahmood, K. (1987). *Reservoir sedimentation: Impact, extent, and mitigation* (No. WTP71; p. 1). The World Bank. <http://documents.worldbank.org/curated/en/888541468762328736/Reservoir-sedimentation-impact-extent-and-mitigation>
- Meshkati, M. E. M., Dehghani, A. A., Sumi, T., Naser, G., & Ahadpour, A. (2010). Experimental investigation of local half-cone scouring against dam. *Proceedings of the International Conference on Fluvial Hydraulics*, 1267–1273.
- Miller, R. L. (2015). *The Role of Surface Tension in Breaking Waves*. 433–449. <https://doi.org/10.1061/9780872620490.025>
- Mohammad, B. T., Daham, F. A., & Bilal, Z. Z. (2018). Experimental Investigation to study the Hydraulic Performance of Pressure Flushing in Straight Wall Reservoirs. *Zanco Journal of Pure and Applied Sciences*, 30(1), 113–121. <https://doi.org/10.21271/ZJPAS.30.s1.13>
- Morgan, J. A., Brogan, D. J., & Nelson, P. A. (2017). Application of Structure-from-Motion photogrammetry in laboratory flumes. *Geomorphology*, 276, 125–143. <https://doi.org/10.1016/j.geomorph.2016.10.021>
- Morris, G. L., & Fan, J. (2010). *Reservoir sedimentation handbook: Design and management of dams, reservoirs, and watersheds for sustainable use*. McGraw-Hill.
- Oliveto, G., & Hager, W. H. (2005). Further Results to Time-Dependent Local Scour at Bridge Elements. *Journal of Hydraulic Engineering*, 131(2), 97–105. [https://doi.org/10.1061/\(ASCE\)0733-9429\(2005\)131:2\(97\)](https://doi.org/10.1061/(ASCE)0733-9429(2005)131:2(97))

- Paul, T. C., & Dhillon, G. S. (1988). Sluice dimensioning for desilting reservoirs. *International Water Power and Dam Construction*, 40(5), 40–44.
- Powell, D. N. (2007). *Sediment Transport Upstream of Orifices* [PhD Thesis, Clemson University]. https://tigerprints.clemson.edu/all_dissertations/140
- Powell, D. N., & Khan, A. A. (2012). Scour upstream of a circular orifice under constant head. *Journal of Hydraulic Research*, 50(1), 28–34. <https://doi.org/10.1080/00221686.2011.637821>
- Pugh, C. A., & Dodge, R. A. (1991). *Design of sediment models* (Technical Report PAP-586; p. 8). https://www.usbr.gov/tsc/techreferences/hydraulics_lab/pubs/PAP/PAP-0586.pdf
- Reynolds, O. (1901). On certain laws relating to the regime of rivers and estuaries, and on the possibility of experiments on a small scale. In *Papers on mechanical and physical subjects* (Vol. 2, pp. 326–335). Cambridge University Press.
- Rouse, H., Siao, T. T., & Nagaratnam, S. (1958). Turbulence Characteristics of the Hydraulic Jump. *Journal of the Hydraulics Division*, 84(1), 1–30.
- Scheuerlein, H. (1993). *Estimation of flushing efficiency in silted reservoirs*. First international conference on Hydro-science and Engineering, Washington, DC.
- Scheuerlein, H., Tritthart, M., & Gonzalez, F. N. (2004). *Numerical and physical modelling concerning the removal of sediment deposits from reservoirs*. Conference Proceeding of Hydraulic of Dams and River Structures, Tehran. https://www.civilica.com/Paper-HDRS-HDRS_28.html
- Schleiss, A. J., Franca, M. J., Juez, C., & De Cesare, G. (2016). Reservoir sedimentation. *Journal of Hydraulic Research*, 54(6), 595–614. <https://doi.org/10.1080/00221686.2016.1225320>
- Schmocker, L., & Hager, W. H. (2009). Modelling dike breaching due to overtopping. *Journal of Hydraulic Research*, 47(5), 585–597. <https://doi.org/10.3826/jhr.2009.3586>
- Shahmirzadi, M. E. M., Dehghani, A. A., Meftahh, M., & Mosaedi, A. (2010). Experimental Investigation of Pressure Flushing Technique in Reservoir Storages. *Water and Geoscience*, 1(1), 132–137.
- Shields, A. (1936). Anwendung der Aehnlichkeitsmechanik und der Turbulenzforschung auf die Geschiebebewegung. *PhD Thesis Technical University Berlin*. <https://repository.tudelft.nl/islandora/object/uuid%3A61a19716-a994-4942-9906-f680eb9952d6>
- Sloff, C. J. (1991). Reservoir sedimentation; a literature survey. *Communications on Hydraulic and Geotechnical Engineering*, No. 1991-02. <https://repository.tudelft.nl/islandora/object/uuid:27232f02-0e81-43ac-bebf-8e2459d6f076?collection=research>
- Sutherland, J., & Soulsby, R. (2011). *Guidelines for physical modelling of mobile sediments HR PP 4 63*.
- Taylor, B. D. (1972). Temperature effects in alluvial streams, Dissertation (Phd), California Institute of Technology, <https://doi.org/10.7907/9XZ5-FA91>, <https://resolver.caltech.edu/CaltechTHESIS:09062016-161209389>

- Taylor, R. N. (1994). *Geotechnical Centrifuge Technology*. CRC Press.
<https://doi.org/10.1201/9781482269321>
- UNESCO. (2009). *Water in a Changing World* (The United Nations World Water Development Report 3).
- Vollmers, H.-J. (1990). Examples for Using Sand and Lightweight Material in Movable Bed Models. In H. W. Shen (Ed.), *Movable Bed Physical Models* (pp. 125–140). Springer Netherlands. https://doi.org/10.1007/978-94-009-2081-1_13
- Wei, B. Q., Xun, H. Y., Xiao, R. G., & Meng, W. Q. (2011). Similarity Laws of Distorted Model with a Movable Bed and its Validity. *Advanced Materials Research*, 383–390, 4413–4423. <https://doi.org/10.4028/www.scientific.net/AMR.383-390.4413>
- Wen Shen, H. (1999). Flushing sediment through reservoirs. *Journal of Hydraulic Research*, 37(6), 743–757. <https://doi.org/10.1080/00221689909498509>
- Westoby, M. J., Brasington, J., Glasser, N. F., Hambrey, M. J., & Reynolds, J. M. (2012). ‘Structure-from-Motion’ photogrammetry: A low-cost, effective tool for geoscience applications. *Geomorphology*, 179, 300–314. <https://doi.org/10.1016/j.geomorph.2012.08.021>
- White, R. (1990). Reservoir sedimentation and flushing. *Hydrology in Mountainous Regions II*.
- White, R. (2001). *Evacuation of sediments from reservoirs*. Thomas Telford Publishing. <https://doi.org/10.1680/eosfr.29538>
- Yalin, M. S. (1971). Similarity in Sediment Transport. In M. S. Yalin (Ed.), *Theory of Hydraulic Models* (pp. 145–186). Macmillan Education UK. https://doi.org/10.1007/978-1-349-00245-0_6
- Zarn, B. (1992). *Lokale Gerinneaufweitung – eine Massnahme zur Sohlstabilisierung der Emme bei Utzendorf* (Mitteilungen 118; pp. 98–103). Laboratory of Hydraulics, Hydrology and Glaciology, Swiss Federal Institute of Technology.
- Zwamborn, J. A. (1966). Reproducibility in hydraulic models of prototype river morphology. *La Houille Blanche*, 3, 291–298. <https://doi.org/10.1051/lhb/1966020>

Annex-A

Research Articles

Paper I

Application of 'Structure from Motion' (SfM) technique in physical hydraulic modelling

Sanat Kumar Karmacharya, Meg Bishwakarma, Ujjwal Shrestha, Nils R  ther

CRHT IX, 2019, Journal of Physics: Conference Series 1266 012008

Application of ‘Structure from Motion’ (SfM) technique in physical hydraulic modelling

Sanat Kumar Karmacharya^{1,2}, Meg Bishwakarma², Ujjwal Shrestha¹ and Nils R  ther ^{*1}

¹*Department of Civil and Environmental Engineering, NTNU, Trondheim, Norway*

²*Hydro Lab Private Limited, Lalitpur, Nepal*

* *Corresponding author (nils.r  ther@ntnu.no)*

Abstract. There are many methods available for measurement of bed morphology in physical hydraulic model studies considering mobile bed sediment. Among which, there are sophisticated instrumentations which provide quality results in shorter time but are vastly expensive and requires special training for execution. Whereas the conventional surveying methodology, which is simple and inexpensive, requires plenty of time for the measurement and processing of the data. That is why the recent developments in ‘Structure from Motion’ (SfM) technique have made it a potential candidate for an inexpensive and efficient tool for measurement of bed morphology in physical hydraulic model studies. SfM method allows to simultaneously determine both the parameters of the camera and the 3D structure of a scene by combining 2D images taken from multiple viewpoints. SfM tools can create a dense point cloud out of a set of partially overlapping photographs taken even by a budget friendly digital camera. The SfM method have already been used as an alternative for topographic surveying to create high-resolution digital elevation models (DEM). Some researchers had also used it for measurement of bed morphology in laboratory experiments. In this study, different freely available SfM tools were used to create a dense point cloud from a set of photographs representing a short reach in a river model in the hydraulic laboratory at Hydro Lab. The selected tools were compared with each other and against a commercial software, based on the methodologies used, processing time and quality of the output. Then the results from SfM method were compared with actual measurements in the physical model done with a conventional surveying technique using a theodolite and a level machine. The results showed that free SfM tools can also produce efficient results compared to commercial tools and SfM method can be used as an inexpensive and efficient alternative for bed morphology measurements in physical hydraulic models.

1. Introduction

With aggressive advancement in technology, currently various methodologies are available, over conventional ground surveying techniques, for creating a high-resolution digital elevation models (DEM) of a topography. Aerial photogrammetry, airborne lidar and ground based terrestrial laser scanners (TLS) are some advanced technologies, which have revolutionized the quality of DEMs extending their spatial extent, resolution and accuracy [1]. Recently, easy access to unmanned aerial vehicles (UAV) and drones has made the aerial imaging surveys more convenient and inexpensive.

Besides the development in large-scale terrestrial surveying, there has also been a huge advancement in data acquisition and processing technologies for hydraulic laboratories. Producing DEMs of physical hydraulic models and/or recording bed morphologies in fluvial sediment transport studies in hydraulic laboratories can be carried out more accurately by using laser scanning or acoustic sounding systems. These systems can be tailored for semi or fully automatic data acquisition curtailing the experiment

time. Despite these sophisticated instrumentations are useful in producing high quality DEMs in shorter time, they require high logistical cost and specialized user expertise. Therefore, many hydraulic laboratories still use conventional measurement techniques that are inexpensive and simple though more time demanding. In conventional techniques, measurements are taken at selected points/cross-sections and those data are interpolated in-between. The accuracy of such measurements can be improved by increasing the density of measured points especially at desired details to be captured but it will ultimately increase the time required for measurement and data processing. On the contrary, the laser and acoustic scanning can record highly dense point cloud in shorter time ensuring higher resolution DEM.

In this study, an advanced yet inexpensive and easy to perform photogrammetric method, called 'Structure from Motion' (SfM), was used to produce high resolution DEM of a physical hydraulic river model. Basic principle governing SfM method is similar to stereoscopic photogrammetry in which a 3D structure is developed from a series of overlapping 2D images [1]. Unlike conventional photogrammetry, SfM method utilizes advanced algorithms by which it automatically solves the relative camera positions, orientation and geometry of the target object based on the features extracted from the set of images [2]. Possibility of using low-cost consumer level digital cameras and availability of free and open-source processing tools has given SfM method boundless potentials. Nowadays, SfM has already been widely used in various fields like archaeology, geosciences, robotics, terrestrial surveying, real state, film and entertainment, sports etc. The possibility of using SfM method in an inexpensive and simple way to record 3D information from laboratory models was assessed in this study.

2. Methodology

2.1 Structure from motion (SfM)

There are various algorithms available for application of SfM but the general principle remains the same and has been described by [1] [3] and [4]. SfM requires a set of overlapping images, capturing the object from multiple viewpoints, as an input. From the images, common feature points across the image set called key point descriptors are identified using a scale invariant feature transform (SIFT) algorithm. With these feature points and camera parameters extracted from the images, camera location, orientation and position of the feature points are simultaneously resolved in a relative 3D coordinate system. Once the spatial positions of the images are established, a sparse bundle adjustment (BA) algorithm is used to create 3D points covering the area of interest. Then, dense point cloud is produced by intensifying the sparse point cloud with multi view stereo (MVS) techniques. Once the dense point cloud is obtained, it can be used for further processing like developing a DEM, mesh generation, creating a 3D model etc. as per requirement.

2.2 Software

Nowadays, due to the application of SfM method in diverse fields, there are various software available for its implementation. Following six software were selected for application of SfM method in this study. First two are commercial software whereas remaining four are free to use.

PhotoScan. PhotoScan (now available as Metashape) is commercial software developed by Agisoft LLC, Russia. It is an easy to use stand-alone software which offers all the capabilities from processing images to 3D model generation and texturing and includes additional pre-processing and post processing

features. Professional edition of the software is priced USD 3,499 and the standard edition is available for USD 179. However, standard edition itself is enough for generation of 3D models and lacks only other extra features that professional edition offers.

ReCap. ReCap (named after abbreviation of Reality Capture) is developed by Autodesk Inc USA and is a cloud-based service tailored for generation of 3D models from photographs or laser scans. ReCap Photo, which is included within ReCap pro, is specifically targeted for support UAV and drone photo capture workflows. ReCap Photo can be used to create photo textured meshes, photo-based point clouds with geo-location and high-resolution orthographic views with elevation maps. It can also be used in object mode to create 3D models of objects. It is a commercial software and ReCap pro subscription is needed to use the service. The subscription costs USD 40 for a month, USD 305 for a year and USD 915 for three years. The service uses cloud credits for each projects and additional cloud credits can be purchased separately once subscribed. Currently, ReCap pro subscription allows you to process up to 1,000 images for one project in aerial mode while the limit is 300 photos for one project in object mode. The software can be used freely under academic license but has the limitation of 100 photos for one project and academic users may also have to wait in long queue for processing. Since it is a cloud-based service, no expensive hardware is required for the processing and the images can be uploaded via smartphone app too. The disadvantage could be it works like a black box and users have very limited control over the quality of the output.

VisualSfM. VisualSfM, developed by Dr. Changchang Wu, is a GUI application for 3D reconstruction using structure from motion (SfM). The reconstruction system integrates different algorithms like SIFT on GPU (SiftGPU), Multicore Bundle Adjustment and Towards Linear-time Incremental Structure from Motion [5–7]. VisualSfM runs fast by exploiting multicore parallelism for feature detection, feature matching, and bundle adjustment. It is one of the first free photogrammetry program to utilize the power of graphical processing unit (GPU). It can process up to sparse reconstruction and utilizes Yasutaka Furukawa's PMVS/CMVS tool for dense reconstruction, which has to be integrated and can be run from the VisualSfM's GUI. However, the sparse point cloud from VisualSfM can be processed in other dense reconstruction tools as well to produce dense point cloud. VisualSfM is free and open source but the licensing restricts its commercial use.

Regard3d. Regard3d is a free and open-sourced structure from motion software which is developed by Roman Hiestand. It offers complete SfM processing up to dense point cloud generation. It can also generate surface, from the dense point cloud, either with colored vertices or with a texture. It has integrated several algorithms and users have a bunch of options to control the quality of the output.

Meshroom. Meshroom is a free and open-source 3D reconstruction software based on the Alice Vision framework. It can perform complete 3D reconstruction up to textured surface creation. It has a node-based workflow that gives its users a lot of control on setting the processing and once its set whole processing can be completed in one click. The advantages of this software are it supports augmented reconstruction i.e. more pictures can be added for better detailing while the processing is on-going. Additionally, it can also perform live reconstruction. The disadvantage of Meshroom could be that it requires CUDA enabled GPU with at least computing capability of 2.0. It should be noted that it does not warn users if they lack the mandatory GPU requirement and the processing seems to be frozen without any notifications. Despite of its promising features and capabilities, there is not any official user manual or guide available yet.

COLMAP. COLMAP is a free and open-sourced Structure-from-Motion (SfM) and Multi-View Stereo (MVS) pipeline with a graphical and command-line interface. It offers a wide range of features for reconstruction of ordered and unordered image collections [8]. It uses MVS technique for dense point cloud reconstruction and uses screened Poisson surface reconstruction algorithm to recover 3D surface geometry from the dense point cloud. However, COLMAP requires CUDA-enabled GPU (at least CUDA version 7.x) to perform dense reconstruction and surface creation processes. But processes up to sparse reconstruction can be carried out without CUDA-enabled GPU and the output can be exported to do dense reconstruction with other tools. For beginners, COLMAP has an automatic reconstruction tool that simply takes a folder of input images and produces a sparse and dense reconstruction in a workspace folder.

Meshlab. Meshlab is the open source software for processing and editing 3D point clouds and 3D triangular meshes and creating 3D models [9]. In this study, Meshlab was used for transformation of 3D dense point cloud in arbitrary coordinates created by SfM software to 3D dense point cloud in actual coordinates.

2.3 Hardware

2.3.1. Camera. Sony α 6300 (model ILCE-6300) camera was used for taking pictures for this study. It was a mirrorless digital camera with 24-megapixel Exmor RS sensor, and 425 phase detection autofocus points. The camera setting has a significant impact on the image quality which ultimately affects the quality of the output. After various trials with different settings, following camera settings were used for this study:

- Shooting mode: Shutter Priority (S)
- Shutter speed: 1/80 sec
- ISO: 640
- Aperture: F9-F11
- Focal length: 16 mm
- Image format: JPEG

Workstation. The specification of the workstation determines the total processing time except for the cloud-based processing as with ReCap. For fair comparison, same workstation with following specifications were used for processing with all the selected software:

- Operating System: Microsoft Windows 7 Ultimate 64-bit
- Processor: Intel® Core™ i7-4790 CPU @3.60GHz
- Installed memory (RAM): 32 GB
- GPU: NVIDIA GeForce GTX 750 Ti -18 GB available memory

2.3.2 Ground control points (GCPs)

With SIFT algorithm, the 3D structure is created based on relative spatial relationships between the original image locations in an arbitrary 3D coordinate system [10]. That means the structure (shape) of the object is recovered but the size is scaled to some arbitrary scale factor. Hence, the final output, either the dense point cloud or 3D surface model, must be transformed using rotation, translation and scaling.

To perform this transformation, several ground control points (pre-defined set of points with known coordinates) are needed in the study area. For large scale terrestrial surveying, in order to obtain high accuracy of final output ($RMSE < 1$) 1GCP per $200m^2$ is needed to be placed in the interest area [11]. But, at least 5 control points are needed to acquire a precise 3D point cloud [12]. Total 8 control points were used in this study and these control points were marked such that it covered all the concerned area. Image acquisition process was started after setting the control points. Also, it is possible to get a scaled final product without placing manual markers if the images from a GPS enabled camera is used for processing. However, the manual marker placement with pre-defined coordinate system is usually more accurate allowing more precise geo-referencing.

3. Case Study

3.1 Study area

A small reach of a physical hydraulic model of a river, in the hydraulic laboratory of Hydro lab at Kathmandu, was taken as the object for this study. The model was built in 1:40 scale. The length of the study area is about 3 m which represents 120 m long river reach in prototype. Eight ground control points covering all the region was marked on the model as shown in the Figure 1.

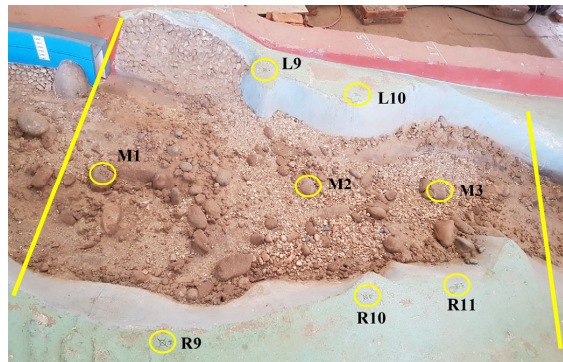


Figure 1. A small reach of a river model in Hydro Lab used as object for this study

3.2 Image acquisition

Several images were taken from varying camera position and angle covering the whole study area. Few close-up images of the boulders were also taken to obtain better detailing. It was ensured that there was enough light in the model with no direct sunlight and sharp shadows. Each feature and control points were captured in at least three images from different viewpoints.

3.3 Image processing and dense reconstruction

At first, the images were filtered removing very bright, dark, blurred and shadowed images if any. 46 images were selected for further processing. The set of images were processed using all the selected software individually and 3D dense point clouds were created. Meshroom and ReCap created 3D mesh as output, which were later converted to 3D dense point cloud using Meshlab. Total time for feature extraction/feature matching, sparse reconstruction and dense reconstruction by each software was

recorded and compared as one of the major performance parameters. The processing time up to dense reconstruction for the selected software is shown in Table 1. The processing was done mostly with default settings of the software to assess the possibility of using them by a complete beginner.

Table 1. Processing time up to dense reconstruction for selected software.

Tools	Feature extraction and Feature matching	Sparse reconstruction	Dense reconstruction	Total processing time
Colmap	1 hr 51 min	31 min	8 hr 4 min	10 hr 26 min
Meshroom	2 min	3 min	1 hr 41 min	1 hr 46 min
Photoscan	5 min		3 hr 34 min	3 hr 39 min
ReCap	-	-	-	2 hrs
Regard3d	1 hr 38 min	29 min	35 min	2 hr 42 min
VisualSfM	3 min	31 sec	24 min	58 min

3.4 Post processing

The 3D dense point clouds created by the selected software were transformed from arbitrary 3D coordinates to the real prototype coordinates (not model coordinates) using rotation, translation and scaling in reference to the coordinates of GCPs. It was done in Meshlab using ‘roto-translation’ with ‘uniform scaling’ in geo-referencing tool. During the transformation, GCPs with error (RMSE) greater than 1 were eliminated to ensure better accuracy [13]. Thus, the georeferenced point cloud is generated. The point cloud data was exported to create a contour map with 1m X 1m grid resolution as shown in Figure 2.

3.5 Manual measurements

For assessing the accuracy of outputs by selected software, 4 cross-sections in the river model were manually measured using a level machine and bar scale. These cross sections were compared with the corresponding cross-section profiles extracted from the contour plots produced by using dense point clouds from the selected software.

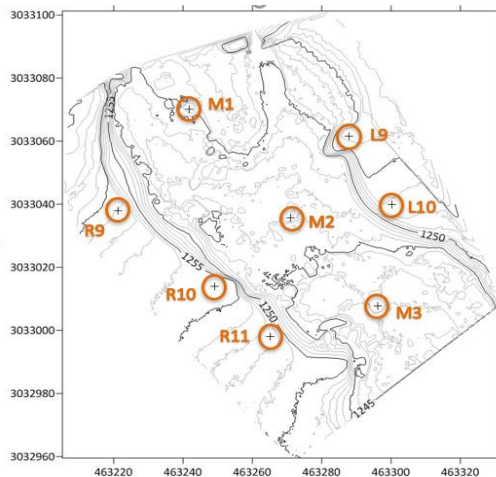


Figure 2. Contour Map plotted from 3D point cloud created by PhotoScan

4. Results and discussion

It was observed that SfM method created high density point cloud thus captured better details compared to the manual measurement. The total number of points in the final 3D dense point clouds vastly varies from 2.03 million for Meshroom to 29.2 million for PhotoScan. Although point cloud by Meshroom contained minimum number of vertices, the quality of the output was not lesser. Hence, bigger number of vertices may not necessarily mean better quality of the output. The final output by each software and the total number of vertices forming the 3D output are shown in Figure 3. Finally, 4 cross-sections profiles within the study area were extracted from the contour map plotted using 3D dense point cloud from each software. Each of the cross-section profiles were plotted together with that obtained from manual measurements and compared with each other as shown in Figure 4 where comparison for two cross-section profiles are shown. The plots show that the cross-section profiles generated with selected SfM tools are in close agreement with each other and with the manually measured cross section profile.

To quantify the capability of the SfM tools to predict the vertical dimension, elevation of the 150 points, where manual measurements were done, were extracted from the point clouds generated by each of the selected software. Those elevations were compared with measured elevations and mean absolute error (MAE), root mean square error (RMSE) and coefficient of determination (R^2) were calculated as shown in Table 2. It is to be noted that MAE and RMSE values shown in Table 2 are in meters as the analysed results were in prototype scale. The results show that each of the selected software is good at predicting the vertical dimension with MAE below 0.24 m and RMSE below 0.30 m in prototype scale which represents MAE below 6 mm and RMSE below 7.5 mm in model scale. Here, Photoscan stood out as ‘the best among equals’ by scoring lowest MAE and RMSE, and highest R^2 value. However, the quality of results is dependent on various factors like choice of different algorithms and respective parameter values within SfM technique, resolution of DEM generated from dense point cloud and accuracy of GCPs used for geo-referencing. Also, the acceptable limit for error or discrepancies varies with the purpose of the model study, scale factor and measurement techniques. Therefore, there is an immense possibility to obtain better results with free and open-source software by tweaking various parameters whereas commercial software like Photoscan and ReCap work as a black box model and give their users lesser control. On the other hand, Photoscan and ReCap are user friendly, easy to use and can deliver quality results with minimum involvement of the user.

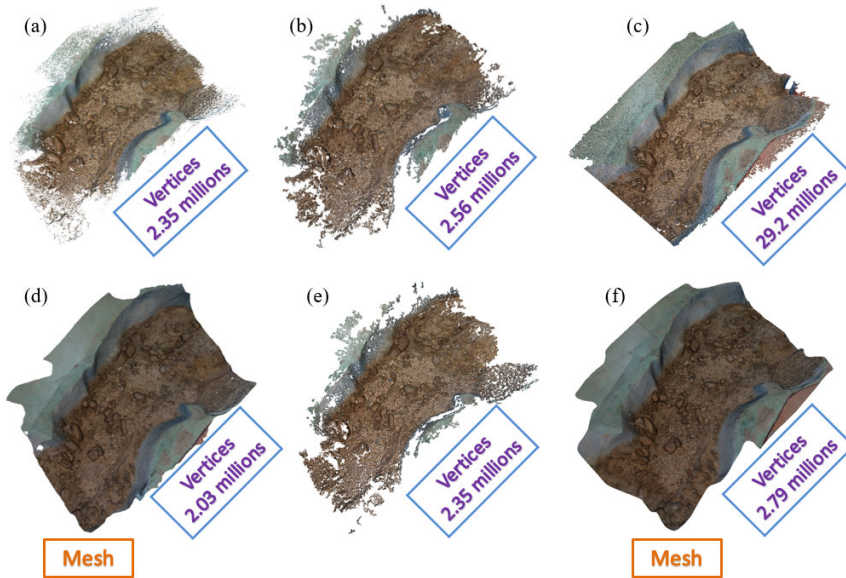


Figure 3. Outputs by (a) COLMAP, (b) Regard3d, (c) PhotoScan, (d) Meshroom, (e) VisualSfM and (f) ReCap and total number of vertices in respective outputs

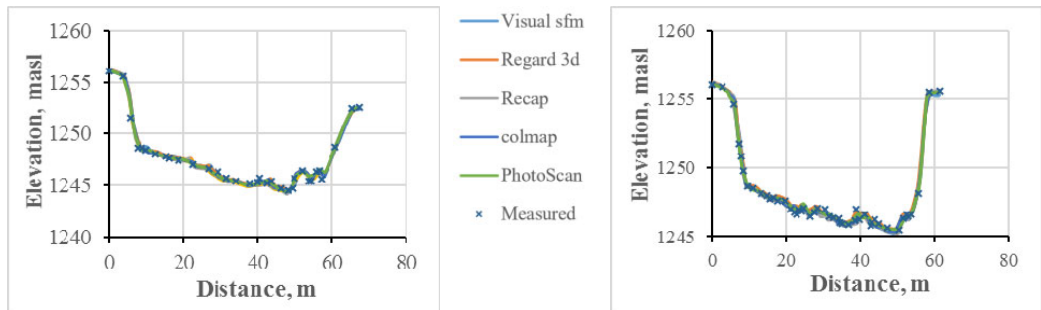


Figure 4. Cross section profiles (a) L9-R11 and (b) L9-R10

Table 2. Analysis of the error in predicting elevations by the selected software.

Tools	MAE	RMSE	R ²
Colmap	0.161 m	0.216 m	0.9958
Meshroom	0.176 m	0.232 m	0.9956
Photoscan	0.155 m	0.195 m	0.9965
ReCap	0.165 m	0.222 m	0.9962
Regard3d	0.232 m	0.294 m	0.9946
VisualSfM	0.175 m	0.228 m	0.9956

5. Conclusion

From the results of this study, it can be said that SfM method can be used in hydraulic laboratories to efficiently capture 3D geometry from a physical hydraulic model in shorter time yet with better details and within acceptable accuracy. It is also concluded that the free and open source software are also capable of producing good results as compared to results from commercial software. Moreover, free and open sourced software offers more control to the users and hence have huge potential for researchers to produce even better-quality results. But for commercial purposes, where quality results are required in shorter time with minimum involvement of the user, commercial software are recommended. For example, Photoscan and ReCap can perform all the processes including scaling of the final model output and DEM generation within one platform and hence provide the complete solution. Whereas, free and open sourced software requires additional third-party software to perform different processes e.g. Meshlab for geo-referencing the output model. Lastly, it should be noted that the first criterion to achieve better quality output is to take better quality photographs.

References

- [1] Westoby M J, Brasington J, Glasser N F, Hambrey M J and Reynolds J M 2012 “Structure-from-Motion” photogrammetry: A low-cost, effective tool for geoscience applications *Geomorphology* **179** 300–14
- [2] Snavely N, Seitz S M and Szeliski R 2008 Modeling the World from Internet Photo Collections *Int. J. Comput. Vis.* **80** 189–210
- [3] James M R and Robson S 2012 Straightforward reconstruction of 3D surfaces and topography with a camera: Accuracy and geoscience application *J. Geophys. Res. Earth Surf.* **117**
- [4] Micheletti N, Chandler J H and Lane S N 2015 Investigating the geomorphological potential of freely available and accessible structure-from-motion photogrammetry using a smartphone *Earth Surf. Process. Landf.* **40** 473–86
- [5] Wu C 2013 Towards Linear-Time Incremental Structure from Motion *2013 International Conference on 3D Vision - 3DV 2013* 2013 International Conference on 3D Vision - 3DV 2013 pp 127–34
- [6] Wu C VisualSFM: A Visual Structure from Motion System <http://ccwu.me/vsfm/>, 2011
- [7] Wu C, Agarwal S, Curless B and Seitz S M 2011 Multicore bundle adjustment *CVPR 2011* CVPR 2011 pp 3057–64
- [8] Schönberger J L and Frahm J 2016 Structure-from-Motion Revisited *2016 IEEE Conference on Computer Vision and Pattern Recognition (CVPR)* 2016 IEEE Conference on Computer Vision and Pattern Recognition (CVPR) pp 4104–13
- [9] Cignoni P, Callieri M, Corsini M, Dellepiane M, Ganovelli F and Ranzuglia G 2008 *MeshLab: An Open-Source Mesh Processing Tool* (The Eurographics Association)
- [10] Micheletti N, Chandler J H and Lane S N 2015 Structure from motion (SfM) photogrammetry
- [11] Oniga V-E, Breaban A-I and Statescu F 2018 Determining the Optimum Number of Ground Control Points for Obtaining High Precision Results Based on UAS Images *Proceedings* **2** 352
- [12] Goldstein E B, Oliver A R, deVries E, Moore L J and Jass T 2015 Ground control point requirements for structure-from-motion derived topography in low-slope coastal environments (PeerJ PrePrints)
- [13] Alfredsen K, Haas C, Tuhtan J A and Zinke P 2018 Brief Communication: Mapping river ice using drones and structure from motion *The Cryosphere* **12** 627–33

Paper II

**Evaluating the Structure from Motion technique for measurement of bed
morphology in physical model studies**

Sanat Kumar Karmacharya, Nils R  ther, Ujjwal Shrestha, Meg Bahadur Bishwakarma

Water 2021, 13(7), 998; <https://doi.org/10.3390/w13070998>

Evaluating the Structure from Motion technique for measurement of bed morphology in physical model studies

Sanat Kumar Karmacharya^{1,2,*}, Nils Ruther¹, Ujjwal Shrestha¹ and Meg Bahadur Bishwakarma²

¹ Department of Civil and Environmental Engineering, Norwegian University of Science and Technology (NTNU), S.P. Andersens veg 5, 7491 Trondheim, Norway. nils.ruther@ntnu.no (N.R.); ujjwalshrestha21@gmail.com (U.S.)

² Hydro Lab Pvt. Ltd., GPO Box no 21093, Kathmandu 44600, Nepal. mb@hydrolab.org

* Correspondence: sanat.k.karmacharya@ntnu.no, sanat.karmacharya@gmail.com;

Abstract: The selection of instrumentation for data acquisition in physical model studies depends on type and resolution of data to be recorded, time frame of the model study, available instrumentation alternatives, availability of skilled personnel and overall budget of the model study. The available instrumentation for recording bed levels or three-dimensional information on geometry of a physical model range from simple manual gauges to sophisticated laser or acoustic sensors. In this study, Structure from Motion (SfM) technique was applied, on three physical model studies of different scales and study objectives, as a cheap, quicker, easy to use and satisfactorily precise alternative for recording 3D point data in form of colour coded dense point cloud representing the model geometry especially the river bed levels in the model. The accuracy of 3D point cloud generated with SfM technique were also assessed by comparing with data obtained from manual measurement using conventional surveying technique in the models and the results were found to be very promising.

Keywords: Structure from Motion; physical hydraulic model; river bed morphology; experiments; instrumentation; photogrammetry

1. Introduction

The use of physical hydraulic models to study different hydraulic phenomena has a history spanned over a few centuries. Since the fundamental theoretical background on producing hydraulically similar models were already put forward by past researchers, the advancement in physical hydraulic modelling since then were mostly focused on measurement, data acquisition and processing technologies. The laboratory instrumentation for physical hydraulic models have been evolved from simple manual gauges to highly sophisticated acoustic, ultrasonic and laser-based measurement systems [1]. However, various laboratories around the world still use the simple manual/mechanical instrumentation for measurements in physical hydraulic models because of their simplicity in operation as well as in data interpretation and their low logistical cost, though the measurement processes with those instruments are more time consuming. Whereas, relatively sophisticated thus expensive instrumentations are more accurate and less time consuming but require high logistical cost and specialized user expertise for data acquisition and analyses. These advanced measurement systems can be tailored for semi or fully automatic data acquisition curtailing the experiment time. However, the availability of instrumentation facilities, skills of the operator, time and budget for a given experiment ultimately govern the selection of measurement techniques for the experiment.

Traditional close-range digital photogrammetry was successfully used, in both field and laboratory measurements, as a cost-effective method to create 3D surface of a topography [2–4]. But the traditional photogrammetry is time consuming and the user is required to have a keen knowledge of mathematical foundations of photogrammetry in order to reconstruct an accurate 3D model [5]. When 3D laser scanning technology was released, it was supposed to completely replace the traditional photogrammetry, because of its accuracy and automation level [6]. But recent developments in photogrammetry and computer vision have made many improvements in the automated extraction of three-dimensional information from 2D images to generate accurate and dense models. Hence, image-

based techniques are still widely used as the most complete, economical, portable and flexible method to generate 3D models [7]. Backed by complex algorithms, various commercial and open-source software are available to implement photogrammetric techniques, most of which can be used even by non-vision experts [8].

Structure from Motion (SfM) is a widely used photogrammetric technique which utilizes multi-view 3D reconstruction technology to produce high-resolution 3D models of a target object from a series of overlapping 2D images [9–11]. The fundamental advantage of SfM over traditional photogrammetry is its capability to automatically determine geometry of the target object, camera positions and orientation without prior need for a set of defined control points [9,12,13]. SfM solves these parameters simultaneously using a highly redundant, iterative bundle adjustment procedure based on a dataset of distinct features extracted automatically from the given set of images [14]. All the processes in SfM, from identification of key features to 3D reconstruction of scene geometry, can be automated which makes it more practical and cheaper alternative compared to traditional photogrammetry. SfM can be a low-cost but reliable alternative to other sophisticated measurement techniques also as it can be applied with images taken from low-cost consumer level digital cameras [9,15,16] or even from smartphones and complete processing can be carried out with freely available tools/software. With easy access to unmanned aerial vehicles (UAVs) and drones, which can be equipped with camera and sensors, SfM technique has also been widely used in medium to large-scale terrestrial surveying [17,18]. The accuracy of SfM for generation of high-resolution 3D topography has been validated by multiple studies [15,19,20] with some results being highly comparable to laser-based techniques [8,21,22].

The advantages of photogrammetric method over laser scanning are low operation cost, short data acquisition time, high quality of colour information and scalable 3D point clouds as output [23]. For example, Lane [3] spent about 8 hours just to collect the data, using a laser sensor on a motorized cart, required to create a DEM with 0.5 mm resolution on a 0.25 m x 0.25 m area. To achieve the similar output using SfM technique, the required images can be acquired in few minutes and can be processed to produce 3D models within a couple of hours. Additionally, SfM technique is capable of producing better detailed 3D surface since images can be taken from various angles and distances unlike the laser-based measurements with limited measurement angles. The SfM technique has the potential to bridge the spatial scales between detailed measurement of small areas and coarser large-scale measurements [23]. However, SfM technique has some shortcomings like: majority of the users are not aware of the fundamental mathematics behind it; the accuracy of final output is hugely affected by lighting conditions during photography; difficulty in reproducing smooth or transparent surfaces with indistinct features/textures [22,24–26]. SfM technique have been widely applied in field-scale terrestrial surveying [27,28], geosciences [9,10,15,17,29], archaeology [30–33] and also in robotics [34–36], real estate and even in film productions. A few researchers have used it to study fluvial geomorphology in laboratory flumes and physical river models [3,37–43].

This study presents the evaluation of SfM technique in different model scale case studies to record 3-dimensional bed topography for different stages of tests and to quantify the extent and volume of change in riverbed topography in each case studies. In this study, images were acquired using handheld photography, instead of using camera installed in fixed orientation on moving trolleys, to reduce the logistical cost and image acquisition time. With handheld photography, it is also possible to put more focus on important details by taking images from different angles and distances specially in irregular shaped physical river models. The objective of this study is to evaluate the applicability of SfM technique with close range handheld photography in physical hydraulic model studies to capture 3D topography for each test event and to quantify the changes in riverbed topography. The applicability of SfM technique was evaluated by comparing the accuracy of 3D point clouds produced using SfM technique against the manual measurement data acquired using conventional surveying techniques.

2. Method

2.1. Ground Control Points (GCPs) and Georeferencing

The 3D model produced by SfM technique is created based on relative spatial relationships among locations of extracted feature points on multiple images taken from different viewpoints [19]. Therefore, the 3D model output preserves the shape of the target object but the size is arbitrarily scaled [44]. Hence, georeferencing of the 3D model output shall be done by transforming it to original scaling and

coordinates in reference to a set of pre-defined ground control points (GCPs). The GCPs with known coordinates shall be marked on the model before capturing the images. The accuracy in defining these GCPs is crucial to avoid structural errors in resulting 3D models [15]. The structural errors are caused by erroneous scaling of the 3D model output in reference to the inaccurately defined control points. For better results, the GCPs should be distributed in such a way that it covers all the concerned area [45]. Micheletti [19] recommended to use at least 5 GCPs. The accuracy of output 3D model can be increased by increasing the number of GCPs [46] since the accuracy in reproducing elevations in 3D model output increases with decreasing distance to GCPs [47]. For better accuracy in 3D model output, each GCP should be visible in at least three images from different viewpoints [9]. It is recommended to define GCPs beforehand and then process the images for generating 3D model output in actual scaling and coordinates. However, it is also possible to produce a 3D model output in arbitrary scaling and coordinates and then transform it into original scaling and coordinates by using rotation, translation and scaling in reference to the GCPs. If the camera captures geotagged images, then the GCPs are not required but the accuracy of results may not be satisfactory for small scale objects [48]. Although scale river models were used in this study, the GCPs were defined with actual prototype coordinates to avoid ambiguities. Hence, the 3D model outputs were generated in original prototype scaling and coordinates.

2.2. Image Acquisition

A Sony α 6300 (model ILCE-6300) camera was used for capturing images for the study. It was a mirrorless digital camera with 24-megapixel Exmor RS sensor and 425 phase detection autofocus points. For flexibility and time saving in image acquisition, the camera was operated in hand-held condition without using tripods or trolleys. Since handheld camera operation is prone to camera shaking at lower shutter speed resulting blurry images, the maximum exposure time (associated with slowest shutter speed) was kept below 1/100 sec to avoid ‘motion blur’ effect in images due to camera shaking. The camera’s aperture was allowed to vary for optimum image exposure under the normal laboratory lighting condition, which resulted in camera aperture ranging from F9 to F11. The focal length of the camera lens was fixed at 16 mm. With these settings, the camera was operated in handheld condition to capture sets of overlapping images from varying viewpoints and orientations covering the whole study area. Additional closeup images of important features were taken from different angles to achieve better detailing.

2.3. Digital Photogrammetry

Nowadays various commercial and free software are available to cater the implementation of SfM technique in different applications. Based on the comparison among different SfM software made in [49], Agisoft Photoscan was selected for this study. Agisoft Photoscan (now available as Agisoft Metashape) is a commercial software developed by Agisoft LLC, Russia. It is a complete package loaded with all the capabilities from processing images to generating 3D models in form of a dense point cloud, a mesh and a Digital Elevation Model (DEM). It also includes additional pre-processing and post processing features. It is capable of processing both aerial and close-range photographs, and is efficient in both controlled and uncontrolled conditions. The software has a linear project-based workflow [8] consisting of: feature matching and aligning photographs; building dense point cloud; building mesh; generating texture; and exporting results [50]. In this study, dense point clouds and DEMs were generated with Photoscan. The quality of dense point clouds designated as Ultra high, High, Medium, Low and Lowest can be selected in Photoscan to specify the desired reconstruction quality. Mentioned quality settings were relative to the resolution of original input images and it provides the users to keep a balance between the quality of output and the processing time. In this study, we have used “medium” and “high” quality settings for different case studies. The DEMs were then exported to compute volume between two point-cloud surfaces using 2.5D volume computation tool in ‘CloudCompare’ software.

The total processing time is largely determined by specification of the workstation used and the extent of the study area. In this study, a workstation with Intel® Core™ i7-4790 CPU @3.60GHz processor, 32 GB RAM and 18 GB NVIDIA GeForce GTX 750 Ti GPU was used.

2.4. Manual Measurements

Manual measurements of a few cross-sections were also carried out in the physical models using a level machine, a staff gauge and a distance measuring bar with an accuracy of ± 1 mm. These data were used for comparison with the corresponding cross-section profiles extracted from the 3D model outputs by SfM technique. In addition, a few distances between random pairs of the established GCPs were also measured manually to assess the accuracy of SfM output models.

3. Case Studies

3.1. Case Study I: Measurement of Changes in Bed Morphology

In case study I, the SfM technique was applied to record changes in bed morphology during a physical model study. The objective of the model study was to simulate evolution of river bed morphology during high sediment transport event and to create a database to validate a 1D numerical model developed for simulating river morphology in sediment laden rivers. The study was conducted on a physical hydraulic model representing 1 km long reach of Trishuli River in Nepal (Figure 1). Trishuli River is a typical Himalayan river with steep bed gradient which becomes relatively flatter after it crosses Betrawati. The selected river reach has an average bed slope of about 1:200 and consists of a sharp bend. The particular reach was chosen for the study since evolution of river bed morphology is prominent in reaches with flatter bed gradient and with bends.

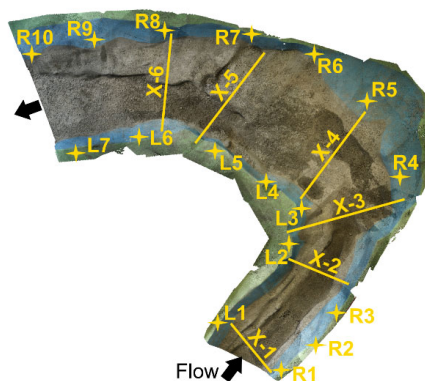


Figure 1. Trishuli River model with locations of 17 GCPs (R1-R10 in the right bank and L1-L7 in the left bank) and 6 measurement cross-sections (X-1 to X-6). The figure shows the fixed bed river model which is then filled with mobile sediment bed.

The 12.5 m long undistorted Froude scaled model at hydraulic laboratory of Hydro Lab in Nepal, representing the 1 km long reach of Trishuli river under study, was built in 1:80 scale. The modelled river channel had a fixed bed which was then filled with sand to provide a mobile bed having an average longitudinal slope of 1:200, in order to match the original bed slope in the prototype. The sand used for preparing mobile bed had median particle diameter (d_{50}) of 0.55 mm, d_{90} of 1.28 mm and geometric standard deviation (σ_g) in particle size of 1.972. Similar sediment was also fed with inlet discharge during the simulation. It is to be noted that d_{50} of the prototype sediment is about 0.1 mm which shall be represented by model sediment with $d_{50} = 1.25$ microns to fulfill the scaling requirements for an undistorted Froude model. But using such a fine sediment in the model will introduce cohesion in the sediment particles and there is possibility of alteration of sediment transport phenomena from bed load in the prototype to suspended load in the model [51]. According to Bretschneider, the particle size of sand in models should be greater than 0.5 mm [52] to avoid the scale effects due to cohesion between sediment particles and changes in flow-grain interaction characteristics. Therefore, a model sediment having $d_{50} = 0.55$ mm was used in this study. A steady discharge of 40 L/s (2290 m³/s in prototype, which is close to the magnitude of 2 years return period flood) was supplied into the model with sediment feeding at the rate of 10 kg/min which corresponds to sediment concentration of 4167 ppm in the flow. The concentration of sediment fed into the model is about 5 times of average concentration for given

discharge as estimated from the site measurement data. The experiment was run for 140 minutes (about 21 hours in prototype) only. Due to high sediment concentration and the flatter river bed gradient, most of the sediment fed with inflow discharge deposited along the channel. The effect of the river bend was clearly visible with the flow concentrating towards the outer bank (the right bank) accompanied with small scour on the initially filled sediment bed while most of the sediment fed was deposited along inner bank (the left bank). A distinct delta front was witnessed propagating to downstream direction, which can be seen in Figure 2.

The river-bed topographies of initial bed and final river bed after simulation were recorded and respective 3D dense point clouds and DEMs were produced in prototype scale with actual coordinates (meters) and elevations (in masl) using SfM technique. The quality and size of the output dense point clouds and total processing time for each stage were given in Table 1.

Table 1. Processing time and output quality for Case study I.

Stage	No. of Images	Time for feature matching and alignment	Time to create dense cloud	Time to create DEM	Quality of dense cloud	No. of vertices in Dense point cloud
Initial Bed	244	31 mins	4 hrs	18 min	medium	30.36 million
After Run	116	46 mins	49 mins	15 min	medium	23.45 million

The DEMs of initial river bed and the river bed after test run are shown in Figure 2a and Figure 2b respectively. Total 17 GCPs, 10 in the right bank (R1-R10) and 7 in the left bank (L1-L7), distributed over the study area (Figure 1) were used for georeferencing the 3D models into actual coordinates.

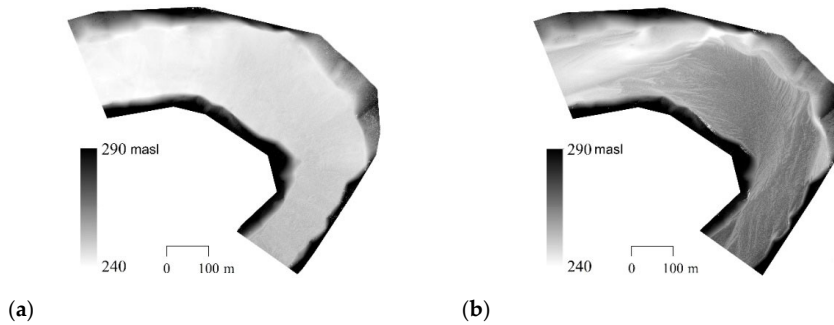


Figure 2. DEMs produced by SfM technique for Case Study I: (a) initial mobile bed; (b) final bed after test run.

The accuracy of these 3D models was investigated by estimating errors in reproducing 3D location of points, horizontal lengths and cross sections in reference to manual measurements. Figure 3 shows errors in X, Y and Z coordinates of the selected 17 GCPs in the 3D model, designated as E_x , E_y and E_z respectively. The locations of these points were reproduced in the 3D model with maximum deviation below 4 mm in each direction and the maximum resultant error (E_R) was below 5 mm. Likewise, 12 distances between random pairs of these GCPs were estimated from the 3D model and compared with respective manually measured distances (Table 2). The estimated lengths matched pretty well against respective measured distances with root mean square error (RMSE) of 1.9 mm and mean absolute error (MAE) of 1.7 mm. Moreover, 6 cross sections designated as X-1 to X-6 (Figure 1) were randomly selected over the study area and their cross-section profiles were extracted from the 3D model output for 'After run scenario'. These estimated cross sections were compared with their respective upscaled cross-section data from manual measurements in the model (Figure 4), which showed that the estimated cross sections were close to the measured cross sections and had more detailing with abundant points.

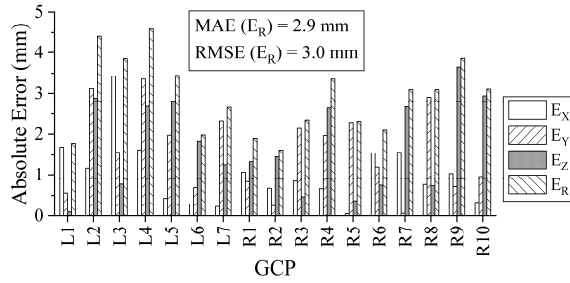


Figure 3. Estimated errors in reproduction of points in a 3D model using SfM, Case Study I. The errors are calculated in model scale.

Table 2. Estimated errors in reproduction of selected distances in the 3D model by SfM, Case Study I.

Distance between GCPs	Distance by manual measurement, mm	Distance from 3D model by SfM, mm	Absolute discrepancy, mm
LA-R1	1,879.15	1,877.00	2.2
L1-R2	1,861.60	1,862.00	0.4
L2-RA	2,466.94	2,465.00	1.9
L2-R3	2,132.04	2,135.00	3.0
L5-R5	3,793.81	3,796.00	2.2
L5-R9	3,909.81	3,912.00	2.2
L7-R10	2,594.69	2,597.00	2.3
L6-R9	2,543.95	2,544.00	0.0
L5-R7	2,893.94	2,895.00	1.1
L6-R8	2,568.95	2,571.00	2.0
L4-R6	3,245.66	3,245.00	0.7
L5-R4	4,422.73	4,425.00	2.3

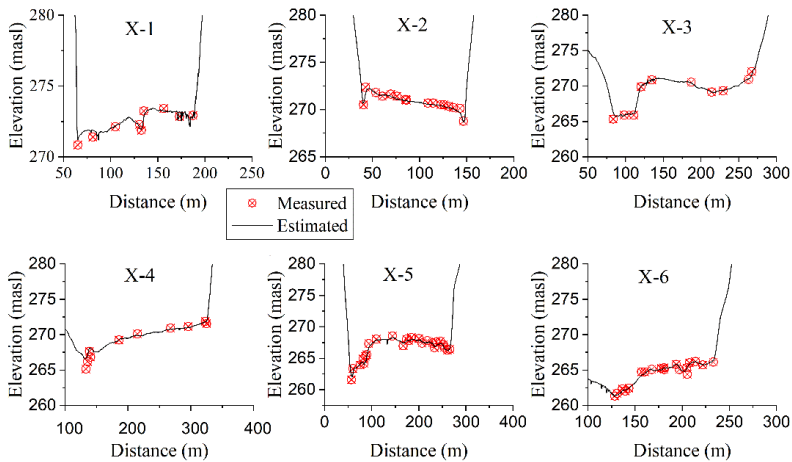


Figure 4. Plots of cross-sections estimated by SfM and manually measured cross-sections upscaled to prototype scale.

After confirming the accuracy of DEMs produced by SfM technique to be within acceptable limits, changes in volume of river bed morphology were calculated using the DEMs generated for initial bed

and after run scenarios mentioned above. At the rate of 10 kg/min for 140 mins, total 1,400 kg sediment was fed with the inflow discharge during the test. Using bulk density of the sediment to be 1,680 m³/s, the total volume of sediment added into the system during the test was calculated to be 0.833 m³. Analysing the difference between DEMs for initial bed and river bed after simulation, it showed that 0.677 m³ (out of 0.833 m³ sediment fed into the system) sediment was deposited into whereas 0.125 m³ sediment from initially filled bed was scoured out of the system; which means total 0.281 m³ of sand was transported to downstream of the modelled river reach. To check the accuracy in estimating changes in volume, the volume of sediment trapped at the outlet tank downstream of the model was measured manually using a calibrated bucket. The measured and estimated volumes in model scale were 0.292 m³ and 0.281 m³ respectively with a discrepancy of 4% only.

After the satisfactory result from the test, SfM technique was further applied in full-fledged model study in which intermediate river bed formations at different time steps during the test were also recorded in addition to the initial and final river bed. Besides measuring the changes in bed morphology precisely, SfM technique also made it possible to record the evolution of bed morphology over time by capturing the river bed at different time steps during the test. Moreover, it provided high resolution river bed data for creating mesh of initial river bed to be used in numerical modelling. It also provided high-resolution river bed data for intermediate time steps for validating the results from the numerical model.

3.2. Case study II: Evaluation of Sediment Flushing Efficiency

A physical hydraulic model of the headworks of a hydropower project in Khimti River of Nepal was selected to apply SfM technique in investigating flushing efficacy of headworks structures. Khimti River is a tributary of Tamakoshi River in Saptakoshi river basin. The Saptakoshi River is one of the tributaries of the Ganges River. The study area covered about 250 m reach of Khimti River upstream of the weir axis (Figure 5). The model was built as an undistorted fixed bed model on a scale of 1:40 using the Froude's Model Law. The headworks design consisted of a free flow type gravity weir, two bed load sluices, a side intake with eight orifices and a forebay from where water is diverted towards settling basins through two gated inlet orifices. A general arrangement of the headwork is as shown in Figure 6. Since Khimti River is a typical Himalayan river with steep gradient, the hydropower plant was designed as run-off-river type. In such headworks arrangement, the pool created upstream of the diversion weir is normally insignificant and gets filled with the incoming sediment in very short time-span of operation. So, the designed headworks arrangement should be able to flush the sediment deposits around the intake area in order to avoid entry of bed sediments into the intakes. Regarding this, one of the main objectives of the model study was to ensure the capability of flushing gates to clean the deposited sediments from area around the intake upstream of the diversion weir. Since the partial opening of flushing gates in normal operation condition could not stop sedimentation in front of intakes, free flushing with annual flood discharge was tested in the model.

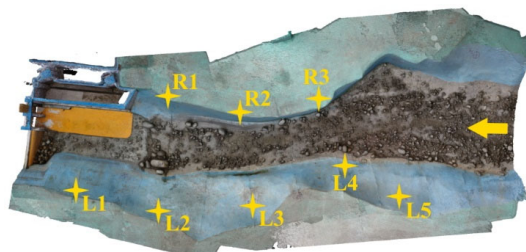


Figure 5. Khimti River model with location of 8 GCPs (R1-R3 in the right bank and L1-L5 in the left bank). The figure shows the fixed bed river model which is then filled with mobile sediment bed.

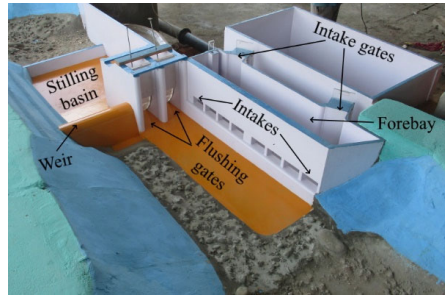


Figure 6. Headworks structure arrangement under study, Case study II

In order to speed up the sedimentation process, the river upstream of the weir was initially filled with bed sediment up to the sill level of intake orifices. The sand used for representing the bed load had median particle diameter (d_{50}) of 1.5 mm, $d_{10} = 0.5$ mm and $d_{90} = 10$ mm. The sediment fed with the inflow discharge during the test also had the same composition. The model was run under normal operating conditions for 12 minutes (1.3 hours in prototype) simulating a river discharge of 14.4 L/s (equivalent to annual flood with the magnitude of 146 m³/s in prototype) with sediment feeding at the rate of 0.580 kg/min which corresponds to sediment concentration of 671 ppm in the flow. Then both flushing gates were opened to allow free gravity flushing of the bed sediment with the annual flood discharge for 38 minutes (4 hours in prototype). Initial bed before flushing and final bed after flushing were photographed and a dense point cloud for each scenario was produced in prototype scale using SfM technique in reference to 8 GCPs defined over the study area. The quality and size of dense point clouds produced with their respective processing times are presented in Table 3. The DEMs generated from the dense point clouds of the two scenarios are shown in Figure 7.

Table 3. Processing time and output quality for Case study II.

Stage	No. of Images	Time for feature matching and alignment	Time to create dense cloud	Time to create DEM	Quality of dense cloud	No. of vertices in Dense point cloud
Initial Bed	61	6 min	57min	9 min	medium	13.21 Million
After Run	74	14 min	1 hr 7 min	11 min	medium	16.13 Million

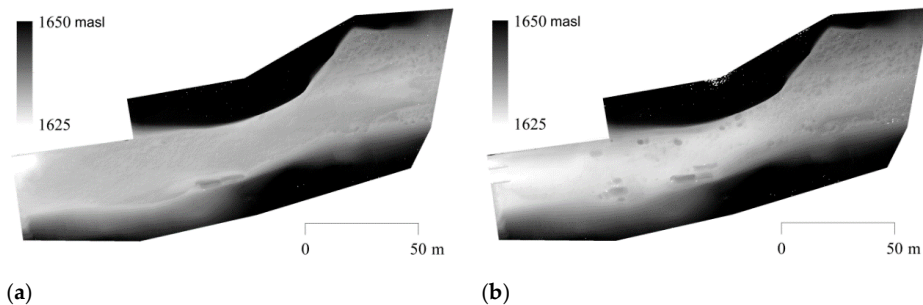


Figure 7. DEMs produced by SfM technique for Case Study II: (a) initial mobile bed; (b) final bed after flushing test.

Errors in reproducing both the locations of GCPs and linear distances were calculated to be below 2 mm in the model as shown in Figure 8 and Table 4 respectively. Finally, flushing scenario was quantified by analysing the dense point clouds in CloudCompare software. Evaluating volume changes

among dense point clouds for given scenarios, about 88% of sum of deposited sediment volume and volume of sediment fed was found to be flushed successfully keeping the area around the intake clean from sediment deposits. The flushed volume of sediment was estimated as a volume difference between dense cloud for initial bed before flushing and that for final bed after flushing in addition to the volume of sediment fed during the experiment. The estimated flushed volume of sediment in model scale was 0.1602 m^3 against the measured volume of 0.162 m^3 with only 1% of discrepancy.

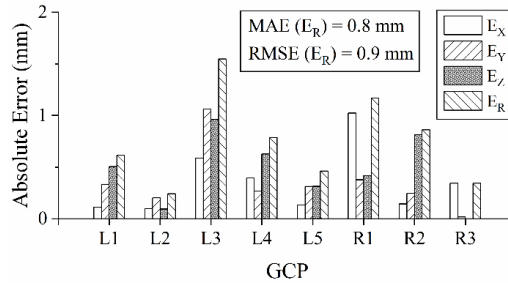


Figure 8. Estimated errors in reproduction of points in a 3D model using SfM, Case Study II. The errors were estimated in model scale

Table 4. Estimated errors in reproduction of selected distances in the 3D model by SfM, Case Study II.

Distance between GCPs	Distance by manual measurement, mm	Distance from 3D model by SfM, mm	Absolute discrepancy, mm
L1-R1	1,550.35	1,550.0	0.35
L2-R1	1,326.82	1,328.0	1.18
L4-R3	1,121.20	1,121.0	0.20
L5-R5	1,858.53	1,857.0	1.53
L2-R5	4,101.46	4,100.0	1.46
R1-R2	851.83	852.0	0.17
R2-R3	911.97	913.0	1.03

In this way, the SfM technique helped to precisely quantify the bed control near intake structure in physical model studies. The SfM technique was also useful in recording spatial distribution of the sediment deposits remained upstream of the headworks after flushing, which was very useful information for the designer to identify the passive zones not cleaned by the flushing operation and to further modify, if required, the components of headworks structure to improve its overall performance. However, in this test the flushing operation was satisfactorily successful as 88% of the sediment were flushed downstream and the area around the intake was clean of sediment deposit.

3.3. Case study III: Measurement of Flushing Cone Volume

Finally, the SfM technique was applied on small scale flume experiments to investigate scour holes, commonly called as flushing cones, created by pressurized flushing of sediment deposit through a bottom outlet under steady flow conditions. The experimental setup consisted of a 0.6 m wide horizontal flume with a 50 mm wide rectangular orifice, the opening height of which was variable, at the centre of the flume. The sill of the orifice was 60 mm above the flume bed. A 120 mm thick layer of plastic grains representing sediment in the model were filled before the tests. Then a desired discharge was supplied into the flume without disturbing the filled sediment layer. When the water surface reached desired level, the bottom outlet was opened for desired opening height, which was meant to maintain the selected water level for the selected discharge, and pressurized flushing of the deposits were allowed to form a flushing cone. Once the flushing cone upstream of the outlet reached an equilibrium, the gate was closed and the flume was drained slowly without disturbing the cone. Then the flushing cone was measured manually with a millimeter precise point gauge as well as using SfM

technique. Total 7 tests were carried out for different combination of discharge, water level and opening height of the outlet as listed in Table 5.

Since it was a small-scale flume test, high quality dense clouds were produced expecting better accuracy. For example, the dense point cloud for Test no. 3 is shown in Figure 9. The contour plot of flushing cone for Test no. 3 produced by SfM superimposed on that produced by manual measurements is presented in Figure 10. It shows that the flushing cone reproduced with SfM technique is comparable against the one produced by manual measurement.



Figure 9. Dense point cloud of flushing cone for Test no. 3, Case study III

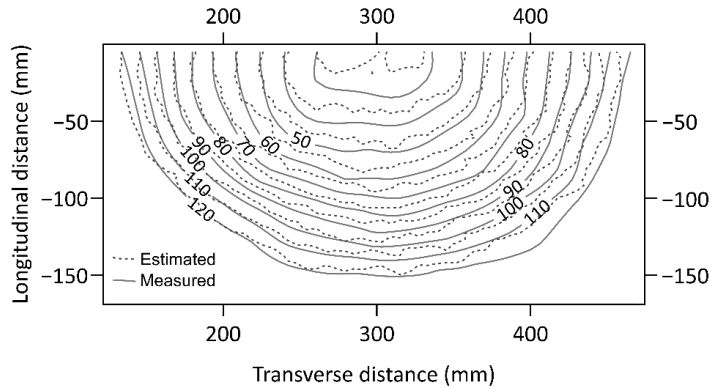


Figure 10. Contour plots for Test no. 3 by SfM estimation and Manual measurement in model scale, Case study III

The size of dense point cloud for each test and their respective processing time is shown in Table 6. The volumes of flushing cones measured manually were compared with volumes of respective cones estimated by SfM technique as shown in Table 5. The absolute discrepancy between measured and estimated volumes for all the tests were below 5% of the measured volume.

Table 5. Boundary conditions and measured volume of flushing cone for tests conducted in Case Study III.

Test no.	Discharge, L/s	Water level, mm	Outlet's opening height, mm	Volume of flushing cone, $\times 10^6 \text{ mm}^3$		Absolute Discrepancy %
				Manual measurement	Measured from 3D model by SfM	
1	2.5	244	40	1.31	1.27	3.05
2	3.2	352	40	1.54	1.54	0.00
3	3.9	455	40	1.72	1.78	3.49
4	4.3	570	40	1.80	1.77	1.67
5	3.2	264	50	1.48	1.41	4.73
6	3.8	327	50	1.63	1.67	2.45
7	5.0	502	50	1.98	1.99	0.51

Table 6. Processing time and output quality for Case study III

Test no.	No. of Images	Total processing time to create dense cloud (hh:mm:ss)	Quality of dense cloud	Points in dense cloud (in millions)
1	18	00:48:27	high	13.7
2	24	01:08:21	high	15.5
3	18	00:31:38	high	12.6
4	28	01:11:44	high	15.3
5	22	01:03:15	high	14.3
6	30	02:54:23	high	15.8
7	27	02:08:32	high	18.6

After achieving satisfactory precision from the SfM technique for such experiments, it was further applied in similar tests to produce high resolution point clouds of flushing cones which was utilized for precisely estimating dimensions and volume of flushing cones. A number of tests were carried out with varying water level, discharge, opening height of outlet, thickness of sediment deposit and density of sediment materials. The results from the experiments were used to develop empirical relations to predict the length and volume of flushing cone for relevant input parameters.

4. Discussion of Results

The overall accuracy of SfM technique was estimated to be below 5 mm for reproducing location of points and below 3 mm for estimating distance measurements in the model. Between two models in case study I and case study II, accuracy of SfM reproduced models was found to be coarser for bigger model. It can be justified with expected precision of derived elevations as defined by Lane [3]:

$$precision (p) = \frac{\text{physical size of pixel in image space } (d_e)}{\text{focal length } (c)/\text{camera flying height } (H)} \quad (1)$$

With $d_e = 4 \mu\text{m}$ and $c = 16 \text{ mm}$, the expected vertical precision for case study I and II were 0.45 mm and 0.3 mm for camera flying height of 1.79 m and 1.25 m respectively. According to Lane [3], the best possible spatial resolution is about 5 times coarser than p . From Equation (1), it can be concluded that the precision will be reduced for bigger model since camera flying height need to be increased to cover bigger area considering same camera with similar settings is used. Morgan et al [37] also concluded that the decrease in model point count with respect to increase in distance between camera and subject follows a power law having the exponent value of approximately 2.15. The other way around to achieve output model with better accuracy is to take more pictures with lower camera flying height but it will increase the time required for image acquisition and processing.

The precision in estimating volume changes was found to be better (below 5% of measured values), most probably due to compensation of errors while subtracting two 3D models (dense point clouds or DEMs). The applicability of SfM method hence depends on acceptable error or discrepancy, which in turn is governed by scale factor for the model, objective of the model study and measurement techniques available as alternative. Analysing the results of this study, it can be concluded that SfM is a quick, economic and comparatively accurate alternative for manual measurements in the model study. The acceptability of the precision of SfM technique is entirely subjective. The same precision could be acceptable for large scale models while on the other hand it might be unacceptable for small-scale models. Besides scale factor, acceptable precision is also limited by purpose of the model study. For model studies with objectives to assess bed evolution pattern (case study I) and to estimate sediment budget (case study II and III), the achieved precision in each case studies seemed to be satisfactory. Since manual measurement with staff gauges of 1 mm precision was the only low-cost alternative available in our laboratory to SfM technique, RMSE error of 1.9 mm in output dense cloud (in model scale) is satisfactory provided with the fact that SfM technique was quicker and reproduced better detailing of important features.

The major advantage of SfM technique over manual measurement is the detailing captured as colour-coded dense point cloud. In general practice with manual measurements, only a few cross sections are selected over the study area for conducting measurements and the measured data are

interpolated in-between. In such case, there is always possibility of loss or even mis-interpretation of detailing in between the measured cross sections. For example, in case study I, the front of sediment deposition was continuously moving downstream. If the deposition front was in between two measurement cross sections for a certain time step, then interpolation of manually measured two cross-section profiles upstream and downstream of that deposition front will not represent the actual pattern. Therefore, for mobile bed model studies with an objective to study patterns of bed evolution, SfM technique can ensure higher detailing of the river bed reproduced in 3D model output. Additionally, SfM technique can be highly beneficial to capture the time-evolution of the river bed morphology by taking set of photographs at certain intervals of model run time. It can save a significant amount of time compared to measurements carried out with manual instrumentation. Though processing time for SfM technique could extend up to couple of hours, e.g., more than 4 hours for producing 3D dense point cloud of initial filled bed in Case study I as shown in Table 1, actual man-hour used will be much lower since the image processing up to production of 3D models can be fully automatized. Moreover, the total processing time can also be reduced considerably by targeting low or medium quality of dense point cloud yet ensuring the quality of result will not be compromised.

The results from all three case studies (see Tables 1, 3 and 6) showed that the image processing time in SfM is not proportional to the number of images to be processed. While doing trials to produce 3D models of different quality (low, medium and high), it was observed that the processing time for same set of images increased as the desired output (dense point cloud) quality was set from low to medium and then to high.

5. Conclusions

SfM photogrammetry technique was successfully applied in three different model studies to estimate changes in mobile river bed. Free handheld photography was used for acquiring images which reduced the logistical cost for camera support setup and also reduced the image acquisition time. The 3D models in form of dense point clouds were produced with satisfactory precision against manual measurement using lesser time and human resources. Hence, SfM is recommended as a low-cost and quicker alternative to manual measurements in physical hydraulic models. However, the selection of measurement technique is always a trade-off between desired precision, time spent for measurement and data analysis, and total budget (cost) incurred.

Author Contributions: Conceptualization: N.R., S.K.K.; Methodology: S.K.K., U.S.; Resources: N.R., M.B.B.; Investigation: S.K.K., U.S.; Formal analysis: S.K.K., U.S.; Software: S.K.K., U.S.; Validation: N.R.; Visualization: S.K.K., U.S.; Data curation: S.K.K., U.S.; Writing-original draft: S.K.K.; Writing-review & editing: S.K.K.; Supervision: N.R.; Project administration: N.R., M.B.B.; Funding acquisition: N.R., M.B.B. All authors have read and agreed to the published version of the manuscript.

Funding: This research was funded by The Research Council of Norway, Hydro Lab, Statkraft and the Norwegian Hydropower Center (NVKS).

Institutional Review Board Statement: Not applicable

Informed Consent Statement: Not applicable

Data Availability Statement: 3rd Party Data

Acknowledgments: We would like to thank all the technicians and colleagues at Hydro Lab, Nepal for the help and support during the study.

Conflicts of Interest: The authors declare no conflict of interest.

References

1. Aberle, J.; Rennie, C.D.; Admiraal, D.M.; Muste, M. *Experimental Hydraulics: Methods, Instrumentation, Data Processing and Management: Volume II: Instrumentation and Measurement Techniques*, 1st ed.; Aberle, J., Rennie, C., Admiraal, D., Muste, M., Eds.; CRC Press: Boca Raton, FL, USA, 2017. ISBN 978-1-315-15892-1.
2. Lane, S.N.; Richards, K.S.; Chandler, J.H. Developments in Photogrammetry; the Geomorphological Potential. *Prog. Phys. Geogr. Earth Environ.* **1993**, *17*, 306–328, doi:10.1177/030913339301700302.
3. Lane, S.N.; Chandler, J.H.; Porfiri, K. Monitoring River Channel and Flume Surfaces with Digital Photogrammetry. *J. Hydraul. Eng.* **2001**, *127*, 871–877, doi:10.1061/(ASCE)0733-9429(2001)127:10(871).

4. Chandler, J.H.; Shiono, K.; Rameshwaren, P.; Lane, S.N. Measuring Flume Surfaces for Hydraulics Research Using a Kodak DCS460. *Photogramm. Rec.* **2001**, *17*, 39–61, doi:10.1111/0031-868X.00167.
5. Smith, M.W.; Carrivick, J.L.; Quincey, D.J. Structure from Motion Photogrammetry in Physical Geography. *Prog. Phys. Geogr.* **2016**, *40*, 247–275, doi:10.1177/0309133315615805.
6. Skarlatos, D.; Kiparissi, S. Comparison of Laser Scanning, Photogrammetry and SFM-MVS Pipeline Applied in Structures and Artificial Surfaces. *ISPRS Ann. Photogramm. Remote Sens. Spat. Inf. Sci.* **2012**, *1–3*, 299–304, doi:10.5194/isprsannals-1-3-299-2012.
7. Remondino, F.; El-Hakim, S. Image-Based 3D Modelling: A Review. *Photogramm. Rec.* **2006**, *21*, 269–291, doi:10.1111/j.1477-9730.2006.00383.x.
8. Acuna, M.; Sosa, A. Automated Volumetric Measurements of Truckloads through Multi-View Photogrammetry and 3D Reconstruction Software. *Croat. J. For. Eng. J. Theory Appl. For. Eng.* **2019**, *40*, 151–162.
9. Westoby, M.J.; Brasington, J.; Glasser, N.F.; Hambrey, M.J.; Reynolds, J.M. ‘Structure-from-Motion’ Photogrammetry: A Low-Cost, Effective Tool for Geoscience Applications. *Geomorphology* **2012**, *179*, 300–314, doi:10.1016/j.geomorph.2012.08.021.
10. Favalli, M.; Fornaciai, A.; Isola, I.; Tarquini, S.; Nannipieri, L. Multiview 3D Reconstruction in Geosciences. *Comput. Geosci.* **2012**, *44*, 168–176, doi:10.1016/j.cageo.2011.09.012.
11. Wu, C. Towards Linear-Time Incremental Structure from Motion. In Proceedings of the 2013 International Conference on 3D Vision—3DV 2013, Seattle, WA, USA, 29 June–1 July 2013; pp. 127–134.
12. Eltner, A.; Sofia, G. Structure from motion photogrammetric technique. In *Developments in Earth Surface Processes*; Elsevier, 2020; Vol. 23, pp. 1–24, ISBN 978-0-444-64177-9, doi: 10.1016/B978-0-444-64177-9.00001-1
13. Smith, M.W.; Vericat, D. From Experimental Plots to Experimental Landscapes: Topography, Erosion and Deposition in Sub-Humid Badlands from Structure-from-Motion Photogrammetry. *Earth Surf. Process. Landf.* **2015**, *40*, 1656–1671, doi:10.1002/esp.3747.
14. Snavely, K.N. Scene Reconstruction and Visualization from Internet Photo Collections. Ph.D. Thesis, University of Washington, Seattle, WA, USA, 2009.
15. James, M.R.; Robson, S. Straightforward Reconstruction of 3D Surfaces and Topography with a Camera: Accuracy and Geoscience Application. *J. Geophys. Res. Earth Surf.* **2012**, *117*, F03017, doi:10.1029/2011JF002289.
16. Goesele, M.; Snavely, N.; Curless, B.; Hoppe, H.; Seitz, S.M. Multi-View Stereo for Community Photo Collections. In Proceedings of the 2007 IEEE 11th International Conference on Computer Vision, Rio de Janeiro, Brazil, 14–21 October 2007; pp. 1–8.
17. James, M.R.; Chandler, J.H.; Eltner, A.; Fraser, C.; Miller, P.E.; Mills, J.P.; Noble, T.; Robson, S.; Lane, S.N. Guidelines on the Use of Structure-from-Motion Photogrammetry in Geomorphic Research. *Earth Surf. Process. Landf.* **2019**, *44*, 2081–2084, doi:10.1002/esp.4637.
18. Szabó, G.; Bertalan, L.; Barkóczy, N.; Kovács, Z.; Burai, P.; Lénárt, C. Zooming on Aerial Survey. In *Small Flying Drones: Applications for Geographic Observation*; Casagrande, G., Sik, A., Szabó, G., Eds.; Springer International Publishing: Cham, Switzerland, 2018; pp. 91–126. ISBN 978-3-319-66577-1.
19. Micheletti, N.; Chandler, J.; Lane, S.N. Structure from Motion (SFM) Photogrammetry. In *Geomorphological Techniques (Online Edition)*; Cook, S.J., Clarke, L.E., Nield, J.M., Eds.; British Society for Geomorphology: London, UK, 2015.
20. Lane, S.N. The Measurement of River Channel Morphology Using Digital Photogrammetry. *Photogramm. Rec.* **2000**, *16*, 937–961, doi:10.1111/0031-868X.00159.
21. Hartley, R.; Zisserman, A. *Multiple View Geometry in Computer Vision*, 2nd ed.; Cambridge University Press: Cambridge, UK, 2004. ISBN 978-0-521-54051-3.
22. Leduc, P.; Peirce, S.; Ashmore, P. Short Communication: Challenges and Applications of Structure-from-Motion Photogrammetry in a Physical Model of a Braided River. *Earth Surf. Dyn.* **2019**, *7*, 97–106, doi:10.5194/esurf-7-97-2019.
23. Carrivick, J.L.; Smith, M.W. Fluvial and Aquatic Applications of Structure from Motion Photogrammetry and Unmanned Aerial Vehicle/Drone Technology. *Wiley Interdiscip. Rev. Water* **2019**, *6*, e1328, doi:10.1002/wat2.1328.
24. Alfredsen, K.; Haas, C.; Tuhtan, J.A.; Zinke, P. Brief Communication: Mapping River Ice Using Drones and Structure from Motion. *Cryosphere* **2018**, *12*, 627–633, doi:10.5194/tc-12-627-2018.
25. Atkinson, K. *Close Range Photogrammetry and Machine Vision*; Whittles Publ.: Dunbeath, UK, 1996.
26. Bemis, S.P.; Micklethwaite, S.; Turner, D.; James, M.R.; Akciz, S.; Thiele, S.T.; Bangash, H.A. Ground-Based and UAV-Based Photogrammetry: A Multi-Scale, High-Resolution Mapping Tool for Structural Geology and Paleoseismology. *J. Struct. Geol.* **2014**, *69*, 163–178, doi:10.1016/j.jsg.2014.10.007.
27. Mancini, F.; Dubbini, M.; Gattelli, M.; Stecchi, F.; Fabbri, S.; Gabbianelli, G. Using Unmanned Aerial Vehicles (UAV) for High-Resolution Reconstruction of Topography: The Structure from Motion Approach on Coastal Environments. *Remote Sens.* **2013**, *5*, 6880–6898, doi:10.3390/rs5126880.
28. Gindraux, S.; Boesch, R.; Farinotti, D. Accuracy Assessment of Digital Surface Models from Unmanned Aerial Vehicles’ Imagery on Glaciers. *Remote Sens.* **2017**, *9*, 186, doi:10.3390/rs9020186.

29. Micheletti, N.; Chandler, J.H.; Lane, S.N. Investigating the Geomorphological Potential of Freely Available and Accessible Structure-from-Motion Photogrammetry Using a Smartphone. *Earth Surf. Process. Landf.* **2015**, *40*, 473–486, doi:10.1002/esp.3648.
30. Abdelaziz, M.; Elsayed, M. Underwater Photogrammetry Digital Surface Model (DSM) of the Submerged Site of the Ancient Lighthouse Near Qaitbay Fort In Alexandria, Egypt. *Int. Arch. Photogramm. Remote Sens. Spat. Inf. Sci.* **2019**, *XLII-2/W10*, 1–8, doi:10.5194/isprs-archives-XLII-2-W10-1-2019.
31. Jones, C.A.; Church, E. Photogrammetry Is for Everyone: Structure-from-Motion Software User Experiences in Archaeology. *J. Archaeol. Sci. Rep.* **2020**, *30*, 102261, doi:10.1016/j.jasrep.2020.102261.
32. Sapirstein, P.; Murray, S. Establishing Best Practices for Photogrammetric Recording During Archaeological Fieldwork. *J. Field Archaeol.* **2017**, *42*, 337–350, doi:10.1080/00934690.2017.1338513.
33. Lerma, J.L.; Muir, C. Evaluating the 3D Documentation of an Early Christian Upright Stone with Carvings from Scotland with Multiples Images. *J. Archaeol. Sci.* **2014**, *46*, 311–318, doi:10.1016/j.jas.2014.02.026.
34. Andreff, N.; Horaud, R.; Espiau, B. Robot Hand-Eye Calibration Using Structure-from-Motion. *Int. J. Robot. Res.* **2001**, *20*, 228–248, doi:10.1177/02783640122067372.
35. Schmidt, J.; Vogt, F.; Niemann, H. Calibration-Free Hand-Eye Calibration: A Structure-from-Motion Approach. In *Pattern Recognition*; Kropatsch, W.G., Sablatnig, R., Hanbury, A., Eds.; Springer: Berlin/Heidelberg: Germany, 2005; Volume 3663, pp. 67–74. ISBN 978-3-540-28703-2.
36. Heller, J.; Havlena, M.; Sugimoto, A.; Pajdla, T. Structure-from-Motion Based Hand-Eye Calibration Using L_∞ Minimization. In Proceedings of the CVPR 2011, Colorado Springs, CO, USA, 20–25 June 2011; pp. 3497–3503.
37. Morgan, J.A.; Brogan, D.J.; Nelson, P.A. Application of Structure-from-Motion Photogrammetry in Laboratory Flumes. *Geomorphology* **2017**, *276*, 125–143, doi:10.1016/j.geomorph.2016.10.021.
38. Balaguer-Puig, M.; Marqués-Mateu, A.; Lerma, J.L.; Ibáñez-Asensio, S. Estimation of Small-Scale Soil Erosion in Laboratory Experiments with Structure from Motion Photogrammetry. *Geomorphology* **2017**, *295*, 285–296, doi:10.1016/j.geomorph.2017.04.035.
39. Hwang, K.S.; Hwang, H.H.; Shi, B.T. Applying Photogrammetry in Laboratory Bathymetry Measurement; In Proceedings of the 13th Asian Symposium on Visualisation, Novosibirsk, Russia, 22–26 June 2015.
40. Di Bacco, M.; Scorzini, A.R. Experimental Analysis on Sediment Transport Phenomena in Channels Equipped with Inclined Side Weirs. In Proceedings of the Proceedings of the 8th IAHR International Symposium on Hydraulic Structures ISHS2020, The University of Queensland, Santiago, Chile, 1 January 2020.
41. Ferreira, E.; Chandler, J.; Wackrow, R.; Shiono, K. Automated Extraction of Free Surface Topography Using SfM-MVS Photogrammetry. *Flow Meas. Instrum.* **2017**, *54*, 243–249, doi:10.1016/j.flowmeasinst.2017.02.001.
42. van Scheltinga, R.C.T.; Coco, G.; Kleinhans, M.G.; Friedrich, H. Observations of Dune Interactions from DEMs Using Through-Water Structure from Motion. *Geomorphology* **2020**, *359*, 107126, doi:10.1016/j.geomorph.2020.107126.
43. Kasprak, A.; Wheaton, J.M.; Ashmore, P.E.; Hensleigh, J.W.; Peirce, S. The Relationship between Particle Travel Distance and Channel Morphology: Results from Physical Models of Braided Rivers. *J. Geophys. Res. Earth Surf.* **2015**, *120*, 55–74, doi:10.1002/2014JF003310.
44. Yang, M.-D.; Chao, C.-F.; Huang, K.-S.; Lu, L.-Y.; Chen, Y.-P. Image-Based 3D Scene Reconstruction and Exploration in Augmented Reality. *Autom. Constr.* **2013**, *33*, 48–60, doi:10.1016/j.autcon.2012.09.017.
45. Chandler, J. Effective application of automated digital photogrammetry for geomorphological research. *Earth Surf. Process. Landf.* **1999**, *24*, 51–63, doi:10.1002/(SICI)1096-9837(199901)24:1<51::AID-ESP948>3.0.CO;2-H.
46. Oniga, V.-E.; Breaban, A.-I.; Statescu, F. Determining the Optimum Number of Ground Control Points for Obtaining High Precision Results Based on UAS Images. *Proceedings* **2018**, *2*, 352, doi:10.3390/eers-2-05165.
47. Tonkin, T.; Midgley, N. Ground-Control Networks for Image Based Surface Reconstruction: An Investigation of Optimum Survey Designs Using UAV Derived Imagery and Structure-from-Motion Photogrammetry. *Remote Sens.* **2016**, *8*, 786, doi:10.3390/rs8090786.
48. Turner, D.; Lucieer, A.; Wallace, L. Direct Georeferencing of Ultrahigh-Resolution UAV Imagery. *IEEE Trans. Geosci. Remote Sens.* **2014**, *52*, 2738–2745, doi:10.1109/TGRS.2013.2265295.
49. Karmacharya, S.K.; Bishwakarma, M.; Shrestha, U.; Rüther, N. Application of ‘Structure from Motion’ (SfM) Technique in Physical Hydraulic Modelling. *J. Phys. Conf. Ser.* **2019**, *1266*, 012008, doi:10.1088/1742-6596/1266/1/012008.
50. Agisoft. *Agisoft PhotoScan User Manual—Standard Edition, Version 1.4*; Agisoft LLC: St. Petersburg, Russia, 2018; p. 66.
51. Kamphuis, J.W. Practical Scaling of Coastal Models. *Coast. Eng. Proc.* **1974**, 121–121, doi:10.9753/icce.v14.121.
52. Kobus, H. *Hydraulic Modelling*; German Association for Water Research and Land Development: Berlin, Germany, 1980.

Paper III

**Physical modelling of pressurized flushing of non-cohesive sediment using
lightweight material**

Sanat Kumar Karmacharya, Pierre-Yves Henry, Meg Bishwakarma, Jochen Aberle,
Nils Rüther

CRHT IX, 2019, Journal of Physics: Conference Series 1266 012012

Physical modelling of pressurized flushing of non-cohesive sediment using lightweight material

Sanat Kumar Karmacharya^{1,2}, Pierre-Yves Henry¹, Meg Bishwakarma²,
Jochen Aberle^{1,3} and Nils R  ther^{*1}

¹Department of Civil and Environmental Engineering, NTNU, Trondheim, Norway

²Hydro Lab Pvt. Ltd., Lalitpur, Nepal

³Leichtweiß-Institut f  r Wasserbau, Technische Universit  t Braunschweig, Germany

* Corresponding author (nils.r  ther@ntnu.no)

Abstract. In this study, pressurized flushing of non-cohesive reservoir sediment through a bottom orifice was simulated in laboratory experiments using lightweight material as model sediment. The experiments were carried out by varying flushing discharge, reservoir water level, thickness of sediment deposit layer and opening height of bottom orifice. The volumes of flushing cones formed with lightweight material were compared with volumes calculated using empirical relations proposed by past studies. The good trend observed in variation of dimensionless flushing cone volume against different dimensionless parameters justified the possibility of using the lightweight material as model sediment.

1. Introduction

Reservoir sedimentation is a world-wide problem threatening the capacity and sustainability of large dams. To encounter the sedimentation of reservoirs, several counter and mitigation measures have been proposed ranging from the reduction of the sediment yield in the upstream catchment to hydraulic flushing to scour out deposits and empty the reservoir through low-level outlets [1,2]. Pressurized flushing through bottom outlets scours sediment deposits locally in the vicinity of the outlet openings and creates a funnel shaped crater called flushing cone (also called flushing half-cone because of its shape) [3,4]. During this process, large amounts of sediment are released at the beginning of the flushing [5] and after a short period of time the flushing cone becomes fairly stable in shape and size with no further sediment removal from the cone [6]. This type of flushing is therefore only suitable for reservoirs with small reservoir capacity to water inflow ratio (CIR) and large capacity sluices [7]. Since the effective scour zone is constricted locally near the outlet openings, pressurized flushing is more effective in controlling sediment deposition level at the entrance of the intakes. However, for efficient flushing of large sediment deposits from the reservoir, drawdown of water level is required [8].

Emamgholizadeh et al. [3] carried out laboratory experiments on pressure flushing of non-cohesive sediment. They concluded that the flushing efficiency can be increased by reducing the reservoir level during the flushing while keeping the outlets operating at full capacities and proposed an empirical equation for estimating the volume of the flushing cone:

$$\frac{V_s^{1/3}}{H_{s,net}} = 0.6139 \left(\frac{u}{\sqrt{g H_{w,net}}} \right)^{0.0062} \left(\frac{H_{s,net}}{d_s} \right)^{0.05} \left(\frac{H_{s,net}}{H_{w,net}} \right)^{0.0036} \quad (1)$$

where, V_s = the volume of the flushing cone, $H_{s,net}$ = net sediment height above the centre of the outlet opening, u = flow velocity at the entrance of the orifice, g = acceleration due to gravity, $H_{w,net}$ = net flow depth above the centre of the outlet opening, and d_s = characteristic sediment particle size.

Shahmirzadi et al. [9] showed that the volume of the flushing cone can, for a constant reservoir level, be increased by increasing the outlet opening size i.e. increasing the outlet discharge. They also suggested an empirical relation for predicting the flushing cone volume:

$$\frac{V_s}{H_{w,net}^3} = 0.042 \left(\frac{u}{\sqrt{g H_{w,net}}} \right)^{0.149} \left(\frac{H_{s,net}}{H_{w,net}} \right)^{3.082} \left(\frac{A}{H_{w,net}^2} \right)^{0.174} \quad (2)$$

where, A = cross sectional area of the orifice

Carrying out similar experiments as [9], [4] proposed another empirical relation to determine the volume of the flushing cone:

$$\frac{V_s}{H_{w,net}^3} = 4.6 \left(\frac{u}{\sqrt{g(G_s-1)d_s}} \right)^{0.21} \left(\frac{H_{s,net}}{H_{w,net}} \right)^{2.2} \left(\frac{D}{H_{w,net}} \right)^{0.89} \quad (3)$$

which includes the diameter of the circular bottom outlet (D), specific gravity of sediment particles (G_s) and the characteristic particle size of sediment (d_s), although only a single sand sample was used in their experiments, i.e. their experiments were carried out with constant values for G_s and d_s . Fathi-Moghadam et al. [10] also carried out experiments similar to [3] using three different sand sizes i.e. varying d_s but constant G_s . They concluded that the size of the flushing cone increases with decreasing sediment size. Based on their experimental data, they proposed an empirical relation to predict the flushing cone volume:

$$\frac{V_s^{1/3}}{D} = 5.28 \left(\frac{u}{\sqrt{g(G_s-1)d_s}} \right)^{0.1} \left(\frac{H_{w,net}}{H_{s,net}} \right)^{-0.046} \quad (4)$$

Emamgholizadeh et al. [11] used the data from [3,4] and [10] to train and test an Artificial Neural Network (ANN) and Adaptive Neuro-Fuzzy Inference System (ANFIS), respectively, and concluded that both artificial intelligence based models predicted the flushing half cone volume and length more accurately than the empirical regression-based relations according to equations (1) to (4). They performed a sensitivity analysis which demonstrated that the sediment characteristics, thickness of sediment deposit, mean grain diameter, water depth in reservoir and mean flow velocity through bottom outlet are the most important parameters for predicting the flushing half-cone volume and length.

The present study investigates the practicality of using lightweight materials, having density greater than water but lower than natural sand, as model sediment to simulate pressurized flushing cone in physical hydraulic models. Theoretically, lightweight materials can be used as model sediment in physical hydraulic models if similarity in Froude number and densimetric Froude number are satisfied while compromising similarity in particle Reynolds number, relative density of sediment particles and relative bed roughness. Hughes [12] designated this type of models as Densimetric Froude models. Such a model type is generally applied in studies related to sediment transport processes in fluvial hydraulics when

fine sand is present in the prototype situation which, when downscaled to model scale, would require cohesive sediment to be used in the model. Many researchers have used lightweight sediments for different hydraulic experiments such as studying the beginning of motion and predicting pier scour (as cited in [13]). In this study, a lightweight material was used as model sediment to simulate pressurized flushing through a bottom outlet and to assess the possibility of predicting the flushing cone volume.

2. Methodology

2.1. Previous data

The experiments have been designed to investigate the application of lightweight material as model sediment so that only equations (3) and (4) containing G_s as a variable were considered for further comparison. In total 110 experimental datasets, 65 from [4] and 45 from [10] were extracted from published plots in the respective papers. Experimental data from [4] represented variation in flushing cone volume due to variations in water level, discharge and opening size of the outlet. The experiments were performed with constant sediment layer thickness of 16 cm consisting of sediment with a specific gravity of 2.65 and uniformly sized sediment with a diameter of 1 mm. [10] performed the experiments for different combinations of water levels, discharges and sediment sizes while the sediment layer thickness, specific gravity of sediment and outlet diameter were kept constant. For the whole set of experiments, the sediment layer thickness was 42 cm, specific gravity of sediment was 2.65 and the outlet diameter was 2 inches (5.08 cm). These experimental datasets were used to compare the results according to equations (3) and (4) and with experimental results from this study.

2.2. Dimensional Analysis

The volume of flushing cone (V_s) depends, as outlined above, on various parameters such as geometrical boundary conditions, hydraulic parameters, fluid properties and sediment properties. Hence, it can be written as a function of the following variables [3,4,9,10]:

$$V_s = f(u, H_{w,net}, H_{s,net}, A, B, d_s, \rho_s - \rho_w, \rho_w, \mu, g) \quad (5)$$

where, B = flume width, ρ_s = density of sediment, ρ_w = density of water, and μ = dynamic viscosity. In the present experiments (see Section 2.3), B , ρ_w , μ and g were constant so that the following functional relationship can be established for the dimensionless flushing cone volume [4,9]:

$$\frac{V_s}{H_{w,net}^3} = f\left(\frac{u}{\sqrt{g(G_s - 1)d_s}}, \frac{H_{s,net}}{H_{w,net}}, \frac{A}{H_{w,net}^2}\right) \quad (6)$$

2.3. Experimental setup

The experiments were carried out at the hydraulic laboratory of Norwegian Institute of Science and Technology (NTNU) in Norway. The experimental setup consisted of a 0.60 m wide horizontal flume with a 5 cm wide rectangular orifice at the mid-width of the flume. The orifice was kept 6 cm above the flume bed to allow free formation of the flushing cone and also to avoid the influence of flow downstream. A layer of sediment with uniform thickness H_s was deposited upstream of the orifice at the beginning of each experiments. A simplified sketch of the experimental setup after the formation of the flushing cone is shown in Figure 1.

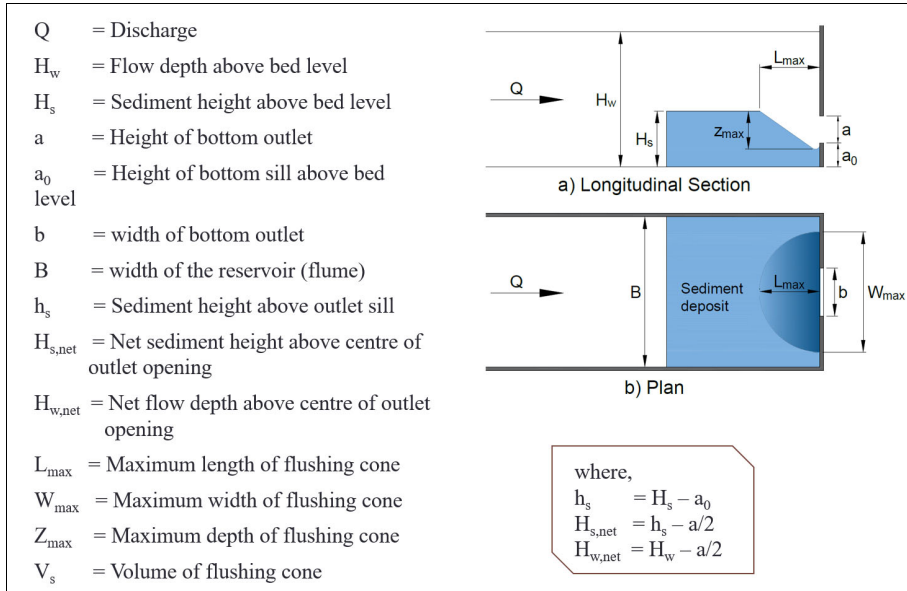


Figure 1. Experimental setup and associated parameters

2.4. Material

Poly-methyl methacrylate (PMMA) grains were used as model sediment for the experiments. The PMMA grains had specific gravity of 1.18 and were uniformly sized ($d_s = 2.4$ mm). They were slightly cylindrical in shape and were light blue in colour.

2.5. Experiments

The experiments were carried out with steady flow condition without any sediment inflow for a range of different parameter values (Table 1). The width of the flume and the width of the orifice were kept constant throughout all the tests. For each test, the flume was initially filled with a sediment deposit of constant thickness H_s . Then, the inflow discharge was slowly fed into the flume without disturbing the initial sediment deposit, and the water level was allowed to rise. When the desired water level was reached, the gate was opened up to the desired opening height. The water level was chosen from the rating curve of the outlet orifice such that the outflow discharge would be equal to the inflow discharge for given opening height of the orifice. The test was run in the steady state until the flushing cone reached the equilibrium state i.e. no more scouring in the flushing cone. Then the orifice gate was closed and water inside the flume was drained slowly without disturbing the shape and size of the flushing cone. The surface profile of flushing cone for each test was measured using SeaTek 5 MHz ranging system consisting 32 acoustic transducers. The transducers were placed in a movable plate to form a 25 mm grid. The plate with the transducers was hovered above the flume bed at different positions to scan the cone surface with finer resolution (<25 mm). Then the data were used to calculate the flushing cone volume for each test with the help of 3D data interpolation function in Matlab.

Table 1. Range of parameters.

Parameters	Range
Discharge (Q)	0.9 – 5.0 lps
Net flow depth ($H_{w,net}$)	107 – 408 mm
Thickness of sediment deposit above flume bed (H_s)	100, 120 and 140 mm
Opening height of outlet orifice (a)	20, 30, 40 and 50 mm



Figure 2. Flushing cone formed with PMMA.

3. Results and discussion

In a first step, the experimental data from [4] and [10] were compared using equations (3) and (4), and Figure 3 illustrates that both equations perfectly fit the data used for their derivation. However, equation (4) overestimates V_s for the data from [4] by about 5 times, and equation 3 over-estimates V_s for data from [10] by about 2 times. This shows that both equations do not comply with the experimental data from the other study because the experiments by [4] were performed with constant d_s and H_s while the experiments by [10] were carried out with constant D and H_s . However, the two datasets complement each other and when combined may be used to capture the effects of variation in d_s , H_s and D . Equations (3) and (4) were further applied to the experimental data from this study to assess whether any of them correctly predicts the volume of the flushing cone formed with lightweight material characterised by a different G_s .

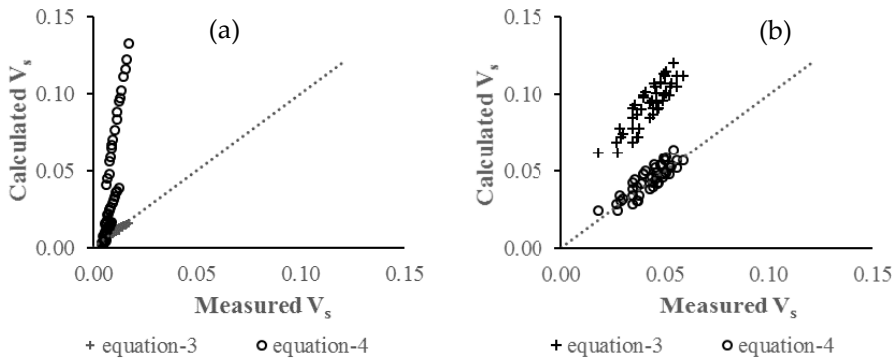


Figure 3. Calculated V_s against measured V_s using equations (3) and (4) for experimental data from (a) Meshkati et al. [4] and (b) Fathi-Moghadam et al. [10]

The empirical relations according to equations (3) and (4) comply with the functional relationship given in equation (6) since both parameters A and D represent the opening size of the outlet. The functional relationship according to equation (6) was further justified with a good trend followed by the variation of each of the chosen dimensionless parameters when plotted against dimensionless flushing cone volume. Figures 4a and 4b show the plots of $\frac{V_s}{H_{w,net}^3}$ against $\frac{u}{\sqrt{g(G_s-1)d_s}}$ and $\frac{H_{s,net}}{H_{w,net}}$ for different outlet opening heights when thickness of sediment deposit was 140 mm, and Figure 4c presents the plot of $\frac{V_s}{H_{w,net}^3}$ against $\frac{A}{H_{w,net}^2}$ for different outlet opening heights and different thickness of sediment deposit. Similar trends were observed for the variation of $\frac{V_s}{H_{w,net}^3}$ against $\frac{u}{\sqrt{g(G_s-1)d_s}}$ and $\frac{H_{s,net}}{H_{w,net}}$ for a thickness of the sediment deposit (H_s) of 120 mm and 100 mm. The dimensionless flushing cone volume decreased with decreasing sediment deposit thickness which can be expected as a smaller sediment deposit thickness means less sediment is available for flushing. Similarly, it can be seen from the plots in Figure 4 that the dimensionless flushing cone volume increases with increasing outlet opening area as concluded by Meshkati et al. [4]. Thus, it can be concluded that the lightweight PMMA in the model experiments behaved similar as natural sediments.

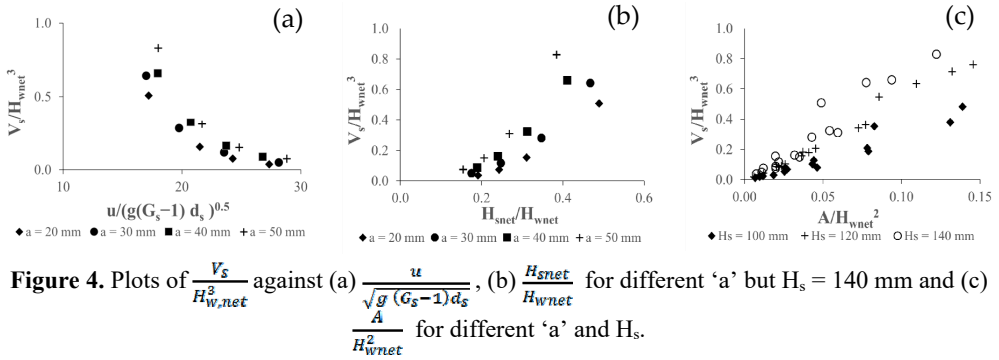


Figure 4. Plots of $\frac{V_s}{H_{w,net}^3}$ against (a) $\frac{u}{\sqrt{g(G_s-1)d_s}}$, (b) $\frac{H_{s,net}}{H_{w,net}}$ for different 'a' but $H_s = 140$ mm and (c) $\frac{A}{H_{w,net}^2}$ for different 'a' and H_s .

Using equation (3) and the experimental data from the present study, $\frac{V_s}{H_{w,net}^3}$ for each experiment was calculated and compared with the measured values as shown in Figure 5. Similarly, $\frac{V_s^{1/3}}{D}$ for each experiment was calculated using equation (4) and compared with measured values as illustrated in Figure 6. Equation (3) underestimated the dimensionless flushing cone volume whereas equation (6) overestimated it. Besides differences in the experimental setup, the deviation of measured values from calculated values using equations (3) and (4) can also be associated with the different shape of the outlets. In this study, a rectangular bottom outlet was used with constant width and varying height whereas [4] and [10] used a circular bottom outlet. In order to apply equations (3) and (4) to our experimental data, the diameter of the bottom outlet was taken as an equivalent diameter of a circle with same area as the rectangular orifice. This assumption is one reason for the observed deviation between measured and calculated values of the dimensionless flushing cone volume. However, [14] showed that the size of flushing cone depends on the shape of the outlet and concluded that flat rectangular and square outlets produced bigger flushing cone compared to a round one. This statement provides thus an explanation for the underestimation of the flushing cone volume by equation (3). On the contrary, the flushing cone volumes were overestimated by equation 4.

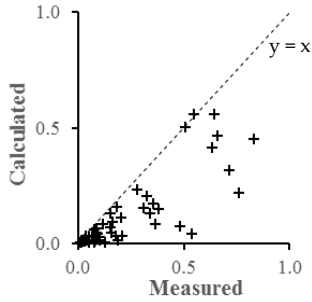


Figure 5. Plot of measured $\frac{V_s}{H_{s,net}^3}$ against calculated values using equation 3

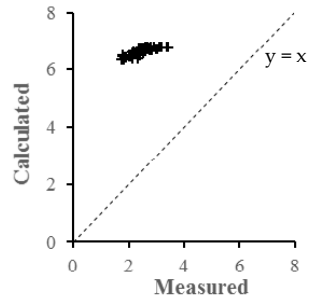


Figure 6. Plot of measured $\frac{V_s^{1/3}}{D}$ against calculated values using equation 4

Another possible reason for the observed deviations is the use of single sediment thickness in the experiments forming the basis for equations (3) and (4). Using only a single sediment thickness, each of the empirical regression-based relations developed from experimental data cannot predict the variation in dimensionless flushing cone volume for varying thickness of sediment deposit above the centre of the outlet opening ($H_{s,net}$). Similarly, equations (3) and (4) were developed from experiments with natural sand i.e., constant G_s and hence might not be effective to predict the effect of variation in G_s . In short, equations (3) and (4) might be applicable to limited range of parameters and hence cannot be applied for the range of parameters in this study.

4. Conclusion

The variation in each of the chosen dimensionless parameters had a good trend against variation in dimensionless flushing cone volume for experimental data with PMMA as shown in Figure 4. This shows the potential of PMMA grains to be used as model sediment to simulate pressurized flushing cone in physical model experiments. However, the experimental data for PMMA cannot be described by the empirical relations according to equations (3) and (4) proposed to predict dimensionless flushing cone volume for sand. The possible reasoning for this deviation have been discussed but should be verified via more experiments using model sediments with different specific gravities and characteristics particle sizes. Experiments with sand in identical experimental setup should also be performed so that the possible deviation due to differences in the experimental setup can be avoided so that the experimental data can be compared directly. Finally, if all the data from previous studies are combined and used to develop a new regression based empirical relation, it will cover a bigger range of parameters and may improve the prediction capability.

References

- [1] Morris G L and Fan J 2010 Reservoir sedimentation handbook : Design and management of dams, reservoirs, and watersheds for sustainable use (New York: McGraw-Hill)
- [2] Schleiss A J, Franca M J, Juez C and Cesare G D 2016 Reservoir sedimentation J. Hydraul. Res. **54** 595–614
- [3] Emamgholizadeh S, Bina M, Fathi-moghadam M and Ghomeyshi M 2006 Investigation and Evaluation of the Pressure Flushing Through Storage Reservoir ARPN J. Eng. Appl. Sci.
- [4] Meshkati Shahmirzadi M E 2010 Experimental investigation of local half-cone scouring against dam
- [5] Fang D and Cao S 1996 An experimental study on scour funnel in front of a sediment flushing outlet of a reservoir 6th Federal Interagency Sedimentation Conference (Las Vegas) p I.78-I.84
- [6] Di Silvio G 1990 Modeling Desiltation of Reservoirs by Bottom-Outlet Flushing Movable Bed Physical Models NATO ASI Series ed H W Shen (Dordrecht: Springer Netherlands) pp 159–71
- [7] Qian N 1982 Reservoir sedimentation and slope stability; technical and environmental effects Fourteenth International Congress on Large Dams vol III (Rio de Janeiro) pp 639–90
- [8] H. Scheuerlein, M. Tritthart and F. Nuñez Gonzalez 2004 Numerical and physical modelling concerning the removal of sediment deposits from reservoirs Conference Proceeding of Hydraulic of Dams and River Structures (Tehran)
- [9] Shahmirzadi M E M, Dehghani A A, Meftahh M and Mosaedi A 2010 Experimental Investigation of Pressure Flushing Technique in Reservoir Storages Water Geosci. **1** 132–137
- [10] Fathi-Moghadam M, Emamgholizadeh S, Bina M and Ghomeshi M 2010 Physical modelling of pressure flushing for desilting of non-cohesive sediment J. Hydraul. Res. **48** 509–14
- [11] Emamgholizadeh S, Bateni S M and Jeng D-S 2013 Artificial intelligence-based estimation of flushing half-cone geometry Eng. Appl. Artif. Intell. **26** 2551–8
- [12] Hughes S A 1993 Physical Models and Laboratory Techniques in Coastal Engineering vol 7 (WORLD SCIENTIFIC)
- [13] Henry P-Y and Aberle J 2018 Hydralab+ Deliverable D8.3 Protocols for scaling morphodynamics in time Zenodo. <http://doi.org/10.5281/zenodo.2420824>
- [14] Dreyer S and Basson G 2018 Investigation of the shape of low-level outlets at hydropower dams for local pressure flushing of sediments SANCOLD 2018 (Cape Town)

Paper IV

Physical modelling of pressure flushing of sediment using lightweight materials

Sanat Kumar Karmacharya, Nils R  ther, Jochen Aberle, Sudhir Man Shrestha,
Meg Bahadur Bishwakarma

Accepted: Journal of Applied Water Engineering and Research

This article is awaiting publication and is therefore not included.

Annex-**B**

Dimensional Analysis and Regression Analysis

B.1 Dimensional Analysis

The volume of flushing cone (V_s) can be written as a function of the following variables:

$$V_s = f(u, H_{wnet}, H_{snet}, A, d_s, \rho_s - \rho_w, \rho_w, g, \mu)$$

Applying Buckingham π theorem,

Parameters	Dimension	Eliminating L using H_{wnet}		Eliminating T using H_{wnet}/u		Eliminating M using $\rho_w H_{wnet}^3$	
		Parameters	Dim.	Parameters	Dim.	Parameters	Dim.
V_s	L^3	V_s/H_{wnet}^3	-	V_s/H_{wnet}^3	-	V_s/H_{wnet}^3	-
u	$L T^{-1}$	u/H_{wnet}	T^{-1}	-	-	-	-
H_{wnet}	L	-	-	-	-	-	-
H_{snet}	L	H_{snet}/H_{wnet}	-	H_{snet}/H_{wnet}	-	H_{snet}/H_{wnet}	-
A	L^2	A/H_{wnet}^2	-	A/H_{wnet}^2	-	A/H_{wnet}^2	-
d_s	L	d_s/H_{wnet}	-	d_s/H_{wnet}	-	d_s/H_{wnet}	-
$\rho_s - \rho_w$	$M L^{-3}$	$(\rho_s - \rho_w)H_{wnet}^3$	M	$(\rho_s - \rho_w)H_{wnet}^3$	M	$(\rho_s - \rho_w)/\rho_w$	
ρ_w	$M L^{-3}$	$\rho_w H_{wnet}^3$	M	$\rho_w H_{wnet}^3$	M	-	-
μ	$M L^{-1} T^{-1}$	μH_{wnet}	$M T^{-1}$	$\mu H_{wnet}^2/u$	M	$\mu/(\rho_w u H_{wnet})$	
g	$L T^{-2}$	g/H_{wnet}	T^{-2}	$g H_{wnet}/u^2$	-	$g H_{wnet}/u^2$	-

The dimensionless parameters obtained are:

$$\pi_1 = \frac{V_s}{H_{wnet}^3}; \pi_2 = \frac{H_{snet}}{H_{wnet}}; \pi_3 = \frac{A}{H_{wnet}^2}; \pi_4 = \frac{d_s}{H_{wnet}}; \pi_5 = \frac{(\rho_s - \rho_w)}{\rho_w} = (G_s - 1);$$

$$\pi_6 = \frac{\rho_w u H_{wnet}}{\mu} = \frac{u H_{wnet}}{\mu/\rho_w}; \pi_7 = \frac{u^2}{g H_{wnet}}$$

Here, π_6 represents Reynolds Number, which can be considered negligible under a fully turbulent flow through the orifice.

The study deals with the orifice flow through the bottom outlet under the influence of gravitational force i.e. $u \propto \sqrt{g H_{wnet}}$ which implies not much variation in outlet's Froude Number (π_7). Since the study is focused more on variations in size and density of sediment particles, π_4, π_5 and π_7 are combined to form a new dimensionless variable given as,

$$\pi_4 = \frac{u^2}{g (G_s - 1) d_s} \approx \frac{u}{\sqrt{(G_s - 1) g d_s}}$$

Hence, the final dimensionless parameters can be written as,

$$\pi_1 = \frac{V_s}{H_{wnet}^3} \approx \frac{V_s^{1/3}}{H_{wnet}}$$

$$\pi_2 = \frac{H_{snet}}{H_{wnet}} \approx \frac{h_s}{H_{wnet}}$$

$$\pi_3 = \frac{A}{H_{wnet}^2}$$

$$\pi_4 = \frac{u}{\sqrt{(G_s - 1) g d_s}}$$

The dimensionless functional relationship for flushing cone volume can be written as

$$\frac{V_s^{1/3}}{H_{wnet}} = f \left(\frac{u}{\sqrt{g (G_s - 1) d_s}}, \frac{h_s}{H_{wnet}}, \frac{A}{H_{wnet}^2} \right)$$

Similarly, the dimensionless functional relationship for maximum length of a flushing cone can be written as

$$\frac{L_{max}}{H_{wnet}} = f \left(\frac{u}{\sqrt{g (G_s - 1) d_s}}, \frac{h_s}{H_{wnet}}, \frac{A}{H_{wnet}^2} \right)$$

B.2 Regression Analysis

From the dimensional analysis of variables influencing the volume of a flushing cone, the dimensionless functional relationship derived is

$$\frac{V_s^{1/3}}{H_{wnet}} = f\left(\frac{u}{\sqrt{g(G_s-1)d_s}}, \frac{h_s}{H_{wnet}}, \frac{A}{H_{wnet}^2}\right)$$

$$\text{Say, } X_1 = \frac{V_s^{1/3}}{H_{wnet}}, X_2 = \frac{u}{\sqrt{g(G_s-1)d_s}}, X_3 = \frac{h_s}{H_{wnet}} \text{ and } X_4 = \frac{A}{H_{wnet}^2}$$

Then, we can write a non-linear relation from the given functional relationship as

$$X_1 = k \cdot X_2^m \cdot X_3^n \cdot X_4^p$$

Transforming to linear equation by applying natural log to both sides,

$$\ln X_1 = \ln(k) + m \ln(X_2) + n \ln(X_3) + p \ln(X_4)$$

From the total 192 experimental data, 120 data were randomly selected to calibrate the regression equation. $\ln(X_1)$, $\ln(X_2)$, $\ln(X_3)$ and $\ln(X_4)$ were calculated for the experimental data and then multiple regression analysis was done in MS-Excel to determine the coefficients of the regression line in the form of

$$y = b_0 + b_1x_1 + b_2x_2 + b_3x_3$$

The coefficients estimated from multiple regression analysis of the selected experimental data are

Coefficients	value	Standard Error	t Stat	P-value	Lower 95%	Upper 95%	Lower 95.0%	Upper 95.0%
b_0	0.1597	0.0281	5.6905	9.53E-08	0.1041	0.2153	0.1041	0.2153
b_1	0.2032	0.0082	24.7923	2.14E-48	0.1870	0.2195	0.1870	0.2195
b_2	0.5216	0.0198	26.3074	5.91E-51	0.4824	0.5609	0.4824	0.5609
b_3	0.2209	0.0093	23.7218	1.60E-46	0.2024	0.2393	0.2024	0.2393

From the results, the actual coefficients can be estimated as

$$\ln(k) = b_0 = 0.1597 \text{ which gives } k = e^{0.1597} = 1.173$$

$$m = b_1 = 0.2032$$

$$n = b_2 = 0.5216$$

$$p = b_3 = 0.2209$$

And the regression statistics are as follows:

<i>Regression Statistics</i>	
Multiple R	0.992521894
R Square	0.985099709
Adjusted R Square	0.98471765
Standard Error	0.044908472
Observations	120

Therefore, the final non-linear regression equation derived from the experimental data for estimating the volume of flushing cone can be written as

$$X_1 = k \cdot X_2^m \cdot X_3^n \cdot X_4^p$$

$$\frac{V_s^{1/3}}{H_{wnet}} = 1.173 \left(\frac{u}{\sqrt{g(G_s - 1)d_s}} \right)^{0.203} \left(\frac{h_s}{H_{wnet}} \right)^{0.522} \left(\frac{A}{H_{wnet}^2} \right)^{0.221}$$

Similarly, regression analysis was carried out on the experimental data to derive the non-linear regression equation for estimating maximum length of flushing cone as

$$\frac{L_{max}}{H_{wnet}} = 1.311 \left(\frac{u}{\sqrt{g(G_s - 1)d_s}} \right)^{0.286} \left(\frac{h_s}{H_{wnet}} \right)^{0.588} \left(\frac{A}{H_{wnet}^2} \right)^{0.203}$$

Annex-**C**

Statement from co-authors



STATEMENT FROM CO-AUTHOR

(cf. section 10.1 in the PhD regulations)

Sanat Kumar Karmacharyaapplies to have the following thesis assessed:
Name of candidate


Simulating pressurised reservoir flushing in scale models using lightweight sediments ..
title

*) The statement is to describe the work process and the sharing of work and approve that the article may be used in the thesis.

*)
Statement from co-author on article:
Application of 'Structure from Motion' (SfM) technique in physical hydraulic modelling
Current Research in Hydropower Technologies (CRHT IX), 2019

I hereby declare that I am aware that the article mentioned above, of which I am a co-author, will form a part of the PhD thesis by the PhD candidate Sanat Kumar Karmacharya who made major contribution to the work in the experiment, data analysis and writing phase.

Kathmandu, Nepal
Place, date 21/12/2020


.....
Signature co-author



STATEMENT FROM CO-AUTHOR
(cf. section 10.1 in the PhD regulations)

Sanat Kumar Karmacharya.....applies to have the following thesis assessed:
Name of candidate


Simulating pressurised reservoir flushing in scale models using lightweight sediments.....
title

*) The statement is to describe the work process and the sharing of work and approve that the article may be used in the thesis.

*)
Statement from co-author on article:
Application of ‘Structure from Motion’ (SfM) technique in physical hydraulic modelling
Current Research in Hydropower Technologies (CRHT IX), 2019

I hereby declare that I am aware that the article mentioned above, of which I am a co-author, will form a part of the PhD thesis by the PhD candidate Sanat Kumar Karmacharya who made major contribution to the work in the experiment, data analysis and writing phase.

Kathmandu, 21.12.2020
.....
Place, date


.....
Signature co-author



STATEMENT FROM CO-AUTHOR

(cf. section 10.1 in the PhD regulations)

Sanat Kumar Karmacharya.....applies to have the following thesis assessed:
Name of candidate

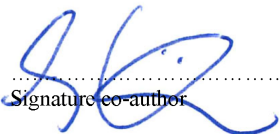
Simulating pressurised reservoir flushing in scale models using lightweight sediments ..
title

*) The statement is to describe the work process and the sharing of work and approve that the article may be used in the thesis.

*)
Statement from co-author on article:
Application of 'Structure from Motion' (SfM) technique in physical hydraulic modelling
Current Research in Hydropower Technologies (CRHT IX), 2019

I hereby declare that I am aware that the article mentioned above, of which I am a co-author, will form a part of the PhD thesis by the PhD candidate Sanat Kumar Karmacharya who made major contribution to the work in the experiment, data analysis and writing phase.

...22.12.2020.....
Place, date


Signature co-author



STATEMENT FROM CO-AUTHOR

(cf. section 10.1 in the PhD regulations)

Sanat Kumar Karmacharyaapplies to have the following thesis assessed:
Name of candidate


Simulating pressurised reservoir flushing in scale models using lightweight sediments ..
title

*) The statement is to describe the work process and the sharing of work and approve that the article may be used in the thesis.

*)
Statement from co-author on article:
Structure from Motion technique to measure bed morphology in physical hydraulic model studies
In Review: Journal of Hydro-environment Research

I hereby declare that I am aware that the article mentioned above, of which I am a co-author, will form a part of the PhD thesis by the PhD candidate Sanat Kumar Karmacharya who made major contribution to the work in the experiment, data analysis and writing phase.

.....22.12.2020.....
Place, date


Signature co-author



STATEMENT FROM CO-AUTHOR

(cf. section 10.1 in the PhD regulations)

Sanat Kumar Karmacharya.....applies to have the following thesis assessed:
Name of candidate


Simulating pressurised reservoir flushing in scale models using lightweight sediments.....
title

*) The statement is to describe the work process and the sharing of work and approve that the article may be used in the thesis.

*)
Statement from co-author on article:
Structure from Motion technique to measure bed morphology in physical hydraulic model studies
In Review: Journal of Hydro-environment Research

I hereby declare that I am aware that the article mentioned above, of which I am a co-author, will form a part of the PhD thesis by the PhD candidate Sanat Kumar Karmacharya who made major contribution to the work in the experiment, data analysis and writing phase.

Kathmandu, 21.12.2020
.....
Place, date


.....
Signature co-author



STATEMENT FROM CO-AUTHOR

(cf. section 10.1 in the PhD regulations)

Sanat Kumar Karmacharya.....applies to have the following thesis assessed:
Name of candidate

Simulating pressurised reservoir flushing in scale models using lightweight sediments ..
title

*) The statement is to describe the work process and the sharing of work and approve that the article may be used in the thesis.

*)

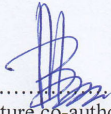
Statement from co-author on article:

Structure from Motion technique to measure bed morphology in physical hydraulic model studies

In Review: Journal of Hydro-environment Research

I hereby declare that I am aware that the article mentioned above, of which I am a co-author, will form a part of the PhD thesis by the PhD candidate Sanat Kumar Karmacharya who made major contribution to the work in the experiment, data analysis and writing phase.

Kathmandu, Nepal
Place, date 21/12/2020


.....
Signature co-author



Encl. to application for assessment of PhD thesis

STATEMENT FROM CO-AUTHOR

(cf. section 10.1 in the PhD regulations)

Sanat Kumar Karmacharya.....applies to have the following thesis assessed:
Name of candidate

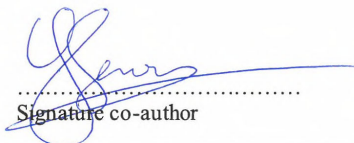
Simulating pressurised reservoir flushing in scale models using lightweight sediments..
title

*) The statement is to describe the work process and the sharing of work and approve that the article may be used in the thesis.

*)
Statement from co-author on article:
Physical modelling of pressurized flushing of non-cohesive sediment using lightweight material
Current Research in Hydropower Technologies (CRHT IX), 2019

I hereby declare that I am aware that the article mentioned above, of which I am a co-author, will form a part of the PhD thesis by the PhD candidate Sanat Kumar Karmacharya who made major contribution to the work in the experiment, data analysis and writing phase.

Trondheim
..21.12.2020
Place, date


.....
Signature co-author



STATEMENT FROM CO-AUTHOR

(cf. section 10.1 in the PhD regulations)

Sanat Kumar Karmacharya.....applies to have the following thesis assessed:
Name of candidate

Simulating pressurised reservoir flushing in scale models using lightweight sediments ..
title

*) The statement is to describe the work process and the sharing of work and approve that the article may be used in the thesis.

*)

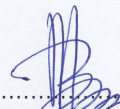
Statement from co-author on article:

Physical modelling of pressurized flushing of non-cohesive sediment using lightweight material

Current Research in Hydropower Technologies (CRHT IX), 2019

I hereby declare that I am aware that the article mentioned above, of which I am a co-author, will form a part of the PhD thesis by the PhD candidate Sanat Kumar Karmacharya who made major contribution to the work in the experiment, data analysis and writing phase.

Kathmandu, Nepal
Place, date 21/12/2020


.....
Signature co-author



STATEMENT FROM CO-AUTHOR

(cf section 10.1 in the PhD regulations)

Sanat Kumar Karmacharya.....applies to have the following thesis assessed:
Name of candidate


Simulating pressurised reservoir flushing in scale models using lightweight sediments.....
title

*) The statement is to describe the work process and the sharing of work and approve that the article may be used in the thesis.

*)
Statement from co-author on article:
Physical modelling of pressurized flushing of non-cohesive sediment using lightweight material
Current Research in Hydropower Technologies (CRHT IX), 2019

I hereby declare that I am aware that the article mentioned above, of which I am a co-author, will form a part of the PhD thesis by the PhD candidate Sanat Kumar Karmacharya who made major contribution to the work in the experiment, data analysis and writing phase.

Braunschweig, 21.12.2020
Place, date


.....
Signature co-author



STATEMENT FROM CO-AUTHOR

(cf. section 10.1 in the PhD regulations)

Sanat Kumar Karmacharyaapplies to have the following thesis assessed:
Name of candidate

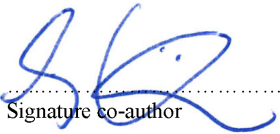
Simulating pressurised reservoir flushing in scale models using lightweight sediments ..
title

*) The statement is to describe the work process and the sharing of work and approve that the article may be used in the thesis.

*)
Statement from co-author on article:
Physical modelling of pressurized flushing of non-cohesive sediment using lightweight material
Current Research in Hydropower Technologies (CRHT IX), 2019

I hereby declare that I am aware that the article mentioned above, of which I am a co-author, will form a part of the PhD thesis by the PhD candidate Sanat Kumar Karmacharya who made major contribution to the work in the experiment, data analysis and writing phase.

...22.12.2020.....
Place, date


Signature co-author



NTNU

Encl. to application for assessment of PhD thesis

STATEMENT FROM CO-AUTHOR

(cf. section 10.1 in the PhD regulations)

Sanat Kumar Karmacharyaapplies to have the following thesis assessed:
Name of candidate

Simulating pressurised reservoir flushing in scale models using lightweight sediments.....
title

*) The statement is to describe the work process and the sharing of work and approve that the article may be used in the thesis.

*)

Statement from co-author on article:


Physical modelling of pressure flushing of sediment using lightweight material

Journal of Applied Water Engineering and Research, Under Review

I hereby declare that I am aware that the article mentioned above, of which I am a co-author, will form a part of the PhD thesis by the PhD candidate Sanat Kumar Karmacharya who made major contribution to the work in the experiment, data analysis and writing phase.

...22.12.2020.....

Place, date


.....
Signature co-author



STATEMENT FROM CO-AUTHOR

(cf. section 10.1 in the PhD regulations)

Sanat Kumar Karmacharya.....applies to have the following thesis assessed:
Name of candidate


Simulating pressurised reservoir flushing in scale models using lightweight sediments.....
title

*) The statement is to describe the work process and the sharing of work and approve that the article may be used in the thesis.

*)
Statement from co-author on article:
Physical modelling of pressure flushing of sediment using lightweight material
Journal of Applied Water Engineering and Research, Under Review

I hereby declare that I am aware that the article mentioned above, of which I am a co-author, will form a part of the PhD thesis by the PhD candidate Sanat Kumar Karmacharya who made major contribution to the work in the experiment, data analysis and writing phase.

Braunschweig, 21.12.2020
Place, date


.....
Signature co-author



STATEMENT FROM CO-AUTHOR

(cf. section 10.1 in the PhD regulations)

Sanat Kumar Karmacharyaapplies to have the following thesis assessed:
Name of candidate

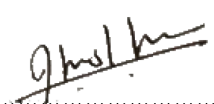
Simulating pressurised reservoir flushing in scale models using lightweight sediments
title

*) The statement is to describe the work process and the sharing of work and approve that the article may be used in the thesis.

*)
Statement from co-author on article:
Physical modelling of pressure flushing of sediment using lightweight material
Journal of Applied Water Engineering and Research, Under Review

I hereby declare that I am aware that the article mentioned above, of which I am a co-author, will form a part of the PhD thesis by the PhD candidate Sanat Kumar Karmacharya who made major contribution to the work in the experiment, data analysis and writing phase.

Kathmandu, 21.12.2020
.....
Place, date


.....
Signature co-author



STATEMENT FROM CO-AUTHOR

(cf. section 10.1 in the PhD regulations)

Sanat Kumar Karmacharya.....applies to have the following thesis assessed:
Name of candidate

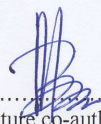
Simulating pressurised reservoir flushing in scale models using lightweight sediments ..
title

*) The statement is to describe the work process and the sharing of work and approve that the article may be used in the thesis.

*)
 Statement from co-author on article:
Physical modelling of pressure flushing of sediment using lightweight material
 Journal of Applied Water Engineering and Research, Under Review

I hereby declare that I am aware that the article mentioned above, of which I am a co-author, will form a part of the PhD thesis by the PhD candidate Sanat Kumar Karmacharya who made major contribution to the work in the experiment, data analysis and writing phase.

Kathmandu, Nepal
 Place, date 21/12/2020


 Signature co-author